Investigating microbial habitats and carbon pools associated with a high Arctic glacier

by

Charvanaa Dhoonmoon

A thesis submitted in partial fulfillment of the requirements for the degree of

Master of Science

Department of Earth and Atmospheric Sciences
University of Alberta

ABSTRACT

Glacial systems are reservoirs of nutrients, labile organic matter, and microbes. Glaciers contain diverse environments (supraglacial (surface), subglacial (base), and ice-marginal) with variable organic matter pools shaped by different physical processes and site-specific microbial communities and metabolisms. The ecological interactions between organic matter and microbial communities, including the bioavailability of organic matter to these communities, in glacial environments remain to be constrained. Samples of supraglacial ice, meltwaters from an ice-marginal channel, and basal ice were collected from Sverdrup Glacier, a polythermal tidewater glacier in the Canadian high Arctic. We assessed microbial diversity (from the 16S rRNA gene) and functional potential (from taxonomy) and correlated community composition with solute (nutrient and major ions) concentrations and dissolved organic matter (DOM) composition measured via fluorescence spectroscopy and ultra-high resolution mass spectrometry (FT-ICR-MS). We also incubated melted debris-rich and debris-poor basal ice to monitor microbial uptake of glacial organic carbon to gain insight into the lability of this carbon pool and the effects on microbial diversity and functional potential. Distinct microbial communities and different patterns of correlations with solute and DOM properties among the glacial environments suggest that site-specific compositions of solutes and DOM shape community structures. The presence of both putative heterotrophic and autotrophic metabolisms across these glacial environments further supported the potential for in-situ microbial carbon cycling in glacial ecosystems. Fluorescence spectroscopy and FT-ICR-MS results revealed significant but varying labile fractions of DOM among the glacial environments, largely derived from in-situ microbial activity. Our experimental incubations showed that this DOM was bioavailable to in-situ microbial communities and stimulated glacial heterotrophs in both incubations. A higher carbon uptake was also observed in

the debris-rich incubation versus the debris-poor incubation, suggesting a differential supply of labile DOM by debris in basal ice. This study helps to establish a baseline from which to assess future physical and ecological changes in glacial labile DOM reservoirs and microbe-DOM interactions driven by climate warming. As glaciers shrink and glacial meltwater and associated labile carbon fluxes increase, this study provides insight into the role of in-situ microbial communities in shaping DOM bioavailability and the effect of DOM on glacial microbial community ecology.

PREFACE

This thesis is a result of collaborative research efforts with Professor Maya Bhatia from the University of Alberta being the lead collaborator and the supervisory author. The samples used in this study were collected and logged by Dr. Ashley Dubnick and Patrick Williams during their field expedition to Sverdrup Glacier in May 2018. They also provided the field pictures of samples used here in Chapter 2 (*Methods*). I melted the samples, filtered them for various analyses, and monitored the incubations (Chapter 2). I was responsible for running/coordinating the laboratory analyses of the samples and conducting all statistical analyses (Chapter 2). Dr. Ryan Hutchins from the University of Waterloo analyzed the samples via ultrahigh-resolution mass spectrometry during his visit to the University of Alberta and processed the output from this instrument to make it suitable for statistical analyses. Professor Erin Bertrand from Dalhousie University and Dr. Ashley Dubnick provided regular insights and feedback on the results and their interpretations throughout this project. The literature review in Chapter 1, data analysis in Chapter 3, and concluding analysis in Chapter 4 are my own work. No part of this thesis has been previously published.

ACKNOWLEDGEMENTS

The completion of my thesis would not have been possible without the efforts, support, and inputs from my mentors, collaborators, and peers. Thank you to Maya who has been a remarkable mentor and devoted much of her time and energy to help me produce this thesis, achieve my professional goals, overcome personal hurdles, and overall become a better scientist. I also want to extend my gratitude to Erin, who as part of my committee and as a mentor, also offered great support both in an academic and personal capacity during my journey. While our interactions have only been online, I am truly appreciative of her insights and guidance in interpreting the data I had. Maria, to whom I will be long grateful, has been instrumental in training and guiding me during laboratory work, especially in microbiological analyses. Thank you, Maria, for making my lab experience truly educational and as smooth as it can be; I will miss our fun chats. I am also thankful to Ashley and Patrick (Williams), who collected the samples I used in my thesis, for their additional contributions to this work. Ashley's expertise was invaluable in correctly shaping the storyline for my thesis, and I am very appreciative of her ongoing contributions and support to this work. Much of my knowledge about TOC maintenance stems from shadowing Patrick, and I cannot thank him enough for taking the time out of his busy schedule to help me with the TOC, and more recently, to provide feedback on my writing. Finally, I cannot thank enough Jill, Hayley, and Patrick (White) enough, who have been wonderful, cooperative, and helpful lab peers and supportive friends during our hangouts.

Thank you to all sources of funding which made this project possible, which include the grants from the University of Alberta Start-up and the Campus Alberta Innovates Program awarded to Maya Bhatia. Thank you to Ming and his team at the Biological Analytical Services Laboratory and the Analytical Services in the Earth & Atmospheric Sciences department at the University of

Alberta for assisting me with the knowledge and completion of several analyses. I would also like to thank Suzanne Tank and Joanna for being welcoming hosts and providing me with the necessary training to use their flow cytometer and the Aqualog in their lab space. I am also extremely grateful to Ryan Hutchins for running and processing my DOM samples and for always responding to my questions promptly.

This journey would also not be possible without the support of my family and best friends. Mum, Yash, and Dad – I can never thank you enough for your patience and prayers and your support of my career. Khoshik – thank you for your entertaining company (including the silly jokes), and your encouragement and confidence in me. Ana, Junaid, and David – thank you for some of the best times I had in this place and for helping me stay sane throughout.

TABLE OF CONTENTS

LIST OF TABLES

LIST OF FIGURES

1. Introduction

Glacial systems (glaciers, ice caps, and ice sheets) are extreme ecosystems characterized by cold, oligotrophic conditions. These systems serve as repositories of nutrients (such as phosphate, nitrate) (Hodson et al., 2005; Tranter et al., 2005; Hawkings et al., 2015), organic matter (Barker et al., 2006; Bhatia et al., 2010; Dubnick et al., 2010; Stubbins et al., 2012; Antony et al., 2014; Lawson et al., 2014b; Hood et al., 2015; Feng et al., 2018; Kellerman et al., 2021), and psychrophilic microbial communities (Skidmore et al., 2000; Bhatia et al., 2006; Lanoil et al., 2009; Simon et al., 2009; Stibal et al., 2015; Cameron et al., 2016; Garcia-Lopez and Cid, 2017). A glacial system is comprised of distinct environments, broadly represented by the supraglacial (glacier surface), englacial (within glacier), subglacial (glacier bed), proglacial (front of the glacier), and ice-marginal (glacier margins) regions (Hodson et al., 2008; Hotaling et al., 2017). These diverse regions are governed by site-specific physical conditions, including light, oxygen, and liquid water availability, and allochthonous inputs (e.g., bedrock, atmospheric, and hydrological supply of solutes, organic matter, and microbes). These environments can also become hydrologically connected during the melt season and circulate nutrients, organic matter, and microbes from one region to another (Tranter et al., 2005; Wynn et al., 2007; Bhatia et al., 2010; Dubnick et al., 2017; Weisleitner et al., 2019; Kellerman et al., 2020). For example, supraglacial meltwaters can drain via the glacier margins (Luckman, 1988; Boon et al., 2010) and also englacially through holes (moulins) and cracks (crevasses) at the surface (Bingham et al., 2005; Rada and Schoof, 2018; Chandler et al., 2021) to the subglacial or proglacial environments. Proglacial zones can include terrestrial areas, rivers, and lakes at land-terminating glaciers, and coastal environments like fjords and bays at tidewater glaciers. Overall, nutrients, organic matter, and microbes are introduced into glacial environments via different physical and hydrological processes including atmospheric deposition, bedrock contact, and meltwater drainage. The allochthonous nutrient and organic matter can then be reshaped by the activity of in-situ microbial communities, whose structure may in turn be influenced by the evolving nutrient and organic matter pools.

1.1. Physical inputs of organic matter and microbes in glacial environments

There is a stark contrast between the two primary glacial environments, the supraglacial and subglacial, with regards to physical inputs of organic matter and microbial inoculum. The

supraglacial represents the snow, ice, and meltwater on the glacier surface that is in direct contact with the atmosphere. The deposition of windblown dust, soot, and aerosols onto the glacier surface constitutes a low but key source of organic matter (Bhatia et al., 2010; Stubbins et al., 2012; Feng et al., 2018), microbial cells (Zhang et al., 2007; Xiang et al., 2009; Cameron et al., 2015; Weisleitner et al., 2019) as well as sediments and solutes (nitrate (NO_3), mineral phosphate, sodium (Na), chloride(Cl)) (Hodson et al., 2005; Price et al., 2009; McCutcheon et al., 2021) to this ecosystem. Once on the glacier surface, sediments and organic matter can melt into surface ice and form water-filled depressions (i.e. cryoconite holes), which become seasonal hotspots for microbial activity (Stibal and Tranter, 2007; Cameron et al., 2012; Telling et al., 2012). Annually, when surface snow and ice melt and drain away during the summer, the supraglacial solutes, organic matter, and microbes are transported out of this system, preventing their long-term accumulation in this environment (Stibal et al., 2008a, 2008b, 2010, 2017).

In contrast, the subglacial environment consists of the ice and meltwater beneath the glacier in direct contact with the underlying sediments and bedrock. Physical interactions such as grinding between the glacier and the bed erode the bedrock and produce comminuted sediments, and crustal solutes (e.g., phosphate (PO_4), sulfate (SO_4), silica (Si), Na, magnesium (Mg), calcium (Ca), potassium (K)) (Tranter et al., 2002; Wadham et al., 2004a; Hawkings et al., 2016). Subglacial organic matter derives in part from previously overridden soil and vegetation at the glacier bed (Barker et al., 2006, 2010; Bhatia et al., 2010; Dubnick et al., 2020; Kellerman et al., 2020, 2021), while subglacial microbial cells may originate from basal sediments and the overridden soil and vegetation. Since the bed of the glacier is inaccessible, samples of basal ice, subglacial sediments, and meltwaters from subglacial streams, channels, and lakes are often used as proxies for this environment (Skidmore et al., 2000; Bhatia et al., 2006; Dubnick et al., 2010; Kayani et al., 2018; Sułowicz et al., 2020). Basal ice is the layer of debris-laden ice (4 – 20 m high) found at the glacier base (Lawson et al., 1998; Iizuka et al., 2001; Barker et al., 2010; Montross et al., 2014). Basal ice is produced during physical glacier–bedrock interactions (Hubbard and Sharp, 1989, 1993; Knight, 1997; Lawson et al., 1998) and thus, can be useful to infer solute, organic matter, and microbial properties shaped by bedrock inputs. As basal ice forms, subglacial debris comprised of the eroded sediments, organic matter, and resident microbial cells is entrained into the ice matrix. As a result of the variability inherent in this formation process, wide-ranging debris concentrations (< 1 g/L to > 1 kg/L) are commonly observed in the basal ice layer and lead to the

formation of debris-rich and debris-poor basal ice zones (Skidmore et al., 2000; Hubbard et al., 2009; Montross et al., 2014). Past studies have linked higher solute and carbon concentrations, elevated microbial cellular densities, and increased heterotrophic activity to higher basal ice debris concentrations (Skidmore et al., 2000; Montross et al., 2014), demonstrating a heterogeneous ecosystem in basal ice. Finally, while largely shaped by bedrock interactions, the organic matter and microbial properties of the subglacial ecosystem can also be influenced by seasonal supraglacial inputs via the hydrological drainage network. These inputs can include atmospherically deposited and microbially derived organic matter (Bhatia et al., 2010; Lawson et al., 2014a; Kellerman et al., 2020) and potentially supraglacial microbial cells (Bhatia et al., 2006).

The ice-marginal environment hydrologically links the glacier surface to subglacial and proglacial environments and contains diverse features such as surface ice margins, ice-marginal lakes and channels, and glacial moraines (Luckman, 1988; Carrivick and Quincey, 2014; Ewertowski et al., 2016; Armstrong and Anderson, 2020). Supraglacial meltwaters drained through the glacier margins (Luckman, 1988; Boon et al., 2010; Armstrong and Anderson, 2020) can accumulate and reside in marginal lakes (Carrivick and Quincey, 2014; Armstrong and Anderson, 2020; How et al., 2021), and in marginal channels (Dubnick, 2018) before draining subglacially and proglacially. This drainage can occur catastrophically, with ice-marginal lake drainage in Greenland shown to contribute up to 2 km^3 of meltwater to a fjord system over one week (Kjeldsen et al., 2017). The passage and storage of meltwaters in marginal lakes and channels could impact the chemical and microbiological properties of the supraglacial meltwaters transiting ice-marginally. Similar effects are commonly observed at the glacier base, where supraglacial meltwaters draining subglacially become enriched in crustal solutes (Hodson et al., 2005; Lilbæk and Pomeroy, 2008), organic matter (Bhatia et al., 2010; Kellerman et al., 2020), and microbial cells (Dubnick et al., 2017). Overwinter storage of supraglacial meltwaters in marginal channels is also possible (Dubnick, 2018), with ensuing potential for microbial reworking of in-situ organic matter composition (Bhatia et al., 2010). The combination of supraglacial inputs and ice-marginal storage can lead to the formation of carbon pools and microbial habitats located at the ice margins that may be distinct from supraglacial and subglacial ecosystems. As climate warming leads to increased meltwater fluxes, ice-marginal ecosystems, which store meltwater and its associated sediment and carbon in marginal ponds, lakes, and streams for varying periods (Carrivick and Quincey, 2014), may become more prevalent (Carrivick and Quincey, 2014; Shugar et al., 2020;

How et al., 2021). These understudied glacial environments (Hodson et al., 2008; Anesio et al., 2017; Hotaling et al., 2017) thus warrant further investigation.

1.2. Glacial DOM composition shaped by in-situ microbial metabolism

The type of microbial metabolism occurring in glacial environments is largely dictated by broad physical conditions such as light and oxygen availability. Supraglacial microbial activity is driven by light energy available at the glacier surface, with photoautotrophic taxa like cyanobacteria (Edwards et al., 2014; Cameron et al., 2015; Musilova et al., 2015) and microalgae (Takeuchi, 2013; Lutz et al., 2014, 2017) being major members of surface snow, ice, and cryoconite microbial communities. Aerobic heterotrophs are also present in supraglacial communities, which can respire surface organic matter (Anesio et al., 2010; Telling et al., 2012). Meanwhile, the metabolic reactions that characterize the subglacial ecosystem are distinct from the photoautotrophic lifestyles on the glacier surface. The subglacial is a dark environment with variable oxygen concentrations that result in seasonally dynamic oxygenated and anoxic zones. As a result, chemolithotrophic metabolism is typical in subglacial systems, including aerobic chemoheterotrophy, anaerobic respiration via sulfate and nitrate reduction, methanogenesis, and chemoautotrophy (Foght et al., 2004; Skidmore et al., 2005; Boyd et al., 2011, 2014; Thór Marteinsson et al., 2013; Montross et al., 2014; Kayani et al., 2018).

The presence of autotrophic and heterotrophic metabolisms in the glacial ecosystems entails that resident microbial communities can play a direct role in carbon and nutrient cycling and in reshaping the composition of glacial organic matter. In glacial systems, microbial transformations have been characterized as a source of labile DOM (i.e., carbon that can be readily consumed by microbes). These transformations can include autotrophic organic matter production, the respiration and reworking of allochthonous organic matter, and the production of proteins, peptides, and free amino acids (Barker et al., 2010; Bhatia et al., 2010; Dubnick et al., 2010; Antony et al., 2014; Lawson et al., 2014b). Fluorescence spectroscopy (Barker et al., 2006, 2010; Dubnick et al., 2010, 2020; Feng et al., 2018) and ultrahigh-resolution mass spectroscopy (Grannas et al., 2006; Bhatia et al., 2010; Antony et al., 2014, 2017) are common techniques which have been used to examine the characteristics of glacial organic matter, including its lability. These methods target different subsets of organic matter, i.e., fluorescing organic compounds in the case of the former and polar organic compounds in the latter case. Past applications of these techniques,

individually or in tandem, have shown that glaciers can be significant sources of autochthonously produced microbial DOM (Barker et al., 2006; Hood et al., 2009; Dubnick et al., 2010; Stubbins et al., 2012; Feng et al., 2018), with glaciers representing a unique carbon pool that is distinct from terrestrial rivers, which typically have allochthonous DOM signatures dominated by degraded plant and soil organic matter (Stedmon and Markager, 2005; Stubbins et al., 2012; Riedel et al., 2016; Kellerman et al., 2021).

Between the supraglacial and subglacial environments, DOM composition can vary widely (Bhatia et al., 2010; Stubbins et al., 2012; Dubnick et al., 2020; Kellerman et al., 2021). Together, these two, hydrologically connected regions, can shape the composition of organic matter ultimately exported out of the glacier. Characterizing carbon pools across various glacial ecosystems can serve to yield better estimates of glacial labile carbon budgets and fluxes. Experimental incubations from past studies have shown that glacial DOM, due to its high lability, is bioavailable to downstream aquatic ecosystems with the potential for stimulating downstream secondary production (Hood et al., 2009; Lawson et al., 2014b). However, the bioavailability of glacial DOM to in-situ microbial communities before downstream export and the effects of this DOM pool on the microbial community ecology (structure and function) remain unclear. Glacial microbial activity could alter in-situ DOM compositions, for example, by consuming the most labile fractions and potentially transforming this pool into less labile DOM (Barker et al., 2010), thereby impacting the bioavailability of glacial DOM which is ultimately exported downstream.

1.3. Research goals

Here, we assessed the organic matter and microbial properties of the supraglacial, ice-marginal, and subglacial environments at a high Arctic polythermal glacier in the Canadian Arctic Archipelago (CAA). We used a suite of biogeochemical analyses including solute (nutrient, major ions) measurements, organic matter characterization via fluorescence spectroscopy and ultrahigh-resolution mass spectrometry, and microbial and metabolic diversity analyses (from 16S rRNA gene sequencing) to demonstrate variations in resident microbial communities and organic matter lability across diverse glacial environments. Next, to explore the effects of glacial carbon bioavailability on in-situ microbial ecology, we incubated debris-poor and debris-rich basal ice over 120 days, examining shifts in microbial community structure and function. Given that debris is a highly variable source of microbial cells, sediments, nutrients, and organic matter in the

subglacial environment (Montross et al., 2014), we hypothesized that the labile carbon delivered by debris would vary, with ensuing impacts on carbon uptake and microbial community shifts (e.g., in heterotrophic potential) in the debris-poor and debris-rich treatments.

Our study site is a marine-terminating glacier (Sverdrup Glacier) on the Devon Island Ice Cap, where meltwaters predominantly drain ice-marginally (Cress and Wyness, 1961; Boon et al., 2010; Williams et al., 2021). This study site is of interest as it is situated in the CAA, a region cumulatively representing 14% of the global ice mass but significantly understudied compared to the polar ice sheets. Sverdrup glacier itself has, however, been intensively studied since the 1960s with previous work characterizing the glacier dynamics and hydrology (Cress and Wyness, 1961; Boon et al., 2010), the lithology beneath the ice cap (St-Onge et al., 2009; Whalen et al., 2010), as well as the solute, organic matter, and microbial properties of surface ice and basal ice (Dubnick et al., 2020; Williams et al., 2021). We build on this previous literature to examine the interactions between resident microbial communities and in-situ DOM in glacial ecosystems. To generate hypotheses about specific microbial carbon cycling processes, we compare putative metabolic functions derived from microbial taxa associated with different environments on Sverdrup Glacier, using marker-gene based pipelines, specifically the Functional Annotation of Prokaryotic Taxa pipeline (FAPROTAX) (Louca et al., 2016). These pipelines (e.g., FAPROTAX, PiCRUST2) can predict functional information from taxonomic data (Langille et al., 2013; Louca et al., 2016; Raes et al., 2021) and are being applied extensively to gain insight into microbial functional diversity in a variety of aquatic and terrestrial ecosystems (Louca et al., 2016; Bomberg et al., 2019; Raes et al., 2021; Sansupa et al., 2021; Toubes-Rodrigo et al., 2021). We further pair ultrahigh-resolution mass spectrometry and fluorescence spectroscopy to characterize glacial DOM pools. Collectively, our microbial and carbon data provide insight into the lability of DOM in different environments at Sverdrup Glacier and, a basis to assess the ecological effects of glacial carbon bioavailability to subglacial microbial communities, which we examine using incubations with basal ice.

1.4. Rationale and significance

The ice masses in the CAA and the wider Arctic region, where tidewater glaciers are prevalent with over 300 such glaciers in the CAA (Cook et al., 2019) and over 215 on Greenland (Choi et al., 2021), are rapidly retreating and shrinking due to climate change (Gardner et al., 2011; Noël et al., 2018; Cook et al., 2019). Increased Arctic temperatures may also alter the extreme

conditions to which glacial microbes are adapted, potentially impacting overall glacial microbial biodiversity (Hotaling et al., 2017; Milner et al., 2017). By investigating the chemical and microbiological properties of different glacial environments, this study highlights the potential for variable pools of labile DOM and distinct ecosystems to be present on tidewater glaciers. These findings help establish a baseline from which to assess future physical and ecological impacts on glacial microbial habitats and labile carbon reservoirs as well as their interactions as the climate warms. Glacial fluxes of labile carbon are also predicted to increase in the short term (Hood et al., 2009, 2015; Bhatia et al., 2013; Lawson et al., 2014b). Clarifying the bioavailability of glacial DOM to in-situ microbes could provide insight into the ecological dynamics between glacial microbial habitats and DOM pools as well as the potential utility of the DOM exported to downstream ecosystems after glacial microbial consumption.

2. Methods

2.1. Study site

Our study site is Sverdrup Glacier, a marine-terminating outlet glacier draining Devon Ice Cap on the north coast of Devon Island (Nunavut) in the CAA (Figure 1A). The glacier terminates in Jones Sound, a waterway between Devon Island and Ellesmere Island. It is ~25-km long, has an average width of 2.5 km, and is nestled between valley walls with an average height of 300 m (Cress and Wyness, 1961; Vögtli, 1967). The bedrock underlying the Devon Ice Cap consists of Precambrian metamorphic rocks that are part of the Cumberland batholith (St-Onge et al., 2009). Composed of primarily granitic rocks such as syenogranite, monzogranite, and granodiorite, the batholith has a high silica content (55-70 wt%) coupled with variable levels of potassium oxide, ranging from high-K to shoshonitic lithology (Whalen et al., 2010). Sverdrup Glacier itself is surrounded by Neoarchean and Paleoproterozoic metasedimentary gneiss and orthopyroxene granite (Harrison et al., 2016). Springtime to summer ice flow rates of < 50 m a^{-1} have been observed in the ablation zone (Burgess et al., 2005; Wychen et al., 2017), and basal sliding has previously been inferred to be a contributor to the ice flow beneath some regions of the glacier (Burgess et al., 2005), which suggests that Sverdrup Glacier is a polythermal ice mass (Dubnick et al., 2020; Williams et al., 2021). In summer, surface meltwater predominantly drains the glacier ice-marginally (Cress and Wyness, 1961; Boon et al., 2010), although supraglacial streams likely drain to the bed through larger crevasses and moulins previously observed at ~ 4 km from the

glacier terminus (Boon et al., 2010). The melt season at Sverdrup Glacier generally starts at the end of May, peaks in early July coinciding with the highest surface air temperatures, and ends in mid-to-late September (Williams et al., 2021).

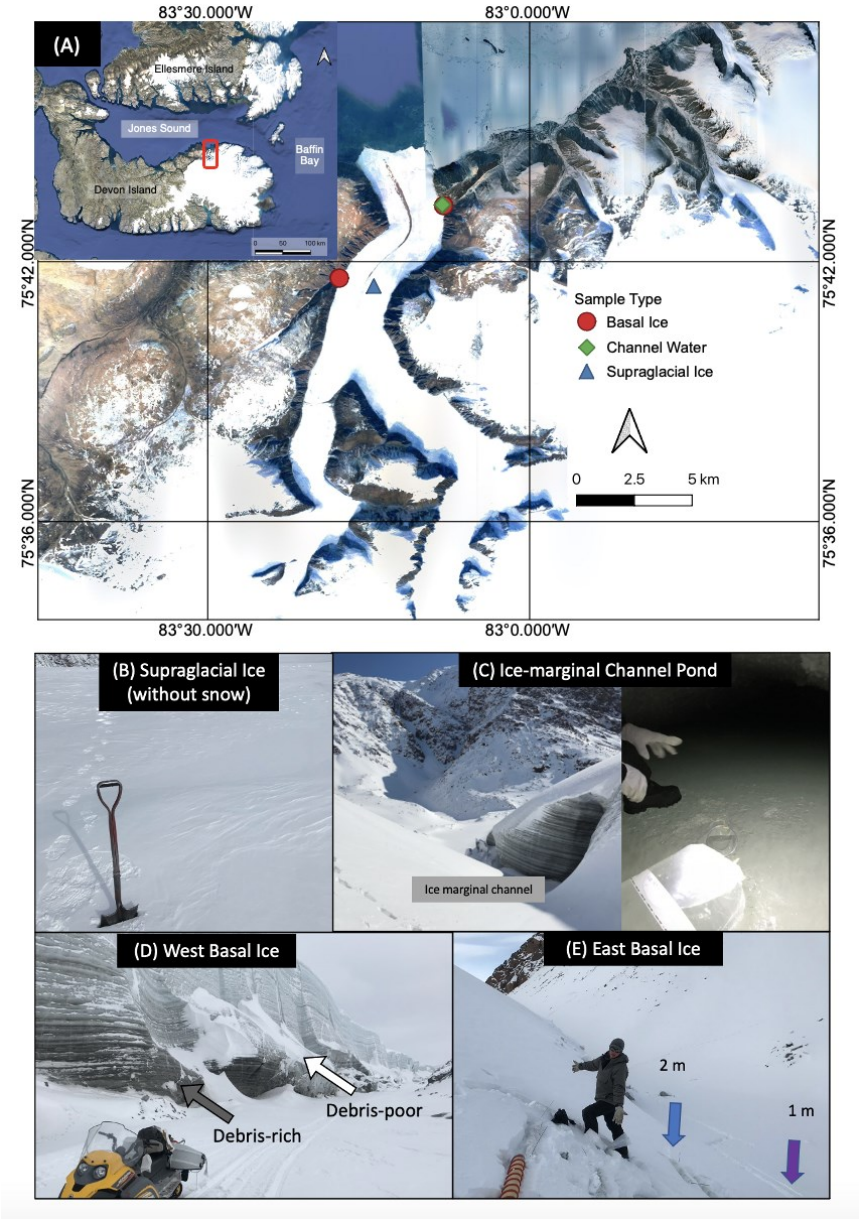

Figure 1. (A) Map showing the location of Sverdrup Glacier, a tidewater glacier draining Devon Ice Cap (Devon Island, Nunavut), and the locations of different glacial samples collected in May 2018. Images of (B) the supraglacial ice collected at the glacier surface after removing the snow cover, (C) the ice-marginal channel on the eastern margin, and the pond of marginal meltwaters located inside the channel, (D) debris-rich and debris-poor basal ice collected on the western margin, and (E) basal ice collected at 1 and 2-m height from the base at the eastern margin.

2.2. Field Sampling

Between 2 and 6 May 2018, we collected 11 large-volume ice and meltwater samples from the supraglacial (n = 1), ice-marginal (n = 6), and subglacial (n = 4) environments associated with Sverdrup Glacier. A previous assessment of melt season progression at Sverdrup Glacier showed the onset of melt in late May (Williams et al., 2021) and established that these samples were collected before the start of the melt season. To represent the supraglacial environment, a single ice sample (SSG) without snow cover was collected at the glacier surface (Figure 1B; Table 1). From the ice-marginal environment, meltwaters were sampled from an unfrozen pond (~ 30 m long and ~ 5 m wide) containing ice lenses at the end of a marginal channel (~ 500 m long) located on the eastern side of Sverdrup Glacier (Figure 1C). Of these "channel waters", four samples (CW1, CW2_3, CW4, CW5) were taken at the surface along the length of the marginal pond, while two samples (CW6, CW7) were collected just below the surface, at a depth of 30 – 40 cm (Table 1). Since ice-marginal drainage predominates at this glacier (Koerner et al., 1961; Boon et al., 2010), these channel waters likely reflect late-season supraglacial meltwaters drained during previous melt seasons that ponded overwinter in the marginal channel (Dubnick, 2018). Finally, basal ice samples were used as a proxy for the subglacial environment and were collected from several locations, targeting samples with variable debris concentrations. From the western margin, samples with visually higher (SWB3; debris-rich) and lower (SWB2; debris-poor) debris concentrations were collected (Figure 1D; Table 1). From the eastern margin, basal ice cores were collected at 1 m (SEBBI) and 2 m (SEMBI) from the glacier base (Figure 1E; Table 1), with the 2-m sample being more debris-rich than the 1-m sample and western basal ice samples. All meltwater samples were collected in sterile 5-L Whirl Pak plastic bags using autoclaved, sample-rinsed plastic beakers. All basal and supraglacial ice cores were collected with 95% ethanol flame-sterilized ice axes and were stored in sterile 5-L Whirl Pak plastic bags. The ice cores and channel water samples were stored at -20 ^{0}C until filtration and analysis in the laboratory. Detailed descriptions for each sample are provided in Table 1.

Table 1. Sample descriptions of supraglacial ice, ice-marginal channel pond waters (i.e., channel waters), and basal ice collected from Sverdrup Glacier in May 2018.

Sample Name (ID)	*Volume/L*	*Date Collected*	*Date Processed*	*Coordinates (Lat, Long)*	*Description*
Supraglacial Ice (SSG)	19.8	6 May 2018	2 Mar 2020	75°41'26.16"N, 83°14'32.28"W	Several chunks of surface ice collected with some debris
Channel Water 1 (CW1)	4.6	2 May 2018	11 Mar 2020	75°43'18.78"N, 83° 8'7.84"W	Sample of Sverdrup East channel pool surface water, no ice
Channel Water 2&3 (CW2_3)	5.6	2 May 2018	13 Mar 2020	75°43'18.78"N, 83° 8'7.84"W	Two samples of Sverdrup East channel pool surface ice slush combined for bulk melt
Channel Water 4 (CW4)	4.9	2 May 2018	12 Mar 2020	75°43'18.78"N, 83° 8'7.84"W	Sample of Sverdrup East channel pool surface slush; surface sample collected near the wall (~30 m from the end of the pool)
Channel Water 5 (CW5)	5.3	2 May 2018	13 Mar 2020	75°43'18.78"N, 83° 8'7.84"W	Sample of Sverdrup East channel pool surface slush; surface sample collected near the wall (~10 m from the end of the pool)
Channel Water 6 (CW6)	4.8	2 May 2018	11 Mar 2020	75°43'18.78"N, 83° 8'7.84"W	Depth sample of Sverdrup East channel pool surface slush; same location as CW5 but down to about 40 cm
Channel Water 7 (CW7)	5.1	2 May 2018	12 Mar 2020	75°43'18.78"N, 83° 8'7.84"W	Depth sample of Sverdrup East channel pool surface slush; near CW1 but down to about 30 cm
West Basal Ice 2 (SWB2)	15.1	5 May 2018	24 Feb 2020	75°41'37.63"N, 83°17'46.76"W	Upper facies of debris-poor basal ice from the west margin of Sverdrup
West Basal Ice 3 (SWB3)	11.1	5 May 2018	6 Mar 2020	75°41'35.52"N, 83°17'43.97"W	Bottom facies of debris-rich basal ice from the west margin of Sverdrup
East Basal Ice Bottom (SEBBI)	10.5	4 May 2018	2 Mar 2020	75°43'17.40"N, 83° 8'1.11"W	Two 1-m ice cores from the eastern margin of Sverdrup collected 1 m from glacier base and combined for bulk melt
East Basal Ice Middle (SEMBI)	11.2	4 May 2018	2 Mar 2020	75°43'17.40"N, 83° 8'1.11"W	Two 1-m ice cores from the eastern margin of Sverdrup collected 2 m from glacier base and combined for bulk melt

2.3. Measurements

2.3.1. Sample processing and filtration

In the laboratory, the glacial samples were first processed to remove any external contamination procured during field sampling, modifying the decontamination protocol for processing glacial ice cores by Christner et al. (2005). In contrast to the 1.5 cm of ice removed by physical scraping and ethanol and Milli-Q washes of the ice core surface (Christner et al., 2005), in this study, only the outer 1-2 mm layer was aseptically shaved off the surface of the frozen samples using combusted razor blades on a sterile surface covered with combusted aluminum foil in a -15 ^{0}C cold room. With up to 35% of ice mass loss possible by the original method by Christner et al (2005), we aimed to minimize mass loss from our samples. To ease safe sample handling, the frozen channel water samples were sawed into smaller pieces before shaving. Sterile

gloves and fresh combusted aluminum foil and razor blades were used between each sample. After the external layer was removed, the shaven ice cores were rinsed with autoclaved, ultrapure water (Milli-Q, 18.2 MΩ.cm). We excluded the ethanol wash due to potential carbon contamination that could affect post-processing carbon concentration and ultra-high resolution composition measurements. Each sample was transferred into a 20-L polycarbonate container lined with an acid-washed (in ~ 3.5% HCl), UV-radiated, 20-L PTFE bags (Welch Fluorocarbon, NH) for melting. Samples were melted in the dark for up to a week at 4 ^{0}C until about 20% of the frozen sample remained before they were filtered for solutes, microbial and organic matter analyses. All plasticware and tubing used in this study were soaked overnight in 3.5 % HCl, rinsed with Milli-Q water three times, and dried before use. The glassware was cleaned in the same manner and then combusted at 560^{0}C overnight before use. All aluminum foil was also combusted before use. Before the samples were filtered for analysis, all filtration equipment was rinsed with at least 10 mL of sample and all filters and vials for filtrates were sample-rinsed three times. Finally, to verify that the acid-washed and/or combusted equipment used to filter the melted samples was a minimal source of contamination, a process blank comprised of 5-L of frozen Milli-Q water was melted and processed following the same procedures as described below.

To determine the total suspended sediment (TSS) load, between 0.3 – 1.1 L of the melted samples were filtered through a pre-weighed 0.7 µm GFF filter until some coloration was observed on the filter or until the volume filtered exceeded 1 L. The filters were subsequently dried in an oven at 60 ^{0}C for 72 hours and re-weighed. The mass change per volume filtered for each sample was used to compute the sediment load. Nutrient samples for total nitrogen (TN) and total phosphorus (TP) were unfiltered. Samples for dissolved nutrients (soluble reactive phosphorus (SRP; PO_4), nitrate + nitrite (NO_3 + NO_2), nitrite (NO_2), ammonium (NH_4), and silica (Si)), and dissolved major anions (sulfate (SO_4) and chloride (Cl)) were filtered through a 0.22 µm PES syringe filter. Samples for major cations (sodium (Na), potassium (K), magnesium (Mg), calcium (Ca)) were filtered through a 0.02 µm Anotop syringe filter. For stable oxygen-18 isotope ($\delta^{18}O$) analyses, samples were filtered through a 0.22 µm PES filter into 2 mL scintillation vials with approximately 0.5 mL of headspace.

To enumerate the microbial cells in each sample, aliquots of 1.6 mL of the unfiltered melted samples were added to cryovials with 0.4 mL of 10% glutaraldehyde and stored at -80 ^{0}C until analysis. To collect microbial biomass for DNA extractions, between 1 – 4 L of bulk meltwaters

for basal ice and channel water samples and 8 L for the single supraglacial sample were filtered through 0.22 µm Durapore PVDF membrane Sterivex filters (MilliporeSigma). Bulk meltwaters were further filtered through a 0.2 µm Omnipore PTFE (MilliporeSigma) membrane using a sequentially acid-washed, combusted, sample-rinsed glass assembly (funnel, frit, flask) to measure dissolved organic carbon (DOC) concentrations (~ 40 mL) and to characterize dissolved organic matter composition using fluorescence spectroscopy (~ 40 mL) and ultrahigh-resolution mass spectrometry (1 L – 2.7 L). A sub-sample for SWB2 (west debris-poor basal ice) was not collected for DOC and fluorescence spectroscopy measurements due to issues during filtration. Filtrates for organic carbon concentration and FT-ICR MS analyses were acidified with trace metal grade 12 M HCl to pH 2 and stored at 4 ^{0}C. Filtrates for fluorescence spectroscopy were unacidified and analyzed within 2 weeks after the first sample was processed (Table 1) due to operational delays caused by the COVID-19 pandemic. Acidified filtrates for ultrahigh-resolution mass spectrometry were passed through 3 mL Bond Elut PPL cartridges to concentrate the DOM. The concentrates were eluted twice with 3 mL of ultrapure methanol into 8 mL amber vials (Dittmar et al., 2008). The eluted samples were dried via vacuum centrifugation, reconstituted in 1 mL of ultrapure methanol, and stored at -20 ^{0}C in the dark. Finally, to measure particulate organic carbon (POC) concentrations and the particulate stable carbon-13 isotope ratios (δ^{13}C-POC), between 0.1 L – 1.1 L of bulk meltwaters were filtered through combusted 25-mm 0.7 µm GFF filter to collect the sediments, and the filters were stored at -20 ^{0}C until analysis.

2.3.2. Nutrients, major ions, and water isotopes

The total (TN, TP) and dissolved nutrient samples (SRP, NO_3 + NO_2, NO_2, NH_4, SiO_2) were measured on a Lachat QuickChem QC8500 FIA Automated Ion Analyzer at the Biological Analytical Service Laboratories (BASL) at the University of Alberta. The reportable LODs were: TN = 6 ppb, TP = 1 ppb, SRP = 1 ppb, NO_3 + NO_2 = 2 ppb, NO_2 = 3 ppb, NH_4 = 3 ppb, and Si = 0.02 ppm. NO_3 concentrations were obtained by subtracting NO_2 concentrations from NO_3 + NO_2 values. Dissolved major anion SO_4 and Cl concentrations were measured on a Dionex DX-600 ion chromatograph at BASL with a reportable LOD of 0.04 ppm and 0.03 ppm respectively. Major cation concentrations (Na, K, Mg, Ca) were measured on a Thermo Scientific ICAP-Q quadrupole ion-coupled plasma mass spectrometer (ICP-MS) at the University of Alberta, run in medium-resolution mode using ^{23}Na (LOD = 0.19 ppb), ^{39}K (LOD = 1.4 ppb), average of ^{24}Mg (LOD =

0.0097 ppb), ^{25}Mg (LOD = 0.012 ppb) and ^{26}Mg (LOD = 0.014 ppb), ^{44}Ca (LOD = 1.2 ppb). Before running on the ICP-MS, 0.32 N trace metal grade nitric acid was used to acidify and dilute samples and prepare calibration standards for each element. Measured concentrations were corrected with an instrument blank made of the same trace metal grade nitric acid. The $\delta^{18}O$ isotope ratios were measured on a Picarro L2130-I at the University of Alberta. Certified water standards (USGS-46, USGS-47, and USGS-48) were used to correct raw isotope ratios to the Vienna Standard Mean Ocean Water-Standard Light Antarctic Precipitation (VSMOW-SLAP) scale, and Milli-Q water was used as instrumental blanks.

2.3.3. Cell counts

Cell densities in each sample were measured on a BD Accuri C6 flow cytometer at the University of Alberta using fluorescent staining of the nucleic acids. Daily validation of the system (all coefficient of variation (CV) peaks at < 5%) was performed using Spherotech 6-peak and 8-peak validation beads. A double viability staining method with 10000x SYBR Green 1 (Millipore) and propidium iodide (10 mg PI powder, Thermoscientific) was used to differentiate between live and dead cells. SYBR Green I can stain cells with both intact and damaged membranes, which fluoresce green, whereas PI, being impermeable to cellular membranes, can only stain cells with damaged membranes, fluorescing red (Habtewold et al., 2016). A 1:100 solution of PI and SYBR Green I was used to stain cells in samples at 1:1 (v/v). Stained samples were incubated at 37 ^{0}C for 12-15 mins before slowly passing through the flow cytometer (27 µL/min). Duplicate measurements were taken for each sample. Live cells were identified from the total (live and dead) cells on the FL3 against FL1 density plot using the Eawag template gate, an established template that marks the region on the density plot associated with live cells (Gatza et al., 2013). Debris was filtered out from the density plot before counting live cells by examining a biplot of forward scatter (FSC) and side scatter (SSC), where debris occurs in regions with low FSC (small size) and low SSC (low complexity) (Habtewold et al., 2016). Finally, total and live cell counts were corrected with the process blank cell counts (total 1.5 x 10^3 cells/mL and live 1.0 x 10^3 cells/mL), which may arise from the un-autoclaved Milli-Q water used for the blank.

2.3.4. DNA extractions and 16S rRNA gene sequencing

DNA was extracted from the Sterivex filters using a phenol-chloroform extraction method (Zaikova et al., 2010) with the following modifications: (1) A mechanical bead-beating step lysis was included (Santoro et al., 2010) at the chemical lysis step where 0.25 mL of detergent-washed, UV-sterilized 0.5 mm zirconia/silica disruption beads (RPI, Corp.) was added with lysozyme (5 mg/mL), RNAase A (10 µg/mL) and tris-acetate-EDTA (TE) buffer to the filters. Subsequently, the filters were incubated at 37 ^{0}C for 60 mins; (2) Incubation with proteinase K (10 mg/mL) and 10% sodium dodecyl sulfate solution was at 55 ^{0}C for 20 mins; and (3) After organic extractions and TE buffer washes and centrifugations in Amicon Ultra-4 Centrifugal Filter Units (1 mL sample volume), the aqueous layer was concentrated to a final volume between 250-500 µL. Genomic DNA concentrations were quantified on a Qubit 4 Fluorometer (Invitrogen, ThermoFisher Scientific), with results ranging between 0.02 to 0.4 ng/µL and being below the detection limit for most basal ice samples (LOD is 0.01 ng/µL). Total DNA yields recovered in this study were therefore low (77 ng for supraglacial ice, 141 – 1351 ng for channel waters, and below detection for all the basal ice samples, except SWB3, which had a yield of 8.96 ng), in line with low DNA yields previously reported in glacial environments (Simon et al., 2009).

To analyze the microbial community composition, we targeted the V4-V5 hypervariable region of the 16S rRNA gene. The primers 515F (5'-GTGYCAGCMGCCGCGGTAA-3') (Parada et al., 2016) and 926R (5'-CCGYCAATTYMTTTRAGTTT-3') (Quince et al., 2011) from Earth Microbiome were used in PCR amplification on a SimpliAmp Thermal Cycler (ThermoScientific), with the following protocol: 3 mins of initial denaturation at 98 ^{0}C, 35 cycles of 30 s of denaturation, 30 s of primer annealing at ~ 60 ^{0}C and 30 s of extension at 72 ^{0}C, and finally, 10 mins of final extension at 72 ^{0}C. Dilutions of genomic DNA with nuclease-free water (undiluted to 1:80), annealing temperatures of 60 – 62 ^{0}C, and extension times of 45 – 60 s were used to optimize the quality of the amplicons. For the SSG sample, high annealing temperatures of 68-75 ^{0}C were used to eliminate non-specific products. All amplicon product was verified on a 1.5% agarose gel. Multiple amplicon products from the same sample were pooled during PCR purification (removing primers, dNTPs, and PCR reagents using magnetic beads (NucleoMag NGS Clean-up and Size Selection kit, Macherey-Nagel)) to further improve the quality of the amplicons. Dual indexing with i7 and i5 adapters (Illumina) was used to construct the V4-V5 library for Illumina sequencing and the quality of the barcoded amplicons was checked on a 1.5% agarose gel. All barcoded amplicons were pooled together (10.7 ng/µL), and the final quality was

checked on the Agilent 2100 Bioanalyzer at the Molecular Biology Service Unit (MBSU) using a high sensitivity DNA assay (Agilent High Sensitivity DNA Kit). Here, in addition to running the pooled library diluted 1:15, 5 random amplicons and 5 random barcoded library samples, diluted 1:10, were run to further confirm the quality of the overall amplification and indexing process. The final prepared 4 nM library containing 50% PhiX Control v3 (Illumina, Canada Inc., NB, Canada) was sequenced on an Illumina MiSeq (Illumina Inc., CA, USA) using a 2 × 250 cycle MiSeq Reagent Kit v3 at MBSU.

2.3.5. DOC, POC, δ^{13}C-POC

DOC concentrations were quantified on a Shimadzu TOC-V (CPH) analyzer using a high-sensitivity platinum catalyst (LOD = 4 ppb). DOC was measured as non-purgeable organic carbon via combustive oxidation at 680 ^{0}C and using a 6-point calibration curve of 0 to 1 ppm with R^2 = 0.9999 made from auto-dilution of a 5 ppm Total Organic Carbon (TOC) Standard stock solution (Accuspec, SCP Science). The calibration curve was validated with 0.5 ppm carbon reference samples prepared from the 5 ppm TOC stock solution. Final DOC concentrations of the samples were corrected with the mean DOC concentration from instrument blanks of acidified Milli-Q and the process blank DOC concentration.

POC concentration and δ^{13}C-POC isotope ratios were measured on an elemental analyzer connected to an isoprime precisION isotope ratio mass spectrometer at BASL (University of Alberta). Prior to quantification, the filters were fumigated to remove inorganic carbon as follows: 24-hour (h) drying of filters at 60 ^{0}C followed by overnight desiccation with drierite; wetting filters with Milli-Q and heating them at 60 ^{0}C in the presence of concentrated trace metal grade 12 M HCl in a desiccator for 24 h; desiccating with NaOH pellets and drierite for 24 h; and finally, 24-h drying at 60 ^{0}C. The carbon masses from the elemental analyzer were corrected with that from a blank filter (processed similarly to the samples). The volume of sample filtered was used to calculate POC concentration.

2.3.6. Dissolved organic matter composition

Fluorescence spectroscopy was used to examine the fluorescent organic compounds (fluorophores) in glacial dissolved organic matter (DOM; ≤ 0.2 μm). This technique tracks the fluorescence emission wavelengths and intensities following light excitation over a specific

wavelength range (UV-visible range), therefore producing excitation-emission matrices (EEMs) for each sample (Coble et al., 1990; Stedmon et al., 2003). The absorbance and fluorescence of DOM in the melted samples were simultaneously measured on a Horiba Aqualog-3 spectrofluorometer equipped with a xenon arc lamp and a 10 mm path length quartz cuvette. The cuvette was rinsed with deionized water and sample water three times. Absorbance spectra and EEMs were measured at intervals of 5 nm over an excitation wavelength range from 230 nm to 600 nm with a 10 s integration time. The emission wavelength range for the EEMs was 245.784 nm to 826.702 nm with a 2.389 nm interval. Corrections for spectral distortions from instrumental biases and inner filter effects were applied to the EEMs by the Aqualog software. A standard ultrapure water reference (SN-RM-H2O) was used for a water Raman test to assess the baseline signal-to-noise ratio of the spectrofluorometer. Daily instrument blanks of deionized water (DI, Milli-Q) were also measured with the same parameters as the samples.

Ultrahigh-resolution Fourier-Transform ion-coupled resonance mass spectrometry (FT-ICR-MS) was used to target the fraction of DOM containing intact polar organic compounds with acidic and basic functional groups (such as carboxyl and amine moieties respectively). Unlike fluorescence spectroscopy, which can only assign broad classifications to DOM components, FT-ICR-MS can identify specific organic compounds in DOM, due to its ultrahigh resolution (> 100,000) and <1 ppm mass accuracy. FT-ICR-MS is coupled with electrospray ionization (ESI). The ESI further ionizes the compounds by protonation (positive ion mode) or deprotonation (negative ion mode). The ion mode used further limits the type of DOM detected to either polar organic compounds containing alkaline moieties (positive) or acidic moieties (negative) at a time (Kujawinski, 2002). ESI is ideal for analyzing environmental DOM as it facilitates the low fragmentation of organic molecules during ionization, thereby keeping them intact for precise identification via molecular formula assignment. Samples were analyzed on a Bruker 9.4T Apex-Qe FT-ICR mass spectrometer with Apollo II electrospray ionization source in the Department of Chemistry at the University of Alberta, run in the negative ion mode with a sample injection flow rate of 120 μL h^{-1}, to obtain 150 scans per sample (MacDonald et al., 2021).

2.3.7. Experimental incubations

To assess glacial organic carbon bioavailability to subglacial microbes and how debris concentration may shape the microbial responses to carbon uptake, unfiltered meltwaters from the

debris-poor basal ice (SWB2) and debris-rich basal ice (SWB3) were incubated in 1-L glass bottles for 120 days at 4 ^{0}C in the dark. The bottles were sealed with gas-tight acid-washed rubber stoppers, wrapped in aluminum foil, and then placed on a shaker between 121 – 135 rpm to prevent sedimentation at the base of the bottles and to maintain a homogeneous environment for microbial growth. Unfortunately, the water budget prevented the inclusion of replicates in this experiment.

Changes in DOC concentration, microbial cell counts, and microbial diversity were tracked throughout the incubation. Samples for DOC, cell counts, and microbial biomass were collected as described in Section 2.3.1. DOC was collected at the start (T_0) and end (T_f) of the incubation period and was measured in duplicates as described in Section 2.3.6. An experimental Milli-Q water control was taken at T_f. Incubation DOC concentrations at T_f were then corrected with this control value. Cell count samples were collected at T_0, two time points mid-incubation, and at T_f and analyzed as described in Section 2.3.3. During cell count collection, bottles were uncapped for < 45 s each time. The remaining meltwater in each incubation at T_f was filtered through a 0.22 μm Sterivex filter (see Section 2.3.1) for microbial biomass and 16S rRNA gene sequencing (see Section 2.3.4.) to characterize shifts in microbial diversity. The sequencing results from the SWB2 and SWB3 environmental samples were used to represent the microbial community composition at T_0 for the debris-poor and debris-rich incubations respectively.

2.4. Data analyses

All data post-processing (mean and standard deviation computations, data filtering and arrangement), visualizations (simple bar plots, stacked bar plots, scatterplots, correlograms), and statistical analyses were conducted in the open-source programming language R (version 4.0.3) with the following packages: *ggplot2, ggpubr, dplyr, tidyverse, corrplot* and *vegan* and other dataset-specific packages described below. To test for significant differences in fluorescent and molecular DOM composition, microbial diversity, and microbial functional potential among glacial environments, a dissimilarity matrix was constructed using the Bray-Curtis distance measure. The dissimilarity matrix was then used to test for significant differences among the glacial environments via pairwise PERMANOVA and to produce a nonmetric multidimensional scaling (NMDS) plot and a cluster dendrogram. Since there was only one supraglacial ice sample (SSG) it was excluded from all significance test results.

2.4.1. Bioinformatics

The MiSeq reads were demultiplexed using the MiSeq Reporter software (version 2.5.0.5). Each read pair was assembled using the paired-end assembler for Illumina sequences (PANDAseq) (Masella et al., 2012) with a quality threshold of 0.9, dictating that 90% of overlapping reverse and forward reads must match to assemble single reads into read pairs. Assembled reads were processed through the Quantitative Insights into Microbial Ecology 2 (QIIME 2) bioinformatics pipeline (Bolyen et al., 2019) with sequence quality control, denoising, and chimera removal performed with the Dada2 pipeline (Callahan et al., 2016). Sequences were resolved into Amplicon Sequence Variants (ASVs) and taxonomy was assigned to each ASV with at least 90% confidence using the SILVA database (SILVA Version 132; April 2018). The database was first trained into a feature classifier using parameters specific to this sample preparation and sequencing, i.e., it was cropped for the regions to which the primers used in this study span to shorten processing times against the SILVA database.

2.4.2. Microbial community composition and functional potential

Raw taxa abundance in the microbial community matrix was Hellinger-transformed (the abundance of each taxon in a sample was divided by the sum of its abundance across all the samples and then square root transformed) to minimize the effects of different total read counts (29,509 – 402,965) among the samples (Legendre and Gallagher, 2001; Legendre and Legendre, 2012; Cameron et al., 2021). The process blank had the lowest total read count (996) and was excluded from any further analysis. The microbial community matrix, taxonomic assignments for the ASVs, and the metadata information (nutrient, major ion, and carbon concentrations, and organic matter properties) were aggregated using the *phyloseq* package for downstream analyses. Beta-diversity was assessed using a dissimilarity matrix made from the Hellinger-transformed data. Spearman rank correlation analysis was used to find significant correlations between the most abundant ASVs in the microbial data and the metadata. The Hellinger-transformed community matrix and taxonomic data from 16S rRNA gene sequencing were compared to the Functional Annotation of Prokaryotic Taxa (FAPROTAX) database (v1.2.1) (Louca et al., 2016). The FAPROTAX database contains metabolic and ecological functions which are associated with prokaryotic genera or species and can be employed to predict functional information from

molecular sequencing data. The abundances of the functions in the samples identified by FAPROTAX from our molecular sequencing data were used to construct a dissimilarity matrix.

2.4.3. Fluorescent and molecular DOM composition

Parallel factor (PARAFAC) analysis is a multivariate statistical tool used to decompose complex, trilinear datasets into the underlying features of interest (e.g., signals, components) (Bro, 1997). This technique has been applied to decompose the intensity signal from the trilinear fluorescent datasets, consisting of excitation and emission wavelengths from the sample EEMs and the sample name/number, into independent, descriptive DOM components (Stedmon et al., 2003; Stedmon and Bro, 2008). Although these fluorescent DOM components cannot be identified as specific organic compounds, they can be compared with previously identified DOM components to infer the source of the observed DOM fluorescence and provide insight into its composition in samples. The drEEM toolbox on MATLAB was used to (1) correct the EEMs, (2) normalize, compute and explore potential component models, and (3) validate the selected component model (Murphy et al., 2013). In this study, 10 samples were used in PARAFAC modeling. First and second-order Rayleigh and Raman scattering were removed from EEMs using the smootheem function (dreem.openfluor.org) without interpolation. Sample EEMs were normalized as we saw high correlations among the fluorescent components modeled from unnormalized sample EEMs. Typically, the fluorescent component model can be validated using split-half analysis in the PARAFAC pipeline, which tests the model's consistency through the pairwise splitting of the sample set into four subsets, fitting a model to each subset, and evaluating the similarities among the solutions (Stedmon and Bro, 2008; Dubnick et al., 2010; Williams et al., 2021). Here, a split-half analysis could not be used to validate our model because of our low sample size that would not generate large enough subsets for robust comparisons (datasets with 20 – 100 samples are acceptable, > 100 samples are ideal). However, it is not uncommon to omit split-half validation of fluorescent component models due to low sample size or high sample variability (e.g. poorly mixed due to geographical differences) as seen in previous glacial and permafrost studies (Dubnick et al., 2010; Woods et al., 2011). Instead, we chose a three-component PARAFAC model using a manual validation protocol described by Dubnick et al. (2010) including steps such as model selection with a relatively lower sum of squared error, visual checks that sample residual spectra mainly contained noise, and inspection of changes in sample leverage

scores in different models (i.e., whether sample leverage scores were similar and if models with higher component models provided higher resolution of the overall sample fluorescence signal). Additional components resolved in models with more than three components primarily arose from the further decomposition of the process blank signal and ultimately led to more dissimilar leverage scores among the glacial samples. The normalization of sample EEMs was reversed before statistical analysis for accurate inferences of inter-sample variations in the fluorescence of modeled components. The result for the process blank was excluded from downstream statistical analyses. The three fluorescent components modeled here using PARAFAC were broadly ascribed to either terrestrial or microbial sources using a combination of past glacial studies (Dubnick et al., 2010, 2020; Feng et al., 2018; Williams et al., 2021), other non-glacial studies (Coble et al., 1990; Coble, 1996; Stedmon et al., 2003; Stedmon and Markager, 2005; Murphy et al., 2008), and open databases (e.g. OpenFluor (Murphy et al., 2014)). The maximum fluorescence intensities (F_{max}) of the three components in each sample were normalized by the total fluorescence (sum of F_{max} of the 3 components) of that sample to compare the fractions of humic-like and protein-like fluorescence among the glacial environments. The unnormalized F_{max} was used to compute a dissimilarity matrix. Absorbance (e.g., SUVA, spectral slopes) and fluorescence (e.g., peak ratios, fluorescence index) optical properties were calculated using R and MATLAB respectively. The computation and interpretation of these optical properties are outlined in Hansel et al (2016).

For the FT-ICR-MS data, the mass-to-charge ratio (*m/z*) peaks resolved were each assigned a molecular formula using the ICBM-OCEAN tool (Merder et al., 2020a, 2020b). Noise was filtered using a signal-to-noise ratio > 4. Limits on the possible abundance of elements present in an organic compound were set as follows: C (0-100), H (0-200), O (0-50), N (0-4), S (0-1) and P (0-1), and these parameters served to define the list of chemically possible molecular formulae that could be assigned to the measured *m/z* values (Merder et al., 2020a). The *m/z* peaks in the process blank were treated as contaminant peaks associated with plasticizers in the WhirlPak bags used for storage and thus were removed from the samples in which they appeared (Bhatia et al., 2010). Peak intensities were used to construct a dissimilarity matrix. The significance of the results did not change if peak presence/absence or relative intensity (normalization by dividing the sum of the intensities of each *m/z* peak across all samples) was used to construct the dissimilarity matrix. H:C and O:C ratios were computed from the molecular formulae assigned to each *m/z* peak. H:C ratios were plotted against O:C ratios in Van Krevalan plots (Kim et al., 2003) for each environment,

where each point represents one *m/z* peak. Different biomolecular classes of compounds with characteristic O:C and H:C ratio ranges are demarked on the Van Krevalan plots as follows: protein-like ($0.28 \leq O:C \leq 0.62$, $1.5 \leq H:C \leq 2$), carbohydrates ($0.7 \leq O:C \leq 0.9$, $1.5 \leq H:C \leq 2$), lignin ($0.2 \leq O:C \leq 0.4$, $1.1 \leq H:C \leq 1.45$), (Kim et al., 2003; Kujawinski et al., 2009; Bhatia et al., 2010; Feng et al., 2020) and terrestrial-like ($0.4 \leq O:C \leq 0.8$, $0.6 \leq H:C \leq 1.5$). The terrestrial-like class was delineated according to the clustering of most *m/z* peaks from a Suwanee River Fulvic Acid (SRFA) standard sample (Supplementary Figure S1), which was not run in this study but previously characterized via the same methods used here. In past studies, the SRFA standard has been used to represent terrestrially-derived DOM (Bhatia et al., 2010; Lawson et al., 2014a). We note that caution should be used when interpreting the ranges of elemental ratios for biomolecular compound classes across different studies, as some variability is evident due to different methods/algorithms used for molecular formula assignments (Kim et al., 2003; Koch et al., 2007; Kujawinski et al., 2009; Merder et al., 2020a; MacDonald et al., 2021). Nonetheless, these broad biomolecular classes are useful to contextualize the bulk molecular formulae obtained from the samples, allowing comparisons of DOM diversity among glacial environments.

2.4.4. Indicator species analysis

Indicator species analysis (ISA) is a statistical tool used to identify the key players in a community (Dufrêne and Legendre, 1997; De Cáceres et al., 2010). In previous works, this tool has been applied to identify the microorganisms (Garcia-Lopez et al., 2019; Malard et al., 2019) or organic matter species (Kujawinski et al., 2009; Bhatia et al., 2010) that can serve as markers for environments and the associated conditions these species appear in. As such, these "indicator species" can be used to monitor the physical and ecological changes in their environments and to distinguish between different environments or sources of organic matter and microbial communities (Kujawinski et al., 2009; Bhatia et al., 2010; Garcia-Lopez et al., 2019; Malard et al., 2019). An ideal indicator species is not only unique to a particular environment (high specificity) but also abundant in all samples collected from within that environment (high fidelity) (Dufrêne and Legendre, 1997). ISA was applied to both the molecular DOM matrices (*m/z* peaks and their peak intensities in samples) and microbial community composition matrices (the ASVs and their untransformed abundances in samples). The samples were grouped according to the environment from which they were collected (supraglacial ice, channel waters, basal ice) before conducting

ISA. An indicator value (IV), ranging from 0 to 1, was calculated for each taxon and *m/z* peak, whereby an IV of 1 indicates high specificity and fidelity to the group assigned (Dufrêne and Legendre, 1997). This analysis also tested the significance of each indicator species and their IV, which is determined using randomization tests (e.g. Monte Carlo with the number of iterations = 999), ultimately assigning a *p*-value to each IV (Dufrêne and Legendre, 1997).

3. Results

3.1. Hydrochemical properties of glacial ice and meltwaters

We assessed differences in the hydrochemical properties (total suspended sediment (TSS), nutrient, major ion, and carbon (DOC, POC) concentrations) of the supraglacial, ice-marginal, and subglacial regions of Sverdrup Glacier using supraglacial ice, meltwaters in an ice-marginal channel pond (hereby referred to as channel waters), and basal ice as representations of these environments. First, oxygen-18 ($\delta^{18}O$) isotope ratios established the provenance of the ice and meltwater in this glacial system (Yde et al., 2010), with the values measured in supraglacial ice (-26.82 ‰), basal ice (mean -25.99 ‰), and channel waters (mean -25.18 ‰) (Table 2) indicative of a glacial source minimally influenced by meteoric water sources (e.g. terrestrial runoff, precipitation). TSS, POC, and DOC measurements in the glacial environments differentiated the basal ice from the supraglacial ice and channel waters. Basal ice had a higher mean TSS (particle size ≥ 0.7 μm) load (0.88 g/L), albeit with large variability (0.0116 g/L – 2.89 g/L), compared to the supraglacial ice and channel waters, which were both below the detection limit (Table 2). Likewise, POC (≥ 0.7 μm) and DOC (≤ 0.2 μm) was higher and more variable in basal ice (POC 1.16 ± 0.68 ppm; DOC 2.04 ± 2.29 ppm), than in the supraglacial ice (POC 0.35 ppm; DOC 0.48 ppm) and channel waters (POC 0.31 ± 0.15 ppm; DOC 0.43 ± 0.38 ppm) (Table 2).

Table 2. Sediment, nutrient, major ion, and organic carbon concentrations, isotopic values, and cell densities in supraglacial ice, channel waters, and basal ice from Sverdrup Glacier. Mean values are reported to 1σ, with the sample number (*n*) indicated. Measurements below the detection limit (< DL) are denoted.

Measurements	Units	Supraglacial Ice	Channel Waters	Basal Ice
Total suspended sediments (TSS)	g/L	< DL (*n=1*)	< DL (*n=6*)	0.88 ± 1.36 (*n=4*)
Oxygen-18 isotope ratio ($\delta^{18}O$)	‰	-26.82 (*n=1*)	-25.18 ± 0.37 (*n=6*)	-25.99 ± 0.13 (*n=4*)
Total phosphorus (TP)	ppb	< DL (*n=1*)	3.17 ± 1.94 (*n=6*)	93.0 ± 90.5 (*n=4*)
Soluble reactive phosphorus (SRP)	ppb	< DL (*n=1*)	2.20 ± 0.87 (*n=6*)	1.75 ± 0.50 (*n=4*)
Total nitrogen (TN)	ppb	24.0 (*n=1*)	158.2 ± 46.6 (*n=6*)	58.0 ± 50.9 (*n=4*)
Nitrate (NO_3)	ppb	8.00 (*n=1*)	117.2 ± 30.2 (*n=6*)	4.5 ± 0.7 (*n=4*)
Nitrite (NO_2)	ppb	< DL (*n=1*)	4.5 ± 0.7 (*n=6*)	< DL (*n=4*)
Ammonium (NH_4)	ppb	32.0 (*n=1*)	12.0 ± 3.0 (*n=6*)	8.0 ± 4.4 (*n=4*)
Silica (Si)	ppm	0.05 (*n=1*)	0.24 ± 0.21 (*n=6*)	0.07 (*n=4*)
Sulfate (SO_4)	ppm	0.04 (*n=1*)	2.23 ± 0.64 (*n=6*)	0.61 ± 0.16 (*n=4*)
Chloride (Cl)	ppm	0.17 (*n=1*)	1.02 ± 0.45 (*n=6*)	0.25 ± 0.24 (*n=4*)
Sodium (Na)	ppb	144 (*n=1*)	581.0 ± 154.5 (*n=6*)	90.0 ± 11.3 (*n=4*)
Potassium (K)	ppb	13.9 (*n=1*)	590.1 ± 140.7 (*n=6*)	182.5 ± 53.5 (*n=4*)
Magnesium (Mg)	ppb	6.4 (*n=1*)	691.3 ± 166.5 (*n=6*)	182.0 ± 75.9 (*n=4*)
Calcium (Ca)	ppb	28.7 (*n=1*)	2484 ± 647.1 (*n=6*)	464.0 ± 123.6 (*n=4*)
Dissolved organic carbon (DOC)	ppm	0.48 (*n=1*)	0.43 ± 0.38 (*n=6*)	2.04 ± 2.29 (*n=3*)
Particulate organic carbon (POC)	ppm	0.35 (*n=1*)	0.31 ± 0.15 (*n=6*)	1.16 ± 0.68 (*n=4*)
POC-13 isotope ratio ($\delta^{13}C$-POC)	‰	-30.80 (*n=1*)	-35.22 ± 1.92 (*n=6*)	-41.05 ± 2.95 (*n=4*)
Total (live and dead) cellular density	10^3 cells/mL	5.5 ± 2.1 (*n=1*)	5.3 ± 3.0 (*n=6*)	66.7 ± 15.1 (*n=4*)
Live cellular density	10^3 cells/mL	4.0 ± 1.4 (*n=1*)	2.3 ± 1.3 (*n=6*)	3.3 ± 0.9 (*n=4*)

The carbon-13 isotope ratios measured in the POC fraction ($\delta^{13}C$-POC) were all depleted (-30.80 ‰ in supraglacial ice and on average -35.22 ‰ in channel waters and -41.05 ‰ in basal

ice), indicating potentially different sources of particulate organic matter in these glacial environments. The total nutrient (total phosphorus, TP; total nitrogen, TN), and dissolved (≤ 0.2 μm) nutrient (soluble reactive phosphorus, SRP; NO_3; NO_2; NH_4) and major ions (SO_4, Si, Cl, Na, K, Mg, Ca) concentrations showed key differences in solute composition among the supraglacial, subglacial, and ice-marginal samples. Generally, the highest solute concentrations (SRP, TN, NO_3, NO_2, SO_4, Si, Cl, Na, K, Mg, Ca) were observed in channel waters (Table 2). One exception to this trend was the TP concentrations (93.0 ± 90.5 ppb) which were highest in the basal ice, but also markedly variable. The solute concentrations were all lowest in the supraglacial ice (Table 2), apart from NO_3, NH_4, and Na, which were lowest in the basal ice.

3.2. Microbial community and functional compositions in glacial environments

Cell counts using a double staining viability technique (SYBR green and propidium iodide) were used to assess the abundance of viable bacterial cells in glacial systems. Total (live and dead) cellular density in basal ice (mean 6.7 x 10^4 cells/mL) was an order of magnitude higher than in channel waters (mean 5.3 x 10^3 cells/mL) and supraglacial ice (mean 5.5 x 10^3 cells/mL) (Table 2). Live cellular densities in supraglacial ice (4.0 x 10^3 cells/mL, channel waters (mean 2.3 x 10^3 cells/mL) and basal ice (mean 3.3 x 10^3 cells/mL) support the presence of viable microbial cells in all three glacial environments.

Molecular sequencing of the 16S rRNA gene provided insight into the microbial community composition in the different glacial environments. The Hellinger-transformed microbial community matrix contained a total of 7169 amplicon sequence variants (ASVs) for all three glacial environments. The microbial assemblages in the basal ice and channel waters were significantly different from each other (pairwise PERMANOVA, $p = 0.018$, $\alpha = 0.05$). A cluster dendrogram was used to identify the hierarchical relationships among samples based on microbial community composition, showing that all channel waters (except for sample CW6 collected at 0.4 m depth and ~ 10 m from the end of the meltwater pond in the ice-marginal channel; Table 1) clustered in one group, separate from basal ice (Figure 2). The supraglacial ice clustered more closely with the basal ice, indicating greater compositional similarities between the resolved microbial communities in these two environments (Figure 2).

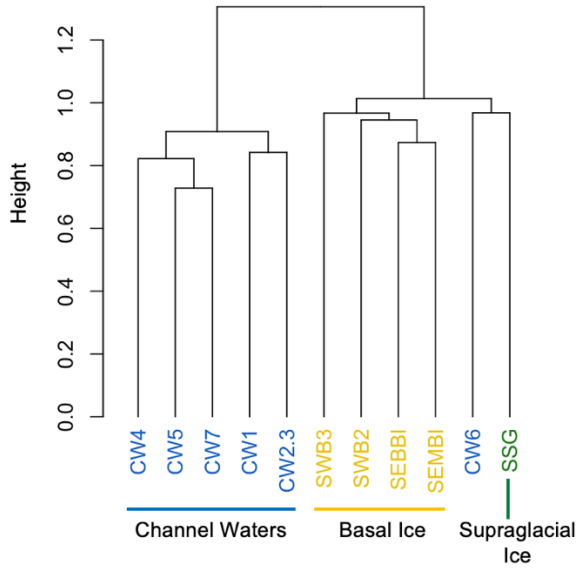

Figure 2. Cluster dendrogram using Ward's distance (squared) showing two major clusters of samples with most channel water samples grouping together (blue labels) on the left, and basal ice (yellow labels) and supraglacial ice (green label) clustering together on the right.

The top ten most abundant phyla in the microbial community matrix and their mean relative abundances in each glacial environment are provided in Table 3. Proteobacteria (39 – 47%) and Bacteriodetes (17 – 29%) were the most abundant phyla in all three glacial environments, followed by Actinobacteria (2 – 12%) and Cyanobacteria (2 – 10%) (Table 3). While generally, the same major phyla occurred in all three glacial environments, their proportions among the supraglacial ice, channel waters, and basal ice differed (Table 3). Stacked bar plots showed that the families detected across all three glacial environments include: *Burkholderiaceae, Caulobacteriaceae, Gemmataceae, Legionellaceae, Methylophilaceae, Nitrincolaceae, Porticoccaceae*, *Rhodobacteracea,e and Sphingomonadaceae* from the Proteobacteria phylum, *Chitinophagaceae, Flavobacteriaceae, Spirosomaceae, Saprospiracea,e* and *NS9 marine group* from the Bacteriodetes phylum, *Microbacteriaceae, Sporichthyaceae* and *Illumatobacteriaceae* from the Actinobacteria phylum, *Pirellulaceae* from Planctomycetes phylum, *Gemmatimonadaceae* from Gemmatimonadetes phylum, and *Nitrosopumilaceae* from the Thaumarchaeota phylum (Figure S2). Only 3 ASVs, all from the *Burkhoderiaceae* family, were shared among all the supraglacial ice, channel waters, and basal ice samples. The same 3 ASVs were also the only ones shared between channel waters and basal ice, whereas 33 ASVs were shared between basal ice and the supraglacial ice (the main families being *Flavobacteriaceae, Rhodobacteriaceae,*

Burkhoderiaceae, NS9/NS11-12 marine group, Spirosomaceae among others, and the order *Chloroplast*). Finally, 10 ASVs were shared between channel waters and supraglacial ice (the families *Burkholderiaceae, Gemmataceae, Methylophilaceae, Sporichthyaceae, Spirosomaceae*).

Table 3. The most abundant microbial phyla found in this study and their mean relative abundances (%) in the supraglacial ice, channel waters, and basal ice samples (reported to 1σ when n > 1).

Phylum (% abundance)	**Supraglacial Ice (*n* = 1)**	**Channel Waters (*n* = 6)**	**Basal Ice (*n* = 4)**
Acidobacteria	2.2	2.9 ± 1.1	2.9 ± 1.4
Actinobacteria	2.7	12.7 ± 0.7	8.9 ± 2.8
Bacteriodetes	29.4	17.7 ± 6.8	25.0 ± 3.2
Chloroflexi	1.5	0.5 ± 0.3	5.5 ± 3.5
Cyanobacteria	10.5	2.5 ± 2.8	7.3 ± 2.8
Patescibacteria	0.5	6.8 ± 4.2	1.2 ± 0.8
Planctomycetes	5.5	6.4 ± 2.8	6.6 ± 2.2
Proteobacteria	44.1	47.1 ± 0.7	39.0 ± 1.0
Thaumarchaeota	0.8	0.3 ± 0.7	1.5 ± 0.8
Verrucomicrobia	2.7	2.8 ± 0.8	2.1 ± 0.6

To gain insight into the metabolic functional potential of glacial microbial communities, we used FAPROTAX, a pipeline that assigns metabolic and ecological functions using molecular sequencing information (Louca et al., 2016). Since this pipeline compares the sample taxonomic data to a reference library of established functions from microbial literature and cultures, taxa resolved at the genera and species level are most useful in this analysis (Louca et al., 2016). Of our 7169 total ASVs, 2249 (31.3%) met this criterion and could be analyzed via FAPROTAX, which produced 47 metabolic functions (Figure S3). Since only about 1/3 of the total ASVs were incorporated into FAPROTAX, the inferred functional potential from this pipeline may not reflect the complete potential of the microbial communities resolved in this study. Nonetheless, a PERMANOVA test revealed that the putative functions resolved with FAPROTAX between basal ice and channel waters were not statistically different ($p = 0.36$, $\alpha = 0.05$).

Of the 47 resolved metabolic functions, 31 (66%) were closely associated with autotrophy, aerobic and anaerobic heterotrophy, methanogenesis, and phototrophy. We used this subset of 31 metabolic pathways for comparisons of functional potential composition among our three glacial environments, as these are the metabolic pathways typically examined or reported in glacial microbial habitats (Skidmore et al., 2000; Boyd et al., 2011, 2014; Stibal et al., 2012; Lutz et al., 2014; Antony et al., 2017; Kayani et al., 2018; Takeuchi et al., 2019; Weisleitner et al., 2019;

Dubnick et al., 2020; Toubes-Rodrigo et al., 2021). The relative abundance of a function was determined by FAPROTAX as the sum of the Hellinger-transformed abundances of the ASVs associated with this function (Louca et al., 2016; Sansupa et al., 2021). Similar to the trends observed in microbial community composition, most metabolic functions were shared among the three glacial environments with variations in their relative abundances (Figure 3). Chemoheterotrophy was the dominant potential metabolic function resolved in all glacial environments, and its abundance in basal ice and supraglacial ice was approximately 10-fold higher than in channel waters (Figure 3). Basal ice also showed greater potential for dark sulfur reactions associated with chemolithoautotrophy and anaerobic respiration with nitrate and sulfate compared to supraglacial ice and channel waters (Figure 3). Nitrification co-dominated in the basal ice and channel waters (Figure 3). Supraglacial ice, unsurprisingly, demonstrated the highest potential for phototrophic metabolism, including photoautotrophy and functions associated with chloroplasts and cyanobacteria (Figure 3). Most of these metabolic functions had the lowest abundances in channel waters, except for reactions associated with methylotrophy, methanol oxidation, and chemoautotrophic dark hydrogen processes (Figure 3).

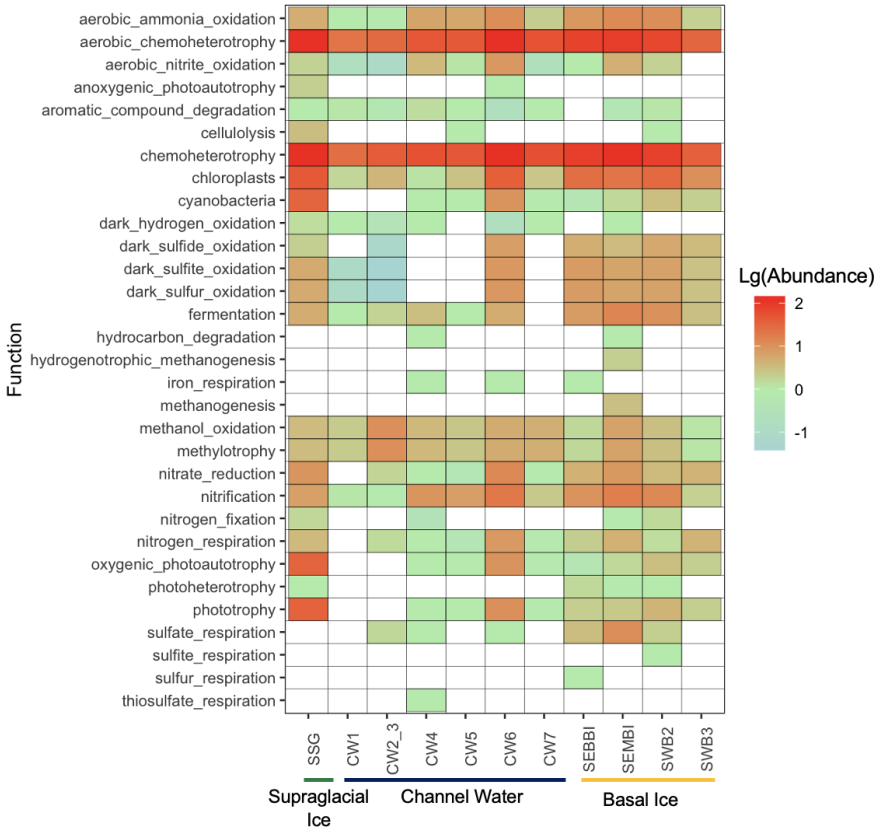

Figure 3. Log abundances of metabolic functions common to glacial ecosystems that were observed in the supraglacial ice (green), channel waters (blue), and basal ice (yellow) samples.

3.3. Fluorescent and molecular glacial DOM pools

The supraglacial, ice-marginal, and subglacial DOM pools were analyzed using fluorescence spectroscopy and ultrahigh-resolution mass spectrometry (FT-ICR-MS). These techniques characterize distinct fractions of DOM. Chemically, fluorescence spectroscopy only targets conjugated organic compounds capable of fluorescing (fluorophores). In comparison, in negative ion mode, FT-ICR-MS targets a much wider fraction of DOM because it can identify intact organic compounds with polar moieties that can be deprotonated. Analytically, fluorescence spectroscopy is limited to broad classifications of DOM as being humic-like or protein-like, whereas FT-ICR-MS can provide more precise classifications based on molecular formula assignments to resolved *m/z* peaks associated with potential DOM compounds. When paired together, these techniques can yield broader insight into the overall character of the DOM pool.

In fluorescence spectroscopy, fluorophores in DOM are excited over a wavelength range and their fluorescence emission wavelengths and fluorescence intensities are measured.

PARAFAC analysis serves to decompose the resulting excitation and emission wavelengths and intensity signals into characteristic fluorescent DOM components that represent the type of DOM present in all the samples. Here, PARAFAC modeling produced three DOM components (labeled C1, C2, and C3), which we identified using the OpenFluor database (Murphy et al., 2014) as well as past literature (Table 4). C1 resembled Peak A (Coble, 1996), associated with humic-like fluorescence (Stedmon et al., 2003; Dubnick et al., 2010; Williams et al., 2021), and was similar to DOM components previously linked terrestrially-derived DOM, such as from forest streams, wetlands and agricultural catchments (Stedmon et al., 2003; Stedmon and Markager, 2005). C1 could also be tied to microbial re-processing of DOM as seen from similar humic-like DOM components with mixed terrestrial and microbial sources reported in past glacial studies (Feng et al., 2018; Dubnick et al., 2020). In contrast, C2 and C3 indicated protein-like fluorescence (Table 4). C2 was similar to peak N and T (Coble et al., 1998; Stedmon et al., 2003) and was indicative of amino acids such as tryptophan (free or within proteins) (Stedmon et al., 2003, 2007; Murphy et al., 2008) and/or autochthonous DOM production (Stedmon et al., 2003; Stedmon and Markager, 2005). C3 likely represented free or protein-bound tyrosine-like amino acids (Stedmon et al., 2007; Shakil et al., 2020; Williams et al., 2021). Our three-component PARAFAC model described 95% of the fluorescence variance in the dataset. Without split-half validation, the ~5% of the unexplained variance in the model represented residuals and could contain other fluorescent components not modeled successfully due to the low sample size (Dubnick et al., 2010).

Table 4. A three-component model (C1-C3) derived from PARAFAC analysis of fluorescent DOM found in supraglacial ice, channel waters, and basal ice samples (n = 10). The peak excitation and emission wavelength pair (at maximum fluorescence) for each component is provided in the table with a description of the DOM type represented by each fluorescent component from the literature.

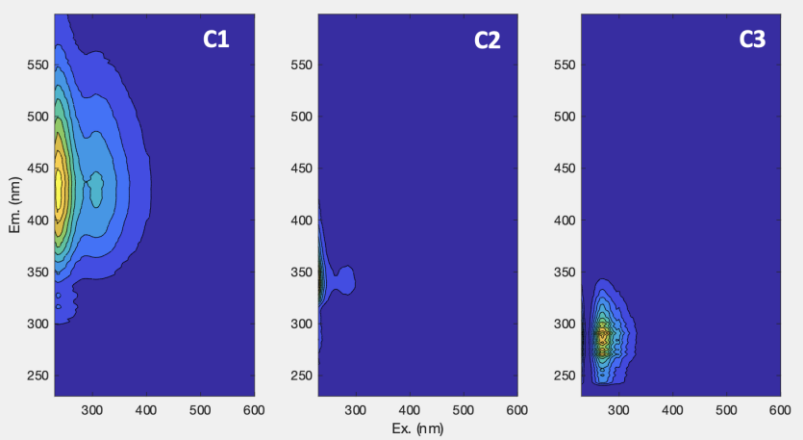

Comp.	Ex:Em (nm)	DOM Type	References
C1	235, 305: 437	Terrestrial humic-like; or microbial DOM reprocessing	(Coble, 1996; Stedmon et al., 2003, 2007; Stedmon and Markager, 2005; Feng et al., 2018; Retelletti Brogi et al., 2018; Dubnick et al., 2020)
C2	230, 285: 341	Protein-like (tryptophan-like)	(Coble et al., 1998; Stedmon et al., 2003; Stedmon and Markager, 2005; Murphy et al., 2008)
C3	270: 284, 290	Protein-like (tyrosine-like)	(Stedmon et al., 2003; Shakil et al., 2020; Williams et al., 2021)

To assess the composition of fluorescent DOM among the supraglacial, ice-marginal, and subglacial environments, we compared the unnormalized (Figure 4A) and normalized (Figure 4B) maximum fluorescence intensities (F_{max}) of C1, C2, and C3 in each sample. Fluorescent DOM composition did not differ significantly between basal ice and channel water (pairwise PERMANOVA, p = 0.084, α = 0.05), but there were still notable variations in DOM character among the three glacial environments. Supraglacial ice and basal ice had higher protein-like C2 and C3 fluorescence than channel waters (Figure 4A). Humic-like C1 fluorescence was higher in channel waters compared to supraglacial ice and basal ice (Figure 4A, 4B). Examining the normalized F_{max} revealed that protein-like C2 and C3 fluorescence represented over 50% of the total fluorescence intensities across all three glacial environments (Figure 4B)

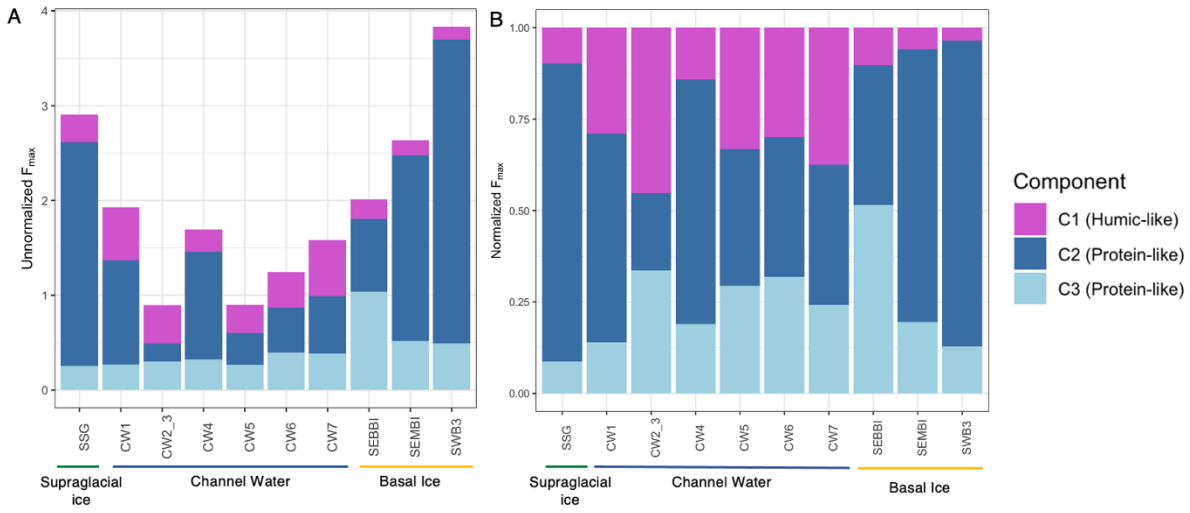

Figure 4. Distribution of the (A) unnormalized and (B) normalized maximum fluorescence (F_{max}) of the three DOM components, humic-like C1 and protein-like C2 and C3, modeled via PARAFAC analysis from the fluorescence signals measured in supraglacial ice, channel waters, and basal ice samples (n = 10).

To quantify DOM characteristics such as aromaticity, lability, and potential sources in each glacial environment, absorbance and fluorescence indices were calculated at specific excitation and emission wavelengths (Table 5). The specific ultraviolet absorbance (SUVA) at wavelengths 254 nm ($SUVA_{254}$) and 280 nm ($SUVA_{280}$), and the slope ratio (S_R) are used as indicators of DOM aromaticity (Hansen et al., 2016). Higher values for these indices were measured in channel waters compared to the supraglacial ice and basal ice (Table 5), indicating a greater amount of aromatic content in the ice-marginal pond DOM. Ratios of the fluorescent peaks A:T, C:A, and C:T are broadly associated with DOM lability (Hansen et al., 2016) and showed more humic-like and recalcitrant DOM in channel waters than supraglacial ice and basal ice (Table 5). High values for the fluorescence index (FI) (e.g., > ~1.4) generally indicate greater contributions of microbial sources compared to terrestrial sources to the DOM pool (McKnight et al., 2001; Cory and McKnight, 2005). FI values for supraglacial ice and basal ice were higher than that of channel waters (Table 5). Finally, high values of the biological index (BI > 0.7) can indicate recent biological production of DOM in glacial environments (Feng et al., 2018, 2020). A BI > 1 measured in all glacial environments Table 5) supports the significant role of in-situ microbial metabolism in shaping fluorescent DOM pools across different glacial environments.

Table 5. Mean values for DOM absorbance and fluorescence indices measured for each glacial environment (supraglacial ice, channel waters, and basal ice), reported to 1σ where $n > 1$. The indices were derived from intensities measured at specific excitation or/and emission wavelengths as summarized by Hansen et al (2016). The '-' indicates that no value was obtained for that environment.

Absorbance measurements (Units)	**Interpretation**	**Supraglacial Ice (n = 1)**	**Channel Waters (n = 6)**	**Basal Ice (n = 3)**
Specific ultraviolet absorbance at 254 nm, $SUVA_{254}$ ($L\ mg.C^{-1}\ m^{-1}$)	Aromaticity index. A higher value indicates greater aromatic content	0.86	2.45 ± 0.9	1.17 ± 0.1
Specific ultraviolet absorbance at 280 nm, $SUVA_{280}$ ($L\ mg.C^{-1}\ m^{-1}$)	Aromaticity index. A higher value indicates greater aromatic content	0.54	1.62 ± 0.65	0.84 ± 0.01
Spectral slope ratio, S_R	High S values relate to low molecular weight or reduced aromaticity	-	0.57 ± 0.17	1.61 ± 0.19
Fluorescence measurements (Units)	**Interpretation**	**Supraglacial Ice (n = 1)**	**Channel Waters (n = 6)**	**Basal Ice (n = 3)**
Peak ratio A:T	Relative amount of humic-like (recalcitrant) to fresh-like (labile) fluorescence	0.47	1.52 ± 0.52	0.32 ± 0.09
Peak ratio C:A	Relative amount of humic-like to fulvic-like fluorescence	0.41	0.54 ± 0.07	0.41 ± 0.05
Peak ratio C:T	Relative amount of humic-like (recalcitrant) to fresh-like (labile) fluorescence	0.19	0.83 ± 0.28	0.13 ± 0.05
Fluorescence index, FI	Relative contributions of microbial to terrestrial sources. Higher values indicate microbial sources	1.79	1.31 ± 0.3	1.77 ± 0.49
Biological index, BI	Indicator of autochthonous DOM production	1.3	1.88 ± 0.73	1.57 ± 0.17

Ultrahigh-resolution mass spectrometry via FT-ICR-MS allowed us to characterize DOM chemical diversity at the molecular level. This technique can detect molecular masses (mass to charge ratio; *m/z* peak) of largely intact, polar organic compounds up to an accuracy of < 1 ppm in a sample. At low molecular masses (< 1000), molecular formulae can be assigned to these *m/z* peaks using computational algorithms based on the highly accurate masses of the resolved peaks (Kujawinski, 2002; Koch et al., 2007; Kujawinski and Behn, 2006; Merder et al., 2020). In this

study, a total of 917 *m/z* peaks were resolved, with 865 *m/z* peaks observed in all channel waters samples and 346 *m/z* peaks in all basal ice samples and with the proportions of peaks containing specific heteroatoms (O, N, S) similar between the two glacial environments (Table 6, top). The supraglacial ice demonstrated an extremely low number of peaks (18 *m/z* peaks), inconsistent with previous molecular DOM studies in supraglacial environments (Bhatia et al., 2010; Stubbins et al., 2012; Antony et al., 2017; Feng et al., 2020; Kellerman et al., 2021). As a result, supraglacial molecular DOM data was excluded from any further analysis.

Table 6. Proportions (in percent) of CHO peaks, CHON peaks, and CHOS peaks from the total number of peaks measured in all channel waters and all basal ice (top); and averaged proportion of protein-like, terrestrial-like, lignin-like, and carbohydrate-like DOM peaks from each sample associated with a glacial environment (channel waters and basal ice) (bottom). Sample number is denoted by *n,* and the average values for DOM type peaks are reported to 1σ for the bottom table.

Molecular Formulae	**Channel Waters (*n* = 6)**	**Basal Ice (*n* = 4)**
Total	865	346
% CHO	100	100
% CHON	25.4	24.2
% CHOS	10.9	10.7
DOM Type	**Channel Waters (*n* = 6)**	**Basal Ice (*n* = 4)**
% Protein-like	16.0 ± 7.1	29.2 ± 4.0
% SRFA Terrestrial-like	31.9 ± 10.0	22.4 ± 12.4
% Lignin-like	20.2 ± 2.3	17.5 ± 9.7
% Carbohydrate-like	1.1 ± 0.5	3.1 ± 2.3

Unlike in the fluorescent DOM fraction, using FT-ICR MS, we observed distinct molecular DOM composition between channel waters and basal ice (pairwise PERMANOVA, $p = 0.042$, $\alpha = 0.05$), whose respective samples clustered within 95% confidence intervals on an NMDS plot (Figure 5A). O:C and H:C elemental ratios, derived from the molecular formulae, were visualized on a Van-Krevalan plot (Kim et al., 2003). Van Krevalan plots enable the visualization of all *m/z* peaks present in a sample and facilitate structural comparisons with major biomolecular classes that have established ranges of H:C and O:C ratios in the literature (Kim et al., 2003). Overall, channel waters exhibited a higher number of *m/z* peaks across the terrestrial-like (demarked by a Suwannee River Fulvic Acid (SFRA) standard, see *Methods*), lignin-like, protein-like, and carbohydrate-like biomolecular classes compared to basal ice (Figure 5B). However, proportionally, basal ice showed higher fractions of protein- and carbohydrate-like DOM, whereas

channel waters demonstrated higher fractions of SRFA terrestrial- and lignin-like DOM (Table 6; bottom).

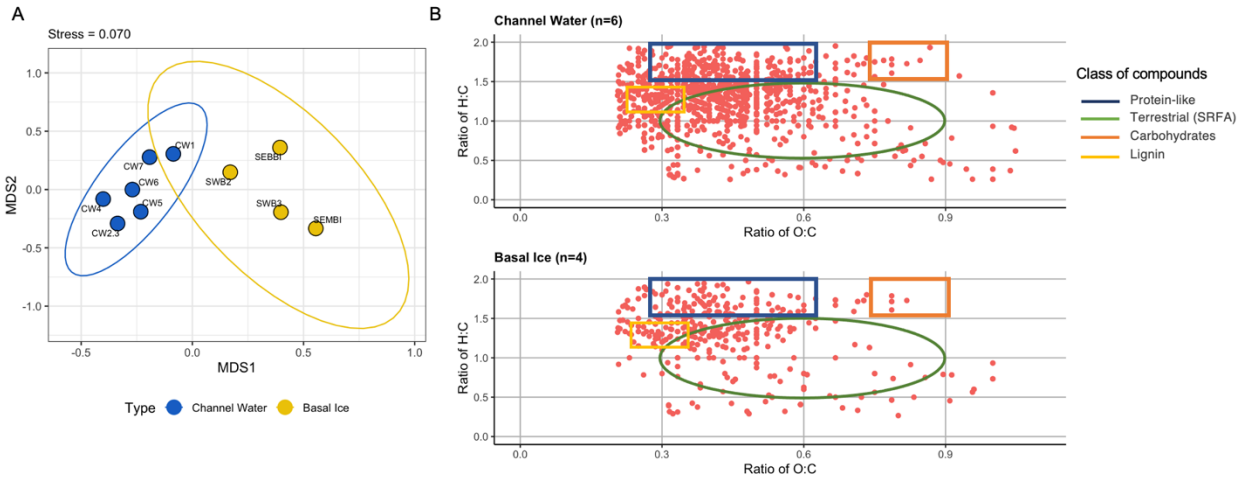

Figure 5. (A) Non-metric multidimensional scaling (NMDS) analysis of the *m/z* peaks (with raw peak intensities) resolved in glacial DOM at the molecular level using FT-ICR-MS. Molecular DOM composition in the channel waters (blue) and basal ice (yellow) were significantly different ($p = 0.042$, $\alpha = 0.05$, PAIRWISE permanova) and clustered separately within the correspondingly colored ellipses representing 95% confidence intervals. (B) Van Krevalan plots of H:C and O:C ratios derived from molecular formulae associated with the resolved *m/z* peaks (red dots) detected in channel waters (top) and basal ice (bottom). The major biomolecular classes of organic compounds are demarked by the colored circle and boxes: protein-like (blue box), terrestrial-like from the Suwanee River Fulvic Acid (SRFA) standard (green circle), lignin-like (yellow box), and carbohydrate-like (orange box). The *n* denotes the number of samples.

To identify characteristic *m/z* peaks for each glacial environment, an indicator species analysis (ISA) was conducted on the FT ICR-MS dataset, following previous studies (Kujawinski et al., 2009; Bhatia et al., 2010). In ISA, a perfect "indicator" for any particular environment is exclusive to and universally present (high fidelity) in all samples from that environment (Dufrêne and Legendre, 1997). Here, an *m/z* peak was defined to be a significant molecular DOM indicator if it had an indicator value (IV) ≥ 0.7 and a *p*-value ≤ 0.05 (as determined by Monte Carlo tests, see *Methods*). For the channel waters, 10 *m/z* peaks were identified as "indicators". Eight of the channel water indicators were associated with the terrestrial-like biomolecular class, one with the protein-like class and one with the lignin class (Figure 6B). In basal ice, only three indicator peaks were identified with their distribution scattered across the Van-Krevalan space (Figure 6B).

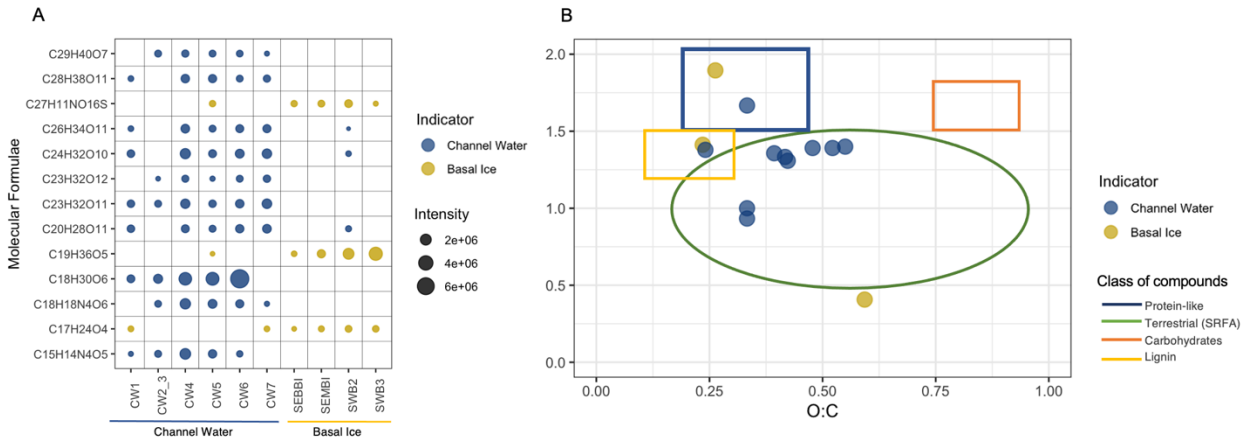

Figure 6. (A) Molecular formulae of significant indicator *m/z* peaks (IV ≥ 0.7 and *p*-value ≤ 0.05) for channel waters (blue) and basal ice (yellow) and their peak intensities across glacial sites. (B) O:C and H:C ratios of indicator peaks in A, displayed on a Van Krevalan plot with major biomolecular organic compound classes as described in Figure 5B.

3.4. Correlations between microbial habitats and DOM and solute pools

Correlations between microbial assemblages and the in-situ environmental parameters (e.g., DOM properties, and solute and carbon concentrations, etc) were used to assess the factors that most influenced the microbial community structure in the different glacial ecosystems. Comparing the correlation results from diverse glacial environments also aided our exploration of variations in glacial biogeochemical interactions among the supraglacial, ice-marginal, and subglacial ecosystems. To implement this analysis, the most abundant or 'top' ASVs in our dataset, defined as those whose total reads across all samples were > 0.5 % of the total reads from the community, were identified. A total of 24 ASVs met this 'top' criterion and were chosen to correlate with the in-situ environmental parameters using Spearman's rank correlation coefficient. Only significant correlations ($p \leq 0.05$) are displayed (Figure 7).

The top ASVs in basal ice were also present in supraglacial ice and some channel waters, including the families *Spirosomaceae, Flavobacteriaceae,* and *NS11-12 marine group* (phylum: Bacteriodetes), *Hydrogenophilaceae* (Thaurmarcheaota), *Hydrogenophilaceae* (Proteobacteria), and *Pirellulaceae* (Planctomycetes) (Figure 7). Channel waters also possessed ASVs that occurred exclusively in the ice-marginal pond, such as from the families *Illumatobacteraceae, Chitinophageaceae, Burkholderiaceae* (ASV 13), and *Nitrospiraceae* (Figure 7). An indicator species analysis was separately run for the entire microbial community matrix with significant microbial indicators (bioindicators) selected if they met the thresholds of IV ≥ 0.7 and *p*-values ≤

0.05. Significant bioindicators that also appeared among the 24 'top' ASVs are marked in Figure 7. Seven of these top 24 ASVs were indicator species for channel waters, occurring in the families *Sporichthyaceae*, *Illumatobacteraceae* (phylum: Actinobacteria), *Chitinophagaceae* (Bacteriodetes), *Nitrospiraceae* (Nitrospirae), *Gemmataceae* and *Pirellullaceae* (Planctomycetes), and *Burkholderiaceae* (Proteobacteria), and three were for basal ice from the families *Hydrogenophilaceae* and *Rhodobacteraceae* (Proteobacteria) and *Nitrospumilaceae* (Thaumarcheaota) (Figure 7).

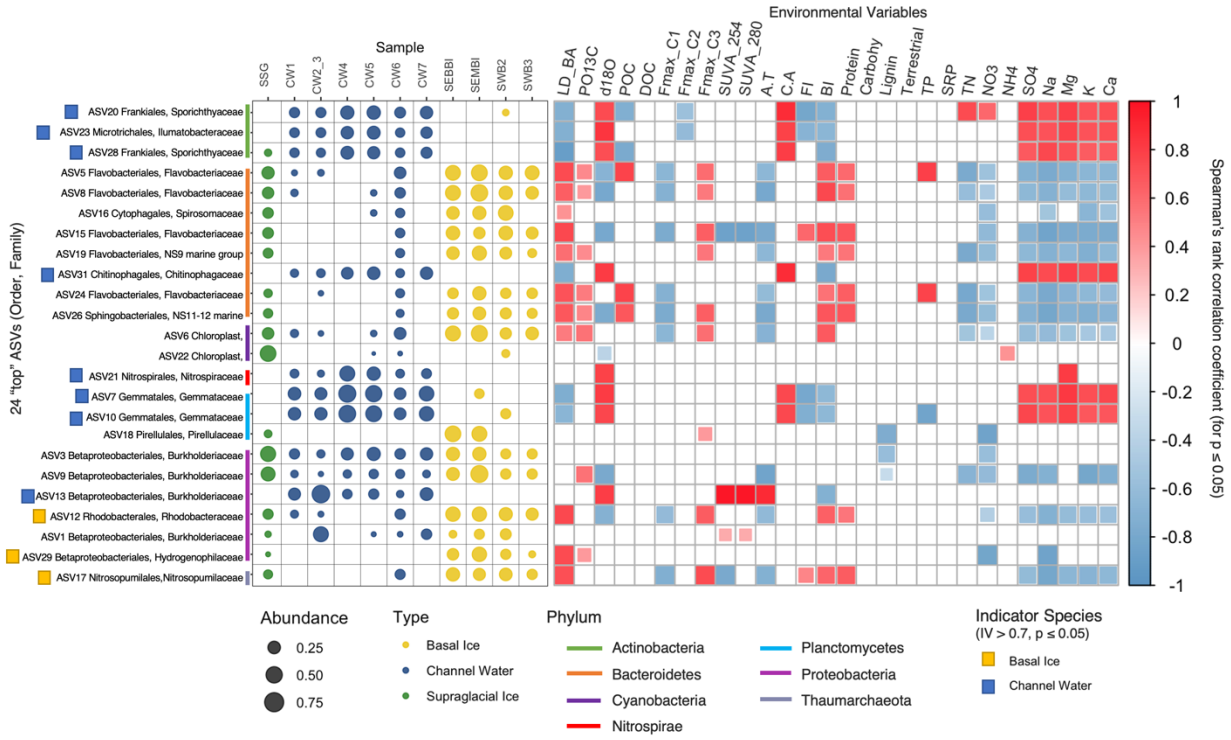

Figure 7. Hellinger-transformed abundances (left bubble plot) of the top 24 ASVs (with total sample reads > 0.5% of the total community reads) in supraglacial ice (green), channel water (blue) and basal ice (yellow) and their Spearman's rank correlation coefficients (right correlation matrix) with measured environmental variables (LD_BA = live/dead bacterial abundance, F_{max}_C1 to F_{max}_C3 = normalized component fluorescence, protein/lignin/carbohy/terrestrial = proportion of DOM peak per sample). In the bubble plot (left), ASVs which are significant bioindicators (IV ≥ 0.7, p-value ≤ 0.05) for specific glacial environments are demarked accordingly. In the correlation matrix (right), a red square indicates a positive correlation, and a blue square indicates a negative correlation. The bigger and darker the square, the stronger the correlation between an ASV and an environmental variable.

The 'top' ASVs that were most abundant and prevalent in the supraglacial ice and basal ice, including the bioindicators for basal ice, correlated positively with live/dead bacterial abundances (LD_BA), $PO^{13}C$, the fluorescent protein-like component C3, the biological index (BI), the fluorescence index (FI), and the fraction of protein-like molecular DOM. These ASVs

also correlated negatively with the fluorescent humic-like component C1, the fluorescent index peak ratio A:T (where a higher value indicates lower lability), and TN, NO_3^-, SO_4^{2-}, Na, Mg, K, Ca concentrations. On the other hand, the top ASVs most abundant and prevalent in channel waters correlated negatively with LD_BA, the fluorescent protein-like C2 component, BI and FI, while correlating positively with SO_4^{2-}, Na, Mg, K, Ca concentrations, and the fluorescent index peak ratio C:A (where a higher value indicates lower lability).

3.5. Changes in microbial growth and diversity, and DOC in melted basal ice incubations

Microbial communities in melted debris-rich and debris-poor basal ice were incubated with in-situ carbon (i.e., unamended incubations) over 120 days to assess microbial carbon uptake and how the community structure shifts due to this uptake. Live cell counts were used to track microbial growth in incubations over the 120-day incubation period. Compared to the debris-poor incubation, the debris-rich microbial community experienced rapid initial growth followed by a steady decline in growth and underwent extensive cell death by the end of the incubation period (T_f). The debris-poor community grew comparatively slowly at the start (up to ~ Day 20) and then showed steady growth until the final time point (Figure 8A). DOC concentrations were measured at the beginning and end of the experiment to monitor heterotrophic carbon consumption, with the DOC pool in the debris-rich incubation being almost exhausted at T_f, whereas a smaller amount of DOC (~0.1 ppm) was consumed in the debris-poor set-up (Figure 8B).

Microbial community and functional (obtained from the taxonomic data via the FAPROTAX pipeline) compositions measured at the start (T_0) and end (T_f) of the experiment showed different changes in diversity between the two incubations over the 120 days. Alpha diversity metrics, such as the Shannon Index, can be used to quantify changes in microbial diversity in an environment with a more positive number indicating greater diversity (considering both species richness and abundance) of microbial species in the community. The debris-rich microbial community showed a small increase in alpha diversity (5.2 at T_0 to 6.7 at T_f) whereas the debris-poor community experienced a larger decrease in alpha diversity (6.2 at T_0 to 3.6 at T_f), signifying a larger loss of microbial diversity in the latter. These changes in alpha diversity are reflected in stacked bar plots of the most abundant (top 20) microbial families present at T_0 and T_f in each incubation (Figure 9). In the debris-rich incubation, most families are retained at the final time point, with some changes to their relative abundances (Figure 9A). We also see the growth

of some new families, such as *Caulobacteriaceae, Saprospiraceae, and Gemmataceae*, by T_f, which were not initially abundant (Figure 10A). The growth of these families may have contributed to the small increase in alpha-diversity values in the debris-rich incubation. On the other hand, most families in the debris-poor incubation were overshadowed by the growth of *Burkholderiaceae and Microbacteriaceae* at T_f (Figure 9B), leading to the observed decrease in alpha-diversity value. These microbial diversity changes also impacted the functional potential composition in the two incubations. The abundance of chemoheterotrophy increased two-fold at T_f in the debris-rich incubation (Figure 10A), suggesting that microbes capable of this metabolic function were actively growing and consuming the DOC. Meanwhile, in the debris-poor incubation, the abundance of chemoheterotrophy decreased and many functions were lost (Figure 10B), reflecting the diversity loss seen at the taxonomic level.

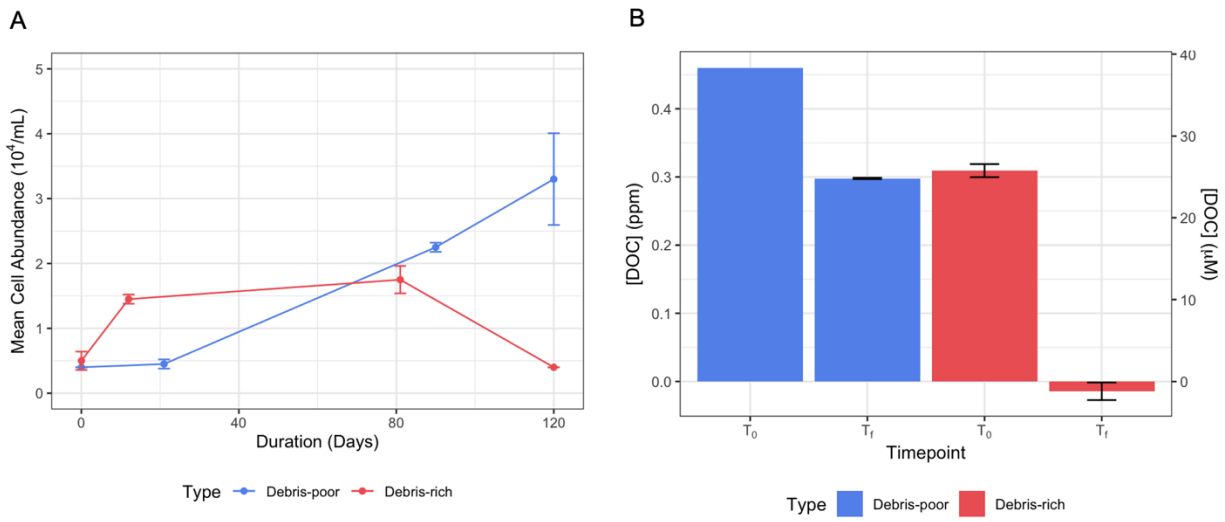

Figure 8. (A) Bacterial growth (live only cell counts) and (B) the change in DOC concentration (reported to 1σ when duplicate DOC measurements were taken) in incubations of melted debris-poor (purple) and debris-rich (red) basal ice microbial communities with their in-situ carbon pool over 120 days. T_0 and T_f indicate the start and end of the incubation period respectively.

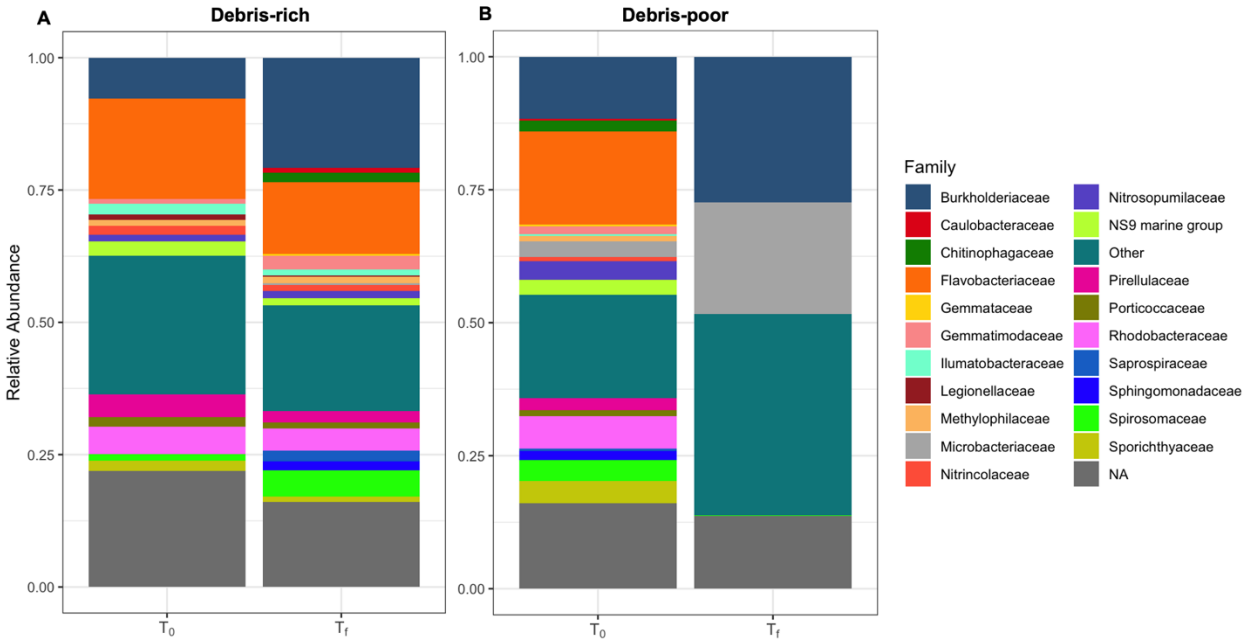

Figure 9. Comparison of microbial diversity using the most abundant microbial families (top 20) and their relative abundances in incubations of melted (A) debris-rich and (B) debris-poor basal ice with in-situ carbon at the start (T_0) and end (T_f) of the 120-day incubation period. 'NA' refers to taxa unresolved at the family rank and higher, and 'Other' indicates resolved taxa that were less abundant than the top 20 families.

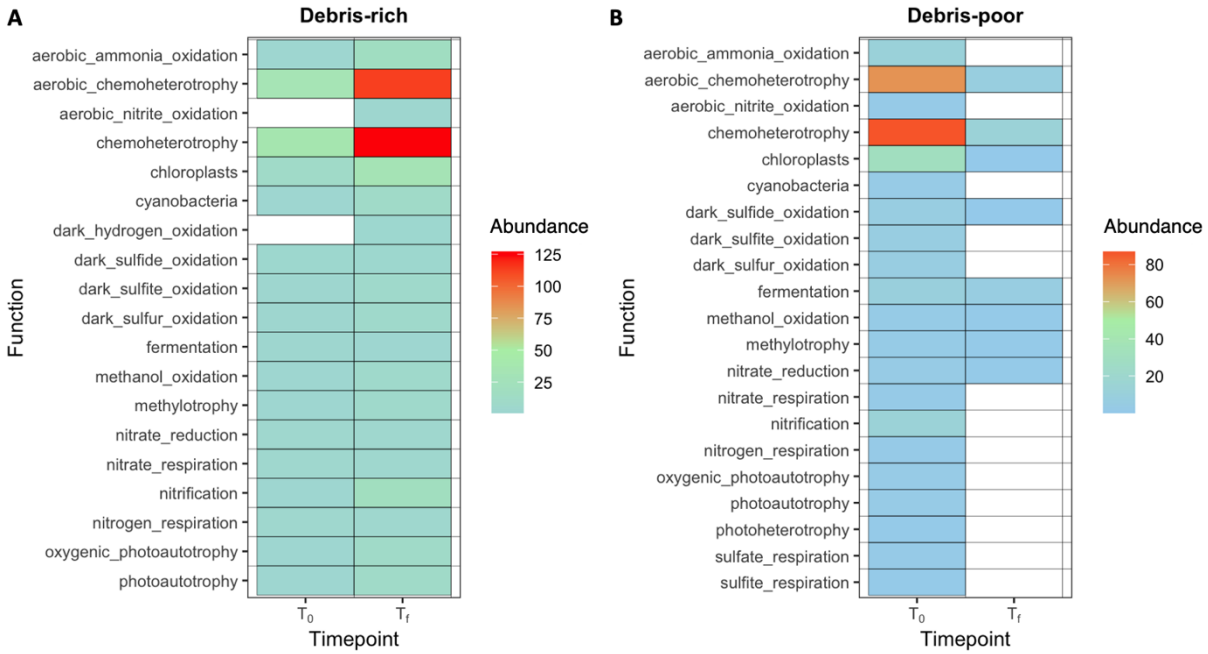

Figure 10. Comparison of metabolic functions (derived from taxonomic data via the FAPROTAX pipeline, Louca et al., 2016 as explained in Figure 3) and their abundances in incubations of melted (A) debris-rich and (B) debris-poor basal ice microbial communities with in-situ carbon at the start (T_0) and end (T_f) of the 120-day incubation period. The abundance of each function represents the sum of abundances of the ASVs associated with the function by the FAPROTAX pipeline.

4. Discussion

4.1. Physical processes shaping the ice and meltwater matrix in glacial environments

The hydrochemical properties of ice and meltwaters showed contrasting solute and organic carbon concentrations among supraglacial ice, basal ice, and channel waters likely shaped by different physical processes occurring in these environments. Direct bedrock contact at the glacier bed differentiates the subglacial environment from the glacier surface. Subglacial debris is produced during frictional interactions between the glacier and the bedrock and gets incorporated into the basal ice matrix during its formation. The debris includes ground sediments (Hodson and Ferguson, 1999; Delaney and Adhikari, 2020), crustal solutes produced from chemical weathering of comminuted minerals (carbonates, silicates, pyrite, apatite) (Tranter et al., 2002; Hodson et al., 2004) and organic matter from previously overridden soil and vegetation (Barker et al., 2010; Bhatia et al., 2010; Dubnick et al., 2020; Kellerman et al., 2020, 2021). Here, the TSS load, a proxy for debris concentration, was highest in basal ice, supporting a bedrock source for this sediment (Table 2). The TSS load was unsurprisingly highly variable among the basal ice samples, reflecting the spatial heterogeneity in debris distribution in basal ice (Montross and Skidmore, 2006; Hubbard et al., 2009). This heterogeneity arises from the different physical mechanisms responsible for basal ice formation, which include (1) supercooling, where supercooled subglacial meltwater flowing across a steep bed steep slope freezes, capturing debris in the ice matrix during its growth (Lawson et al., 1998); (2) regelation, where frictional heat from ice flowing around a bedrock obstacle melts the ice which subsequently refreezes, incorporating debris within the ice (Hubbard and Sharp, 1993); and (3) structural and tectonic deformation such as folding, shearing, and metamorphism of existing subglacial ice that entrain sediments in basal ice (Hubbard and Sharp, 1989; Knight, 1997; Iizuka et al., 2001). The combination of these mechanisms coupled with the variable availability of eroded basal debris ultimately leads to heterogeneous debris incorporation as basal ice forms, with concentrations ranging from < 1 g/L to >1 kg/L (Skidmore et al., 2000; Hubbard et al., 2009; Montross et al., 2014).

This wide range in suspended sediment concentrations drives large (up to two orders of magnitude) variations in solutes (e.g., SO_4), and DOC concentrations in basal ice (Bhatia et al., 2006; Montross et al., 2014; Hood et al., 2015). Thus, the variable TSS loads observed here explains the high variability in the TP, DOC, and POC concentrations in our basal ice samples (Table 2). High mean concentrations of crustal solutes (SO_4 = 0.627 ppm, Na = 1 ppm, K = 353

ppb, Mg = 535 ppb) have also been recorded in basal ice from Sverdrup Glacier and other larger tidewater polythermal glaciers (Belcher, East 7) draining the Devon Ice Cap (Dubnick et al., 2020). Our measurements for the same solutes at Sverdrup Glacier were lower compared to this past study (Table 2), except for SO_4 (0.61 ppm). Sverdrup Glacier flows more slowly (< 50 m a^{-1}) than other glaciers draining Devon Ice Cap (e.g., Belcher (180 – 300 m a^{-1}) and East 7 (80 – 100 m a^{-1}) Glaciers) (Burgess et al., 2005; Wychen et al., 2017). These differential velocities suggest higher subglacial erosion rates and solute production at the larger, faster Belcher and East 7 Glaciers (Boulton, 1979; Waller, 2001; Koppes et al., 2015) compared to Sverdrup Glacier, which may shape the higher mean subglacial solute concentrations measured by Dubnick et al (2020) at these sites compared to the lower solute concentrations measured in this study at Sverdrup Glacier.

In contrast to the subglacial ecosystem, supraglacial debris is limited to atmospherically deposited dust, soot, and aerosols, which can arise from transport of soil and crustal sediments from surrounding deglaciated areas; loose particles and soots from anthropogenic pollution and fossil fuel burning (Stibal et al., 2010; Stubbins et al., 2012; Feng et al., 2018); and/or sea-salt aerosols from oceans and sea ice (Wagenbach et al., 1998; Rankin et al., 2000; Fischer et al., 2007). Measured sediment loads from snow (0.9 – 3 mg/L, Eastern China) (Dong et al., 2009), Greenland surface ice (0.01 – 2 mg/L) and supraglacial streams (0.01 – 0.24 g/L (Lister, 1981) illustrate that atmospheric deposition is a low sediment source to the glacier surface, supporting the negligible supraglacial TSS load measured here (Table 2). However, supraglacial debris remains a key source of life-sustaining solutes. Supraglacial Ca, Mg, and Na (Dong et al., 2009; Price et al., 2009) and bioavailable phosphorus (Hodson et al., 2005; McCutcheon et al., 2021) can be deposited on the glacier surface in windblown mineral dust, sea salt, and sediments, while fixed nitrogen species like NO_3 and NH_4 are derived from atmospheric aerosols that precipitate with snowfall onto glacier surfaces (Hodson et al., 2005; Boyd et al., 2011; Wolff, 2013). On the Devon Ice Cap, Dubnick et al (2020) previously reported low solute (Cl = 0.1 ppm, SO_4 = 0.12 ppm, Na = 70 ppb, K = 13 ppb, Ca = 92 ppb, Mg = 34 ppb, Si = 40 ppb) and phosphorus (SRP = 31 ppb) concentrations in surface ice. At Sverdrup Glacier, Williams et al (2021) also observed low NO_3 (13 ppb), NH_4 (25 ppb), SRP (3 ppb) and negligible Si concentrations in surface ice. The solute concentrations from both of these studies match our measurements in the supraglacial ice (Table 2) except for higher Cl (0.17 ppm) and Na (144 ppb), which may be enriched at different times due to changing atmospheric sea-salt deposition patterns (Fischer et al., 2007). In general, our results support

bedrock interactions at the glacier bed as a more significant source of sediments and solutes to glacial systems than atmospheric deposition at the surface, a finding that is common to many glaciers (Skidmore et al., 2000; Bhatia et al., 2006; Dubnick et al., 2020).

The marginal channel waters may represent a unique ecosystem that is neither in direct contact with the atmosphere nor the bedrock (Dubnick, 2018), which is formed annually when surface meltwaters transit ice-marginally. At Sverdrup Glacier, ice-marginal drainage predominates (Koerner et al., 1961; Boon et al., 2010), although, the presence of some moulins (Boon et al., 2010) and increasing ice flow rates during summer (Cress and Wyness, 1961) suggests that some meltwaters may drain englacially to the bed and facilitate a seasonal glacier acceleration. The channel waters were collected from an ice-marginal pond that likely originated as late-season supraglacial runoff that was stored overwinter (Dubnick, 2018). Our current hypothesis is that the water remained liquid in the pond due to its proximity to a subglacial geothermal heat source (Dubnick, 2018). In the ice-marginal channel waters, solute concentrations of SRP, TN, NO_3, NO_2, SO_4, Si, Cl, Na, K, Mg, and Ca were up to 100-fold higher than both the supraglacial ice and basal ice (Table 2). The ice lenses observed inside the pond suggest that it may be analogous to ice-covered glacial lakes, where cryo-concentration can impact solute concentrations (Belzile et al., 2002; Santibáñez et al., 2019). In the winter, as the pond water freezes, solutes may be extruded out of the ice matrix and concentrate in the water column (Killawee et al., 1998). Laboratory experiments freezing freshwater from ice-covered Antarctic and Alaska lakes to simulate ice formation have shown solutes (such as Mg, K, Na, Ca, SO_4) cryo-concentrating in the water column (Belzile et al., 2002; Santibáñez et al., 2019). These findings support our hypothesis that cryo-concentration likely causes the high solute concentrations observed in the ice-marginal pond, raising these concentrations to levels that even bedrock inputs to basal ice cannot provide (Table 2). To confirm these hypotheses in the future, solute measurements from ice in the pond or the channel floor/walls could be used to constrain the cryo-concentration effects (Belzile et al., 2002; Santibáñez et al., 2019)

The distinct solute pools in the supraglacial, ice-marginal, and subglacial environments provide the necessary inorganic nutrients required to support in situ microbial life. However, microbial communities in different glacial environments have differential access to these essential inorganic nutrients that may limit their activity due to varying solute compositions in these environments. For instance, nutrients such as NO_3 and PO_4 are used in cellular growth. Glacier

surfaces can be P-limited as PO_4 is mainly bedrock-derived, as measured in basal ice but not in supraglacial ice (Table 2) (Stibal et al., 2009; McCutcheon et al., 2021). Meanwhile, the glacier base and margins may obtain NO_3 deposited at the glacier surface during supraglacial meltwater drainage or through nitrification of atmospheric NH_4 (Wynn et al., 2007). The higher supraglacial NH_4 concentration here supports the surface as a source of inorganic nitrogen to the glacier base and margins (Table 2). Past correlations between microbial communities in subglacial channels and proglacial waters with in-situ hydrochemical properties further showed that factors like sediment, nutrient, and ion concentrations can drive significant variations in microbial community structure (Dubnick et al., 2017; Sułowicz et al., 2020). The supraglacial and subglacial ecosystems may expectedly have distinct communities (Bhatia et al., 2006; Dubnick et al., 2020) mainly driven by differences in light availability. In contrast, both the ice-marginal and subglacial environments are dark systems, but the considerable disparities in measured solute concentrations may lead to different resident microbial communities.

4.2. Variations in glacial microbial habitats

Numerous studies over the past two decades have shown that supraglacial (Stibal et al., 2015; Antony et al., 2017; Nicholes et al., 2019), subglacial (Sharp et al., 1999; Skidmore et al., 2000; Yde et al., 2010; Montross et al., 2014), and proglacial environments (Dubnick et al., 2017) contain viable and metabolically active microbial life, despite the cold, oligotrophic conditions in glacial systems. Microbial cells are inoculated onto glacier surfaces via atmospheric dust and bioaerosol (cells, cellular fragments) deposition (Xiang et al., 2009; Stibal et al., 2015; Weisleitner et al., 2019). Supraglacial total cellular densities can be variable: ~ 10^3 cells/mL in snow (Nicholes et al., 2019), between 10^6 – 10^9 cells/mL in cryoconite holes (Anesio et al., 2010; Sanyal et al., 2018), and between 10^3 – 10^4 cells/mL in surface ice (Stibal et al., 2015; Nicholes et al., 2019). Here, we measured 5.5 x 10^3 cells/mL in supraglacial ice from Sverdrup glacier, with live counts consisting of 73% of the total counts (Table 2). At the glacier base, microbial cells from the bedrock and overridden soil are entrained with debris into the basal ice matrix during its formation, leading to variable cellular abundances of between 10^2 – 10^8 cells/mL (Yde et al., 2010; Montross et al., 2014). Total and live cell densities in basal ice here were 6.7 x 10^4 cells/mL and 3.3 x 10^3 cells/mL (4% of the total count) respectively (Table 2). Greater amounts of debris can indicate a higher number of cells in basal ice, particularly when considering large basal ice debris

concentration differences (up to four orders of magnitude; 0.001 – 14 g/L) (Montross et al., 2014). The basal ice TSS values in this study were low (0.01 to 8 g/L) with less variability compared to literature values (Montross et al., 2014), perhaps explaining the lower total and live cell counts found here. In the marginal channel waters, cellular densities were 5.3 x 10^3 cells/mL, with 43% representing live cells, which may be underestimated due to cryo-concentration effects. In contrast to solute extrusion to the water column during laboratory simulations of lake ice cover formation, bacterial cells (particularly free cells) were preferentially incorporated into the ice matrix (Santibáñez et al., 2019). Generally, the cellular densities in the supraglacial, subglacial, and ice-marginal ecosystems at Sverdrup Glacier are in line with the low values characteristic of glacial systems. Given the cold temperatures and limited liquid water availability to support microbial life before the onset of the melt season, these low cellular densities are unsurprising but do not preclude active microbial ecosystems (Anesio et al., 2010; Christner et al., 2014).

While viable cells are present in the diverse, cold glacial ecosystems, the different physical conditions (e.g., light and oxygen availability) and hydrochemistry of these environments can select for microbial taxa most adapted to the in-situ conditions thus generating distinct microbial habitats (Skidmore et al., 2005; Bhatia et al., 2006; Sułowicz et al., 2020). In this study, molecular sequencing showed that microbial community compositions varied among glacial environments in terms of relative taxa abundance and that subglacial and ice-marginal microbial communities were significantly different. Phyla such as Bacteroidetes, Proteobacteria, Actinobacteria, Cyanobacteria, Firmicutes, Chloroflexi, Verrumicrobiota, and Thaumarchaeota were the most abundant in all three glacial environments (Table 3). These phyla have been detected in diverse glacial systems globally, including Antarctic surface and subglacial lakes (Christner et al., 2014; Weisleitner et al., 2019), basal and surface ice from Canadian High Arctic glaciers (Dubnick et al., 2020), and in supraglacial systems of Svalbard and Greenland Ice Sheet (Edwards et al., 2014; Cameron et al., 2016; Takeuchi et al., 2019). Taxa from Bacteroidetes and Cyanobacteria, which can thrive in the oligotrophic, high light environments, dominated the glacier surface at the Devon Ice Cap (Dubnick et al., 2020). Actinobacteria, Acidobacteria, Proteobacteria, Firmicutes, and Chloroflexi, which could arise from overridden glacial soils (Bajerski and Wagner, 2013; Yang et al., 2016; Zhang et al., 2016), dominated subglacially across the Devon Ice Cap (Dubnick et al., 2020). Results from our study are congruent with this previous work, in that Bacteroidetes and Cyanobacteria dominated in supraglacial ice, while Actinobacteria, Acidobacteria, Proteobacteria,

Firmicutes, and Chloroflexi were comparatively higher in basal ice at Sverdrup Glacier (Table 3). Thaumarchaeota was also highest in basal ice (Table 3), in line with its past detection in Antarctic subglacial lake waters and sediments (Christner et al., 2014). The channel waters were differentiated from basal ice by containing the highest abundances of Actinobacteria and Proteobacteria (Table 3). The communities observed in the channel waters are potentially seeded by a combination by supraglacial inputs and marginal bedrock contact with surface runoff (Dubnick, 2018), as has been observed when supraglacial meltwaters drain through the subglacial system and entrain microbes from subglacial waters and sediments (Dubnick et al., 2017) and also seed surface taxa into subglacial ecosystems (Bhatia et al., 2006).

Since the discovery of subglacial microbial life in 1999 (Sharp et al., 1999), molecular sequencing-based studies have been used to explore glacial microbial communities, but focus almost exclusively on the taxonomic realm (Skidmore et al., 2005; Bhatia et al., 2006; Lanoil et al., 2009; Christner et al., 2014; Dubnick et al., 2020). Though informative about the types of microbes present, taxonomic data cannot provide direct insight into the metabolic pathways driving nutrient and carbon cycling in ecosystems. However, the low microbial biomass characteristic of glacial environments often impede non-amplicon functional analyses (e.g., metagenomics) (Brady and Daniel, 2013). This is because large masses of glacial ice (~ 8 kg) (Simon et al., 2009) or subglacial debris (~ 20 g) (Kayani et al., 2018) are often required to isolate sufficient microbial DNA for metagenomic screenings. These sample requirements are often not attainable from glacial systems, particularly those located in the remote high Arctic, like Sverdrup Glacier. Thus, in such scenarios, amplicon-based pipelines like FAPROTAX (Louca et al., 2016) and PICRUSt2 (Langille et al., 2013; Raes et al., 2021) are useful tools to predict functional potential from taxonomic data derived marker gene analysis (e.g., 16S rRNA) in dilute glacial ecosystems. Previously, these two pipelines have been used in marine systems to examine relationships between bacterial taxonomy and function and to find microbial niches over varying depths and latitudes (Louca et al., 2016; Raes et al., 2021). These pipelines allow us to generate hypotheses about microbial metabolism in an environment and are being extensively applied across various ecosystems. Recently, the PICRUSt2 pipeline was used to examine the microbial metabolic potential in basal ice with varying debris loads, finding predominantly chemolithotrophic metabolisms associated with carbon, nitrogen and sulfur cycling (Toubes-Rodrigo et al., 2021). Past studies have specifically used FAPROTAX to probe microbial

functional diversity to infer biogeochemical processes occurring in aquatic (Louca et al., 2016; Bomberg et al., 2019; Yang et al., 2020) and soil ecosystems (Sansupa et al., 2021). Here, we use the FAPROTAX pipeline to examine the variations in major metabolic pathways of different glacial ecosystems.

Functional information derived from FAPROTAX revealed that despite sharing a wide variety of metabolic pathways, the supraglacial, ice-marginal pond, and subglacial microbial habitats are dominated by functions that are most suited for their dominant in-situ conditions (e.g., sunlit versus dark environments). Metabolic functions associated with chemoheterotrophy, autotrophy, and phototrophy were present at varying abundances in all glacial environments (Figure 3). High light availability at the glacier surface can support photoautotrophy (Takeuchi, 2013; Franzetti et al., 2016; Takeuchi et al., 2019), and photoautotrophic functions were expectedly the most abundant in supraglacial ice (Figure 3) and were derived from photoautotrophic taxa such as cyanobacteria (supraglacial ice = 10%, Table 3). Similarly high abundances of cyanobacteria have been observed in surface ice (mean 16%) on the Devon Ice Cap (Dubnick et al., 2020). High abundances of heterotrophy were also seen in supraglacial ice (Figure 3), indicating the potential for organic matter respiration, which has been previously observed in cryoconite holes (Anesio et al., 2010; Smith et al., 2017).

The absence of light in the ice-marginal pond and subglacial environment leads to chemolithotrophic metabolism being dominant in both systems (Figure 3). Second to light, fluctuating oxygen availability defines both the ice marginal and subglacial regions (Wadham et al., 2004b; Montross et al., 2014; Dubnick, 2018; Gill-Olivas et al., 2021). The subglacial environment likely contains both aerated and anoxic zones (Skidmore et al., 2000; Wadham et al., 2004a). Past studies have shown a wide variety of chemolithotrophic functions in basal ice (Skidmore et al., 2000; Montross et al., 2014; Kayani et al., 2018; Toubes-Rodrigo et al., 2021). Aerobic respiration, measured through CO_2 production, was observed in dark incubations of melted basal ice from high Arctic and Alaskan glaciers (Skidmore et al., 2000; Montross et al., 2014). Anaerobic respiration via nitrate and sulfate reduction was also shown via anoxic incubations of basal ice from John Evans Glacier (Skidmore et al., 2000) and in a metagenomic profile of basal ice from Taylor Glacier, Antarctica (Kayani et al., 2018). Functional genes associated with dark sulfide oxidation were also detected in basal ice in this metagenome analysis (Kayani et al., 2018), which could be coupled with subglacial DOM production via autotrophic

sulfide oxidizers (Boyd et al., 2014). Toubes-Rodrigo et al. (2021), using the PICRUST2 pipeline, reported the potential for chemoheterotrophy, sulfur, and nitrogen metabolism and chemoautotrophy in basal ice from an Icelandic glacier. These findings support the putative metabolic pathways also observed here in basal ice, where we found the highest functional potential for aerobic chemoheterotrophy, nitrate and sulfate reduction likely tied to anaerobic respiration, and dark sulfur oxidation potentially linked to autotrophy (Figure 3).

In contrast to the basal ice, as a continuously aerated system, channel water microbial communities showed an elevated potential for aerobic processes, including aerobic chemoheterotrophy, methanol oxidation, and methylotrophy (Figure 3). Methylotrophic clades have been previously linked to well-aerated subglacial zones at Leverett Glacier (Greenland) (Lamarche-Gagnon et al., 2020), supporting the potential for methylotrophic metabolism in oxygenated channel waters. Chemoautotrophic hydrogen oxidation (Boyd et al., 2014; Dunham et al., 2021; Toubes-Rodrigo et al., 2021) dominated in channel waters compared to basal ice. Autotrophic hydrogenotrophs have been previously observed in subglacial sediments (Boyd et al., 2014; Dunham et al., 2021). The hydrogen (H_2) needed to sustain these chemoautotrophs however likely arises from the chemical weathering of Fe and Si-rich bedrock (Dunham et al., 2021), which is not a likely source in the ice-marginal pond due to a lack of direct contact with the bedrock (Dubnick et al, *in prep*). The relative abundance for dark hydrogen reactions in channel waters were low compared to other functions (e.g., aerobic chemoheterotrophy, methanol oxidation) measured in channel waters (Figure 3), potentially limited by the amount of H_2 in this system.

Interestingly, the functional compositions between basal ice and channel waters, which are both dark glacial environments, were not significantly different, despite the presence of taxonomically distinct microbial community structures. Previous studies have shown that local hydrochemistry can directly impact community structure, for instance, in glacial environments (Skidmore et al., 2005; Smith et al., 2018; Sułowicz et al., 2020). However, whether site-specific microbial communities experiencing similar physical conditions (e.g., in subglacial systems of different glaciers) would also be metabolically different remains unclear due to limited studies of functional potential in glacial systems (Anesio et al., 2017). Based on the FAPROTAX-predicted functional potential, taxonomically distinct communities could be functionally similar in terms of major metabolic pathways (aerobic/anaerobic respiration, chemo/photoautotrophy) in glacial

environments, if in-situ physical conditions such as light and oxygen availability were similar (Eng and Borenstein, 2018; Louca et al., 2018).

However, we should note that, functional information from marker gene-based pipelines should be interpreted with caution, as only a portion of the community (in this study ~30%) is often examined by these analyses (Louca et al., 2016; Sansupa et al., 2021). Moreover, the database used to predict function from taxonomy is largely built from cultured species in literature, and the function(s) associated with a cultured taxa are extrapolated to all cultured and uncultured members of that taxa by FAPROTAX (Louca et al., 2016). Finally, since the putative functional diversity identified here does not imply activity, metatranscriptomic and/or metaproteomic analyses are needed to resolve the active metabolic processes driving biogeochemical cycling in glacial ecosystems. Thus far, in part limited by low microbial biomass, glacial proteomic analyses have focused on specific microbial isolates to study microbial adaptations at the molecular level to cold glacial temperatures (Williams et al., 2011) and climate warming (García-Descalzo et al., 2014). Despite the caveats associated with marker gene-based pipelines, they can be useful for generating hypotheses about the functional potential of glacial systems that can then rbe confirmed by metagenomics analyses. Moreoever, the metabolically diverse microbial communities characterized across Sverdrup Glacier hint at active microbial carbon cycling, where autotrophic taxa can fix inorganic carbon and produce organic matter, which could then be respired into CO_2 by in-situ heterotrophs. This carbon cycling via coupled autotrophy and heterotrophy has been measured in cryoconite holes and supraglacial streams (Anesio et al., 2010; Smith et al., 2017) and in subglacial lake waters (Christner et al., 2014). As these different communities metabolize by consuming and producing organic matter, their activities re-shape the composition of organic matter initially supplied by abiotic mechanisms.

4.3. Physical and microbial contributions to glacial DOM pools

DOM, a complex pool of structurally diverse carbon-based organic compounds, is an important substrate for microbial metabolism. Glaciers represent dilute pools of dissolved organic carbon (DOC) with typical concentration ranges of 0.1 – 2 ppm in surface ice, < 1 ppm in englacial ice and glacier meltwater, and < 2 ppm in basal ice across the Greenland Ice Sheet, Antarctic Ice Sheet, and mountain glaciers in North America and Asia (Barker et al., 2006; Lawson et al., 2014b; Hood et al., 2015). Here, DOC in supraglacial ice (0.48 ppm), channel waters, (0.43 ppm), and

basal ice (2.04 ppm) (Table 2) are in line with these previous concentrations, but higher than recent measurements made on Devon Ice Cap (surface ice = 0.15 ppm and polythermal basal ice = 0.46 ppm) (Dubnick et al., 2020) and also previously at Sverdrup Glacier (surface ice = 0.18 ppm and basal ice = 0.28 ppm) (Williams et al., 2021). Although glacial DOC levels are low compared to other aquatic systems like rivers (0.8 – 7 ppm) (Riedel et al., 2016), recent work has shown that glaciers export a unique type of DOM that is distinct from riverine DOM (Hood et al., 2009; Stubbins et al., 2012; Riedel et al., 2016; Kellerman et al., 2021). DOM in rivers draining unglaciated areas is often dominated by a terrestrial or humic-like signature derived from degraded plant and soil organic matter (Stedmon and Markager, 2005; Hood et al., 2009). Comparing watersheds with varied glacier coverage in Alaska, Hood et al (2009) showed that the glacier-fed rivers contained more protein-like DOM derived from in-situ microbial activity than non-glacial rivers where terrestrial/lignin-like DOM predominated. The high protein-like fractions in glacial DOM also made it more bioavailable (i.e., readily consumed) to downstream microbial communities than non-glacial DOM (Hood et al., 2009), supporting glaciers as a dominant source of microbially-derived, labile DOM (Lawson et al., 2014b; Smith et al., 2017; Fegel et al., 2019).

Studies of DOM using fluorescence spectroscopy on a diverse group of sample types (snow, surface melt, englacial ice, and basal ice) collected from Antarctic, Arctic and Norwegian glaciers reveal that it is largely proteinaceous (between 50% – 90%) and therefore labile (Barker et al., 2006; Dubnick et al., 2010; Feng et al., 2018; Smith et al., 2018; Williams et al., 2021). Previously, > 40% of proteinaceous DOM was also measured in a variety of glacial samples specifically on the Devon Ice Cap (Dubnick et al., 2020) and at Sverdrup Glacier (Williams et al., 2021), including surface ice, snow, supraglacial meltwaters, glacier ice and basal ice. In this study we also observed large fractions of proteinaceous (C2 and C3) fluorescent DOM (> 50%) in the supraglacial, ice-marginal pond, and subglacial environments at Sverdrup Glacier (Figure 4B). The protein-like C3 component was also observed by Williams et al (2021), and all three components in this study closely match those found by Dubnick et al (2020). The tryptophan-like C2 fluorescence has been tied to autochthonous microbial DOM production in past studies focused on marine (Coble et al., 1998; Stedmon and Markager, 2005), estuarian (Stedmon et al., 2003), and freshwater environments (Elliott et al., 2006; Dubnick et al., 2020). This component thus points to large microbial autotrophic contributions to glacial fluorescent DOM composition, especially in the basal ice and supraglacial ice (Figure 4). Additional evidence bolstering this

hypothesis is the high BI values (> 0.7) in all three environments (Table 5), also indicative of autochthonous microbial DOM production (Feng et al., 2018, 2020). In sum, the proteinaceous fractions from C2 and C3 may be inferred to be labile. Previously, the tyrosine-like C3 was found to be a direct indicator for DOM bioavailability through significant correlations with total amino acid pools (Yamashita et al., 2015). Moreover, Hood et al (2009) showed that higher fractions of proteinaceous glacial DOM were tied to greater DOM bioavailability, measured as carbon consumed over the course of a 2-week incubation. These past links between protein-like fluorescent DOM and lability (Hood et al., 2009; Yamashita et al., 2015) suggest that all three glacial environments in this study contain dominant fractions of bioavailable, fluorescent DOM derived from in-situ microbial activity.

The high fractions of the humic-like C1 fluorescence in the channel waters (31.4 ± 10.3%) and lower fractions in supraglacial ice (9.8%) and basal ice (6.6 ± 3.4%) (Figure 4B) may derive from terrigenous, degraded plant inputs (Coble, 1996; Stedmon et al., 2003, 2007; Dubnick et al., 2020). Atmospheric deposition of vascular particulates in the supraglacial (Grannas et al., 2004), and overridden soil and vegetation in the subglacial (Bhatia et al., 2010; Kellerman et al., 2020, 2021) support the presence of plant-derived DOM in these ecosystems. Late-season supraglacial DOM inputs and ice-marginal bedrock contact with draining meltwaters may also explain the source of humic-like DOM in channel waters. In addition to plant inputs, the humic-like C1 fluorescence, based on its approximate peak excitation and emission wavelength(s), has also been associated with the microbial reworking of DOM (Stedmon and Markager, 2005; Feng et al., 2018; Dubnick et al., 2020). Basal ice isolates in laboratory incubations have demonstrated the ability to degrade organic matter and produce humic-like, recalcitrant DOM, from labile DOM (Barker et al., 2010). The inference of C1 as microbially sourced humic-like DOM supports the potential for in-situ microbial activity to produce humic-like DOM in glacial ecosystems (Figure 4).

By examining DOM at the molecular level, FT-ICR-MS offers insight into a larger fraction of DOM compared to fluorescence spectroscopy. Here, its application revealed variations in the fractions of protein-like DOM in the ice-marginal and subglacial environments that diverged from the relative dominance of fluorescent protein-like DOM. Following past examinations of glacial DOM at the molecular level (Grannas et al., 2006; Bhatia et al., 2010; Singer et al., 2012; Antony et al., 2014; Feng et al., 2018; Kellerman et al., 2021), diverse biomolecular DOM classes such as protein-like, SRFA terrestrial-like, lignin-like, and carbohydrate-like were observed in the ice-

marginal pond and subglacial environments (Figure 5B). Elevated proportions of SRFA terrestrial-like and lignin-like DOM, associated with terrestrial sources such as plant and soil inputs (Bhatia et al., 2010; Lawson et al., 2014a; Kellerman et al., 2021), were seen in both channel waters (31.9% and 20.2% respectively) and basal ice (22.4% and 17.5% respectively) (Table 6, bottom), along with notable fractions of protein-like DOM in each of these environments (16% in the channel waters and 29% in the basal ice) (Table 6, bottom). This protein-like DOM has been tied to autotrophic DOM production at glacier surfaces (Antony et al., 2014; Feng et al., 2018; Kellerman et al., 2021) and potential in-situ microbial transformations of terrestrially derived organic matter in subglacial environments (Bhatia et al., 2010). The high H:C ratio (>1.5) associated with protein-like DOM can also indicate high carbon bioavailability (D'Andrilli et al., 2015), which suggests that basal ice has higher labile fractions than channel waters. Therefore, the FT-ICR-MS results are congruent with those from fluorescence spectroscopy in that both analyses suggest that glacial environments contain high proportions of labile DOM. However, FT-ICR-MS provides the more nuanced perspective that these labile fractions do not always dominate across all glacial environments.

Past studies have shown that glacial systems can contain distinct pools of molecular DOM, particularly evident between the supraglacial and subglacial regions (Bhatia et al., 2010; Kellerman et al., 2021). Here, we suggest that the ice-marginal molecular DOM pool is also a distinct DOM pool. Compared to basal ice, the channel waters contained overall higher fractions of SRFA terrestrial-like and lignin-like DOM (Table 6; bottom), and higher peak numbers of CHOS and CHON *m/z* peaks, which may arise from in-situ microbial transformations of DOM. Past examination of microbial reworking of molecular DOM in supraglacial snowpack, via incubations that lasted up to 55 days, has shown the addition of more aromatic compounds and the enrichment in heteroatom-containing (N, S-) organic compounds (Antony et al., 2017). Meanwhile, despite significant bedrock inputs, basal ice had higher fractions of protein-like than channel waters (Table 6; bottom), indicating significant microbial reworking of terrestrially sourced DOM into protein-like components (Bhatia et al., 2010).

Despite various recent studies examining the molecular composition of DOM in glacial environments (Bhatia et al., 2010; Stubbins et al., 2012; Kellerman et al., 2021), the topic remains a source of debate. Early studies on the western Greenland Ice Sheet margin found that the supraglacial fractions of both terrestrial/lignin-like and protein-like DOM were lower than in

subglacial and proglacial streams (Bhatia et al., 2010). In contrast, Kellerman et al (2021) observed higher proportions of protein-like DOM in West Greenland and Svalbard supraglacial meltwaters than in proglacial rivers, but similar fractions of polyphenolic compounds (i.e., lignin-like) between the two environments. Stubbins et al (2012) also observed similar supraglacial and subglacial fractions of aliphatic and lignin-like DOM at Mendenhall Glacier, Alaska. Condensed hydrocarbons are another class of DOM associated with atmospheric deposition of aerosols from anthropogenic pollution and fossil fuel combustion (Stubbins et al., 2012), which we did not detect here. They are generally more prevalent in supraglacial systems but can appear in the subglacial system likely as a result of supraglacial meltwater routing to the glacier base (Bhatia et al., 2010; Stubbins et al., 2012; Kellerman et al., 2021). The variations observed in DOM composition among glacial environments in this and past studies may be a factor of sampling year, geographical locations, and the use of different algorithms for molecular formulae assignment. The EnviroOrg Software (Corilo, 2015) and a non-public molecular formula calculator (National High Magnetic Field Laboratory, Florida State University) were used by Kellerman et al (2020) and Stubbins et al (2012) respectively, which both employ set limits for elements (C, H, O, N, S, P) for molecular formulae identification. Bhatia et al (2010) used the Compound Identification Algorithm (Kujawinski and Behn, 2006; Kujawinski et al., 2009), which determines molecular formulae by finding chemical relationships using functional moieties between *m/z* peaks, starting with the lowest molecular mass.

The use of fluorescence spectroscopy and FT-ICR-MS together shows that the different DOM pools at the tidewater Sverdrup Glacier contain dominant fluorescent labile fractions (> 50%) but variable molecular labile fractions (16 – 30 %) associated with in-situ microbial activity and production. These proportions overall diverge from studies at mountain glaciers that have employed one or both of these techniques and observed consistently high labile DOM proportions (> 70%) in the two subsets of DOM in supraglacial and subglacial environments (Hood et al., 2009; Stubbins et al., 2012; Feng et al., 2018). However, in polar glacial systems, while high fluorescent labile DOM fractions (40 – 90%) have been typical (Barker et al., 2006; Dubnick et al., 2010, 2020; Smith et al., 2018; Williams et al., 2021), at the molecular level, labile protein-like/aliphatic DOM proportions have been < 50% across different environments with higher numbers arising from studies that have used FT-ICR-MS analysis in both negative and positive ion modes (Bhatia et al., 2010; Antony et al., 2014, 2017; Kellerman et al., 2021). Although these

fractions come from separate studies and may be subject to both temporal and spatial fluctuations, they support the variable DOM lability between the fluorescent and molecular subsets observed here at Sverdrup Glacier.

Our fluorescent and molecular DOM results are congruent with the spatial variability present in different types (polar, alpine) of glacial reservoirs of labile DOM. Despite this variability, our study supports glacial systems containing a unique type of labile, microbially-sourced DOM that is distinct from aquatic systems such as terrestrial rivers in Alaska and Tibet, which were dominated by high fluorescent humic-like (> 80%) (Hood et al., 2009) and molecular lignin-like/aromatic DOM (60 – 80%) (Stubbins et al., 2012; Spencer et al., 2014). Moreover, although geographical variations are present in glacial DOM composition, incubations of glacial runoff with microbial communities from coastal marine waters at sites in Alaska and Greenland have shown similar ranges of glacial carbon fractions (23 – 66%) being bioavailable to these downstream communities (Hood et al., 2009; Lawson et al., 2014b). We further note that neither fluorescence spectroscopy nor FT ICR-MS can offer a complete assessment of DOM composition. Fluorescence spectroscopy excludes non-fluorescent organic compounds (e.g., aliphatic hydrocarbons) from its analysis, whereas FT-ICR-MS excludes non-polar organic compounds. Also, organic polar compounds that can be protonated (e.g., amine moieties) are not considered in this study, as the FT-ICR-MS was run in the negative ion mode.

4.4. Interactions between glacial microbial habitats and their solute and DOM pools

The cold and dark conditions in ice-marginal and subglacial systems exert a primary control on microbial community composition, selecting for cold-tolerant, chemolithotrophic microorganisms (Anesio et al., 2017; Hotaling et al., 2017). However, a secondary control on microbial community composition in these different dark glacial environments can be the in-situ solute and DOM compositions (Skidmore et al., 2005; Bhatia et al., 2006; Dubnick et al., 2017; Smith et al., 2018; Sułowicz et al., 2020). This geochemical influence on microbial community composition can result in distinct glacial microbial habitats (Skidmore et al., 2005; Bhatia et al., 2006; Dubnick et al., 2017; Smith et al., 2018; Sułowicz et al., 2020). For instance, Skidmore et al (2005) found that the distinct subglacial microbial habitats at Bench Glacier (Alaska) and John Evans Glacier (Canadian High Arctic) were tied to different mineralogical sources of SO_4 (produced via pyrite oxidation or gypsum dissolution) at the glacier bases. In a study at Svalbard,

variations in the species richness (alpha diversity) of microbial assemblages from different subglacial channels were linked to site-specific hydrochemical properties such as pH, and Cl, Br, and NO_3 concentrations (Sułowicz et al., 2020). Moreover, Smith et al (2018) observed that microbial communities in Greenland and Antarctic supraglacial meltwaters were associated with higher protein-like DOM fractions and that these meltwater communities differed from those found in comparatively debris-rich supraglacial habitats like the stream sediments and cryoconite holes containing higher humic-like DOM fractions. Here, we probe microbial relationships with solute and DOM properties to highlight distinct ecosystems and microbial-DOM interactions occurring in glacial systems.

Correlation analysis between the most abundant or 'top' microbial species (> 0.5% of total reads), including the bioindicators for channel waters and basal ice, in the supraglacial, subglacial, and ice-marginal environments and in-situ solute and DOM compositions (Figure 7) showed that the variations in glacial microbial community compositions here are likely driven by differences in in-situ DOM and solute properties. The 'top' species (total sample reads > 0.5% of total community reads) dominating the channel waters and basal ice correlated significantly ($p \leq 0.05$) with in-situ solute concentrations and DOM properties associated with lability in distinct patterns (Figure 7). The presence of high SO_4 and major cations concentrations, humic-like DOM, and highly recalcitrant/aromatic DOM seemed to influence the 'top' species in channel waters, while 'top' species in basal ice seemed to be likely influenced by low SO_4, NO_3, and major cation concentrations, and high fractions of proteinaceous DOM observed in-situ (Figure 7). Thus, the significantly different ice-marginal pond and subglacial microbial communities observed in this study ($p = 0.018$, $\alpha = 0.05$; Figure 2) are likely due to different in-situ solute and DOM compositions influencing resident microbial assemblages, as shown by the correlations (Figure 7).

These significant correlations further indicate that there are different interactions among the site-specific microbial communities and solute and DOM pools in glacial environments, suggesting the presence of distinct ecosystems on glaciers. However, these correlations, while useful to infer significant interactions among glacial microbial, solute and DOM pools, cannot be used to elucidate the exact biogeochemical processes occurring in-situ (Skidmore et al., 2005). In considerations of glacial nutrient and carbon budgets and fluxes reported by past studies (Hood et al., 2009, 2015; Lawson et al., 2014b; Hawkings et al., 2015, 2016), this study highlights the presence of different DOM pools shaped by site-specific physical processes and microbial

metabolism in different environments associated with a single glacier. As glaciers experience accelerated melt due to climate change, the microbial diversity and activity in these environments may change and impact the composition and present estimates of carbon fluxes from glacial systems.

4.5. Glacial carbon bioavailability to subglacial microbial communities

Accelerated glacier retreat, higher melting rates, and prolonged melt seasons are all anticipated effects of climate change that are already being observed in the high Arctic (Gardner et al., 2011; Marzeion et al., 2014; Noël et al., 2016; Rignot et al., 2019; King et al., 2020). One significant predicted impact of this glacier retreat is the short-term increase in meltwater export of solutes and labile carbon to proglacial terrestrial or aquatic ecosystems (Bhatia et al., 2013; Lawson et al., 2014b; Hawkings et al., 2015; Delaney and Adhikari, 2020). However, although studies have shown that glaciers are significant sources of labile DOM to downstream ecosystems (Hood et al., 2009; Lawson et al., 2014b), these studies do not specifically probe the availability of this labile DOM to glacial microbial communities prior to its export downstream. Glacial microbial transformations of in-situ DOM released during melting could impact the bioavailability of DOM to downstream environments and therefore warrant investigation. Here, we used experimental dark incubations of melted debris-poor basal ice (SWB2) and debris-rich basal ice (SWB3) to examine glacial carbon bioavailability to in situ microbial communities and the ecological effects on community structure and function.

Previous studies have shown that debris concentration in basal ice is the primary factor driving variations in in-situ organic carbon and solute concentrations and also bacterial abundances (Skidmore et al., 2000; Bhatia et al., 2006; Yde et al., 2010; Montross et al., 2014). Montross et al (2014) showed that sediment, carbon, and nutrient concentrations and cellular densities can increase as debris concentrations increase drastically (0.001 – 14 g/L) in basal ice. Previous incubations of basal ice with different debris concentrations have shown negligible carbon dioxide (CO_2) production (a proxy for aerobic respiration and microbial growth) in clean basal ice (0.001 – 0.008 g/L), and up to an 8-fold increase in CO_2 production in debris-rich basal ice (10-14 g/L) over a 100-day incubation period (Montross et al., 2014). These prior results point to an effect of debris concentration on subglacial microbial activity, which leads to us to hypothesize that

different levels of carbon uptake and ensuing effects on microbial community structure will be tied to debris content.

The debris-poor incubation initially had a low TSS load of 0.012 g/L and low live cellular density of 4 x 10^3 cells/mL, compared to the debris-rich incubation (TSS = 0.40 g/L; cellular density = 5 x 10^3 cells/mL). A higher initial DOC concentration was measured in the debris-poor incubation (0.40 ppm) than in the debris-rich counterpart (0.31 ppm). However, variations in DOC concentrations, as well as solute concentrations and DOM lability, between the debris-poor and debris-rich incubations could still cause differences in microbial community responses to carbon uptake. In support of this line of reasoning, past studies have tied dissimilarities in community structure in glacial environments to different fluorescent DOM components occurring in supraglacial habitats driven by the presence of debris (Smith et al., 2018) and to different solute concentrations in subglacial and proglacial waters (Dubnick et al., 2017; Sułowicz et al., 2020). Here, initial solute concentrations differed between the debris-poor and debris-rich incubations. Higher TP, K, and Ca concentrations were seen in the debris-rich basal ice, whereas the higher TN, Na, and Mg concentrations were in the debris-poor basal ice; all were on the same order of magnitude except for TP (one order difference) and TN (negligible in the debris-rich ice). The debris-rich basal ice also had higher molecular protein-like DOM (32%) fractions and lower SRFA terrestrial-like (12%) and lignin-like DOM (23%) fractions than the debris-poor basal ice (protein = 12%; SRFA terrestrial = 32%; lignin = 27%), suggesting higher lability of DOM in the debris-rich incubation. Therefore, basal debris in our incubations can supply DOM comprised of different components and lability to subglacial microbial communities despite similar starting DOC concentrations (0.3 – 0.4 ppm).

DOC concentrations decreased by 0.1 – 0.3 ppm in both incubations by T_f (Figure 8B) likely due to microbial heterotrophic activity (Skidmore et al., 2000; Montross et al., 2014). FAPROTAX-predicted functional potential analysis shows an increase in heterotrophic potential in debris-rich microbial community by T_f (Figure 10A). Meanwhile, despite a large decrease in functional diversity, including heterotrophic potential, in the debris-poor incubation (Figure 10B), we observed several aerobic heterotrophic pathways such as chemoheterotrophy, methanol oxidation and methylotrophy remaining in the community at T_f. Moreover, the surviving taxa in the debris-poor incubation were largely limited to two major families (e.g., *Burkholderiaceae, Microbacteriaceae*) (Figure 9B), whose members have been previously associated with aerobic

heterotrophic activity (Tiago et al., 2004; Coenye, 2014; Koo et al., 2017; Hetz and Horn, 2021). Our experimental incubations thus show that DOM released from melting basal ice can be readily consumed by glacial microbial communities, with heterotrophs particularly selected for and stimulated.

The higher DOC uptake in the debris-rich incubation compared to the debris-poor incubation (Figure 8B) likely reflected the consumption of labile DOM components (Hood et al., 2009; Lawson et al., 2014b). The higher inferred lability of DOM in the debris-rich basal ice than in the debris-poor basal ice may explain the greater carbon consumption by the debris-rich microbial communities, which suggests an influence of debris on the bioavailability of glacial DOM. Finally, likely as a result of the different DOM pools present, the debris-rich and debris-poor microbial communities showed different levels of resilience (Allison and Martiny, 2008; Shade et al., 2012; Bölter and Müller, 2016). By T_f, the debris-rich microbial communities had retained most of their original taxonomic and functional diversity (Figure 9A, 10A), demonstrating high community resilience (Allison and Martiny, 2008). On the other hand, microbial communities in the debris-poor incubation experienced extensive microbial and functional diversity losses (Figure 9B, 10B), pointing to comparatively lower community resilience (Allison and Martiny, 2008). We note that besides varying debris concentrations, the difference in community response between the two incubations may also arise from the thaw stimulus (Musilova et al., 2015) or bottle effects (Alcamán-Arias et al., 2021). In the future, the exact role of debris in microbial-DOM interactions could be better elucidated by using replicated experiments with a greater range of debris concentrations and types.

The decrease in DOC seen in both incubations due to heterotrophic activity (Figure 8B, Figure 10) and potentially labile DOM consumption indicates lower carbon concentrations and likely less bioavailable fractions remaining in glacial meltwaters after in-situ microbial activity (Hood et al., 2009; Lawson et al., 2014b). These findings potentially cast a new light on the predicted increases in glacial labile carbon fluxes and downstream heterotrophic activity (Hood et al., 2009; Lawson et al., 2014b; Kellerman et al., 2021; Williams et al., 2021), as glaciers shrink from climate warming. At Sverdrup Glacier, glacial DOM was lower in concentration than downstream coastal levels but contained higher labile fractions, thus still retaining the potential to stimulate heterotrophy in coastal microbial communities (Williams et al., 2021). Our experimental incubations however suggest that the highly labile glacial DOM released during melting may be

first consumed during in-situ heterotrophic activity. The extent of DOM consumption by glacial microbes may depend on the meltwater residence time in the system, with longer times likely facilitating greater microbial processing (Bhatia et al., 2010; Kida et al., 2021). Nonetheless, in-situ DOM consumption by glacial microbes may result in a diluted, potentially less labile DOM pool that gets exported from glaciers to downstream marine and terrestrial ecosystems.

5. Conclusion

In this study, we investigated the supraglacial, ice-marginal channel pond, and subglacial environments to demonstrate varying labile organic matter pools and microbial habitats and how they interact with each other in the high Arctic Sverdrup Glacier. Past work on the Devon Ice Cap and the Sverdrup Glacier established that the supraglacial and basal ice microbial habitats were distinct at this site (Dubnick et al., 2020), and that the subglacial environment contained higher solute concentrations and humic-like DOM fractions than the supraglacial environment (Dubnick et al., 2020; Williams et al., 2021). Here, we added to this existing body of work by characterizing the microbial properties of various glacial environments and providing new insight into the lability of glacial DOM pools by pairing ultrahigh-resolution mass spectrometry with fluorescence spectroscopy. These two techniques provide different perspectives into DOM composition which, when combined, can reveal larger patterns in DOM sources, diversity, and lability in glacial ecosystems. We also inferred metabolic potential from a bacterial marker gene (16S rRNA) in glacial environments to generate hypotheses about potential in-situ microbial carbon cycling and used correlational analysis to examine the associations between microbial habitats, DOM, and solutes among these glacial ecosystems. Finally, we used dark incubations of melted debris-rich and debris-poor basal ice to gain insight into the effects of DOM lability on microbial community structure in basal ice ecosystems.

We found that differences in sediment and solute concentrations among the supraglacial, ice-marginal pond, and subglacial environments at the Sverdrup Glacier were driven by abiotic processes. These processes included atmospheric deposition at the glacier surface, bedrock inputs to basal ice, and a likely combination of supraglacial inputs, ice-marginal bedrock contact, and cryo-concentration in the ice-marginal channel waters. Distinct microbial community compositions were also present between channel waters and basal ice, consistent with past studies of glacial microbial habitats (Bhatia et al., 2006; Dubnick et al., 2020). The most abundant species

in the channel waters and basal ice, including bioindicators, further correlated with different in-situ solute and DOM properties, indicating that the significant variations in community structure between glacial environments was driven by these factors. In contrast to the supraglacial ice where photoautotrophic lifestyles dominated, chemoheterotrophy and autotrophic dark hydrogen/sulfur oxidations dominated in the basal ice and channel waters. Although in-situ physical conditions such as light and oxygen availability shaped the major metabolic lifestyles in glacial ecosystems, all three glacial habitats demonstrated the potential for in-situ carbon cycling through coupled respiration and autotrophy (Anesio et al., 2010; Christner et al., 2014; Smith et al., 2017).

Fluorescence spectroscopy and ultrahigh-resolution mass spectrometry revealed that although fluorescent labile DOM dominated in all environments (> 50%), lower and variable labile fractions (16 – 29%) were observed at the molecular level. These fractions are typical of values measured previously at polar glaciers (Bhatia et al., 2010; Dubnick et al., 2010; Smith et al., 2018; Kellerman et al., 2021) but are lower when compared to alpine glaciers where higher fluorescent and molecular labile fractions have been observed (>70%) (Hood et al., 2009; Stubbins et al., 2012; Feng et al., 2018) . Despite this variability, our results showed that glaciers remain a significant source of microbially-sourced, labile DOM that is unique from riverine systems which are dominated by terrestrial-like DOM signatures. Finally, this glacial DOM is also bioavailable to in-situ microbial communities, as shown by our experimental incubation of basal ice. Glacial heterotrophs were particularly stimulated due to the carbon uptake, even though debris concentration may cause variations in the initial DOM lability and in the response of the microbial communities. Our experimental incubations suggest that the in-situ microbial consumption of glacial DOM may leave behind a diluted DOM pool to be exported out of the glacier, which could be less bioavailable to downstream ecosystems (Hood et al., 2009; Lawson et al., 2014b).

In this work, we show that the supraglacial, ice-marginal, and subglacial environments at Sverdrup glacier contain distinct microbial habitats and significant labile DOM pools, and that the microbe-DOM interactions can be site-specific with the potential for in-situ carbon cycling. We also find that this labile DOM is likely to be first consumed by heterotrophs in the basal ice upon initial thaw. Although we used supraglacial ice, channel waters, and basal ice as a proxy for the different environments associated with a glacier, these environments can also contain additional sub-habitats. These sub-habitats can include snowpack and cryoconite holes at the surface; marginal glacier ice, channel ice, and lakes at the margins; and channels, sediments, and meltwater

at the base, some of which may be hard to access. Incorporating this variety of sub-habitats into future assessments of glacial ecosystems could help capture a greater range of variability pertaining to DOM and resident microbial community compositions. The inclusion of replicated incubations with varying debris concentrations in the future, while also tracking changes in DOM compositions and nutrient concentrations, could help elucidate the role of debris in shaping DOM lability to glacial microbial communities and the ecological responses of these communities.

REFERENCES

Alcamán-Arias, M. E., Fuentes-Alburquenque, S., Vergara-Barros, P., Cifuentes-Anticevic, J., Verdugo, J., Polz, M., et al. (2021). Coastal Bacterial Community Response to Glacier Melting in the Western Antarctic Peninsula. *Microorganisms* 9, 88. doi:10.3390/microorganisms9010088.

Allison, S. D., and Martiny, J. B. H. (2008). Resistance, resilience, and redundancy in microbial communities. *Proc. Natl. Acad. Sci.* 105, 11512–11519. doi:10.1073/pnas.0801925105.

Anesio, A. M., Lutz, S., Chrismas, N. A. M., and Benning, L. G. (2017). The microbiome of glaciers and ice sheets. *Npj Biofilms Microbiomes* 3, 1–11. doi:10.1038/s41522-017-0019-0.

Anesio, A. M., Sattler, B., Foreman, C., Telling, J., Hodson, A., Tranter, M., et al. (2010). Carbon fluxes through bacterial communities on glacier surfaces. *Ann. Glaciol.* 51, 32–40. doi:10.3189/172756411795932092.

Antony, R., Grannas, A. M., Willoughby, A. S., Sleighter, R. L., Thamban, M., and Hatcher, P. G. (2014). Origin and Sources of Dissolved Organic Matter in Snow on the East Antarctic Ice Sheet. *Environ. Sci. Technol.* 48, 6151–6159. doi:10.1021/es405246a.

Antony, R., Willoughby, A. S., Grannas, A. M., Catanzano, V., Sleighter, R. L., Thamban, M., et al. (2017). Molecular Insights on Dissolved Organic Matter Transformation by Supraglacial Microbial Communities. *Environ. Sci. Technol.* 51, 4328–4337. doi:10.1021/acs.est.6b05780.

Armstrong, W. H., and Anderson, R. S. (2020). Ice-marginal lake hydrology and the seasonal dynamical evolution of Kennicott Glacier, Alaska. *J. Glaciol.* 66, 699–713. doi:10.1017/jog.2020.41.

Bajerski, F., and Wagner, D. (2013). Bacterial succession in Antarctic soils of two glacier forefields on Larsemann Hills, East Antarctica. *FEMS Microbiol. Ecol.* 85, 128–142. doi:10.1111/1574-6941.12105.

Barker, J. D., Klassen, J. L., Sharp, M. J., Fitzsimons, S. J., and Turner, R. J. (2010). Detecting biogeochemical activity in basal ice using fluorescence spectroscopy. *Ann. Glaciol.* 51, 47–55. doi:10.3189/172756411795931967.

Barker, J. D., Sharp, M. J., Fitzsimons, S. J., and Turner, R. J. (2006). Abundance and Dynamics of Dissolved Organic Carbon in Glacier Systems. *Arct. Antarct. Alp. Res.* 38, 163–172. doi:10.1657/1523-0430(2006)38[163:AADODO]2.0.CO;2.

Belzile, C., Gibson, J. A. E., and Vincent, W. F. (2002). Colored dissolved organic matter and dissolved organic carbon exclusion from lake ice: Implications for irradiance transmission and carbon cycling. *Limnol. Oceanogr.* 47, 1283–1293. doi:10.4319/lo.2002.47.5.1283.

Bhatia, M. P., Das, S. B., Longnecker, K., Charette, M. A., and Kujawinski, E. B. (2010). Molecular characterization of dissolved organic matter associated with the Greenland ice sheet. *Geochim. Cosmochim. Acta* 74, 3768–3784. doi:10.1016/j.gca.2010.03.035.

Bhatia, M. P., Das, S. B., Xu, L., Charette, M. A., Wadham, J. L., and Kujawinski, E. B. (2013). Organic carbon export from the Greenland ice sheet. *Geochim. Cosmochim. Acta* 109, 329–344. doi:10.1016/j.gca.2013.02.006.

Bhatia, M., Sharp, M., and Foght, J. (2006). Distinct Bacterial Communities Exist beneath a High Arctic Polythermal Glacier. *Appl. Environ. Microbiol.* 72, 5838–5845. doi:10.1128/AEM.00595-06.

Bingham, R. G., Nienow, P. W., Sharp, M. J., and Boon, S. (2005). Subglacial drainage processes at a High Arctic polythermal valley glacier. *J. Glaciol.* 51, 15–24. doi:10.3189/172756505781829520.

Bölter, M., and Müller, F. (2016). Resilience in polar ecosystems: From drivers to impacts and changes. *Polar Sci.* 10, 52–59. doi:10.1016/j.polar.2015.09.002.

Bolyen, E., Rideout, J. R., Dillon, M. R., Bokulich, N. A., Abnet, C. C., Al-Ghalith, G. A., et al. (2019). Reproducible, interactive, scalable and extensible microbiome data science using QIIME 2. *Nat. Biotechnol.* 37, 852–857. doi:10.1038/s41587-019-0209-9.

Bomberg, M., Claesson Liljedahl, L., Lamminmäki, T., and Kontula, A. (2019). Highly Diverse Aquatic Microbial Communities Separated by Permafrost in Greenland Show Distinct Features According to Environmental Niches. *Front. Microbiol.* 10, 1583. doi:10.3389/fmicb.2019.01583.

Boon, S., Burgess, D., Koerner, R., and Sharp, M. (2010). Forty-seven Years of Research on the Devon Island Ice Cap, Arctic Canada. *Arctic* 63, 13–29. doi:10.14430/ARCTIC643.

Boulton, G. S. (1979). Processes of Glacier Erosion on Different Substrata. *J. Glaciol.* 23, 15–38. doi:10.3189/S0022143000029713.

Boyd, E. S., Hamilton, T. L., Havig, J. R., Skidmore, M. L., and Shock, E. L. (2014). Chemolithotrophic Primary Production in a Subglacial Ecosystem. *Appl. Environ. Microbiol.* 80, 6146–6153. doi:10.1128/AEM.01956-14.

Boyd, E. S., Lange, R. K., Mitchell, A. C., Havig, J. R., Hamilton, T. L., Lafrenière, M. J., et al. (2011). Diversity, Abundance, and Potential Activity of Nitrifying and Nitrate-Reducing Microbial Assemblages in a Subglacial Ecosystem. *Appl. Environ. Microbiol.* 77, 4778–4787. doi:10.1128/AEM.00376-11.

Brady, S., and Daniel, R. (2013). "Glacier Metagenomics," in *Encyclopedia of Metagenomics*, ed. K. E. Nelson (New York, NY: Springer), 1–9. doi:10.1007/978-1-4614-6418-1_38-5.

Bro, R. (1997). PARAFAC. Tutorial and applications. *Chemom. Intell. Lab. Syst.* 38, 149–171. doi:10.1016/S0169-7439(97)00032-4.

Burgess, D. O., Sharp, M. J., Mair, D. W. F., Dowdeswell, J. A., and Benham, T. J. (2005). Flow dynamics and iceberg calving rates of Devon Ice Cap, Nunavut, Canada. *J. Glaciol.* 51, 219–230. doi:10.3189/172756505781829430.

Callahan, B. J., McMurdie, P. J., Rosen, M. J., Han, A. W., Johnson, A. J. A., and Holmes, S. P. (2016). DADA2: High-resolution sample inference from Illumina amplicon data. *Nat. Methods* 13, 581–583. doi:10.1038/nmeth.3869.

Cameron, E. S., Schmidt, P. J., Tremblay, B. J.-M., Emelko, M. B., and Müller, K. M. (2021). To rarefy or not to rarefy: Enhancing diversity analysis of microbial communities through next-generation sequencing and rarefying repeatedly. doi:10.1101/2020.09.09.290049.

Cameron, K. A., Hagedorn, B., Dieser, M., Christner, B. C., Choquette, K., Sletten, R., et al. (2015). Diversity and potential sources of microbiota associated with snow on western portions of the Greenland Ice Sheet. *Environ. Microbiol.* 17, 594–609. doi:10.1111/1462-2920.12446.

Cameron, K. A., Hodson, A. J., and Osborn, A. M. (2012). Carbon and nitrogen biogeochemical cycling potentials of supraglacial cryoconite communities. *Polar Biol.* 35, 1375–1393. doi:10.1007/s00300-012-1178-3.

Cameron, K. A., Stibal, M., Zarsky, J. D., Gözdereliler, E., Schostag, M., and Jacobsen, C. S. (2016). Supraglacial bacterial community structures vary across the Greenland ice sheet. *FEMS Microbiol. Ecol.* 92. doi:10.1093/femsec/fiv164.

Carrivick, J. L., and Quincey, D. J. (2014). Progressive increase in number and volume of ice-marginal lakes on the western margin of the Greenland Ice Sheet. *Glob. Planet. Change* 116, 156–163. doi:10.1016/j.gloplacha.2014.02.009.

Chandler, D. M., Wadham, J. L., Nienow, P. W., Doyle, S. H., Tedstone, A. J., Telling, J., et al. (2021). Rapid development and persistence of efficient subglacial drainage under 900 m-thick ice in Greenland. *Earth Planet. Sci. Lett.* 566, 116982. doi:10.1016/j.epsl.2021.116982.

Choi, Y., Morlighem, M., Rignot, E., and Wood, M. (2021). Ice dynamics will remain a primary driver of Greenland ice sheet mass loss over the next century. *Commun. Earth Environ.* 2, 1–9. doi:10.1038/s43247-021-00092-z.

Christner, B. C., Mikucki, J. A., Foreman, C. M., Denson, J., and Priscu, J. C. (2005). Glacial ice cores: A model system for developing extraterrestrial decontamination protocols. *Icarus* 174, 572–584. doi:10.1016/j.icarus.2004.10.027.

Christner, B. C., Priscu, J. C., Achberger, A. M., Barbante, C., Carter, S. P., Christianson, K., et al. (2014). A microbial ecosystem beneath the West Antarctic ice sheet. *Nature* 512, 310–313. doi:10.1038/nature13667.

Coble, P. G. (1996). Characterization of marine and terrestrial DOM in seawater using excitation-emission matrix spectroscopy. *Mar. Chem.* 51, 325–346. doi:10.1016/0304-4203(95)00062-3.

Coble, P. G., Del Castillo, C. E., and Avril, B. (1998). Distribution and optical properties of CDOM in the Arabian Sea during the 1995 Southwest Monsoon. *Deep Sea Res. Part II Top. Stud. Oceanogr.* 45, 2195–2223. doi:10.1016/S0967-0645(98)00068-X.

Coble, P. G., Green, S. A., Blough, N. V., and Gagosian, R. B. (1990). Characterization of dissolved organic matter in the Black Sea by fluorescence spectroscopy. *Nature* 348, 432–435. doi:10.1038/348432a0.

Coenye, T. (2014). "The Family Burkholderiaceae," in *The Prokaryotes: Alphaproteobacteria and Betaproteobacteria*, eds. E. Rosenberg, E. F. DeLong, S. Lory, E. Stackebrandt, and F. Thompson (Berlin, Heidelberg: Springer), 759–776. doi:10.1007/978-3-642-30197-1_239.

Cook, A. J., Copland, L., Noël, B. P. Y., Stokes, C. R., Bentley, M. J., Sharp, M. J., et al. (2019). Atmospheric forcing of rapid marine-terminating glacier retreat in the Canadian Arctic Archipelago. *Sci. Adv.* 5, eaau8507. doi:10.1126/sciadv.aau8507.

Corilo, Y. (2015). EnviroOrg Software.

Cory, R. M., and McKnight, D. M. (2005). Fluorescence Spectroscopy Reveals Ubiquitous Presence of Oxidized and Reduced Quinones in Dissolved Organic Matter. *Environ. Sci. Technol.* 39, 8142–8149. doi:10.1021/es0506962.

Cress, P., and Wyness, R. (1961). The Devon Island expedition, observations of glacial movements. *Arctic* 14, 257–259.

D'Andrilli, J., Cooper, W. T., Foreman, C. M., and Marshall, A. G. (2015). An ultrahigh-resolution mass spectrometry index to estimate natural organic matter lability. *Rapid Commun. Mass Spectrom.* 29, 2385–2401. doi:10.1002/rcm.7400.

De Cáceres, M., Legendre, P., and Moretti, M. (2010). Improving indicator species analysis by combining groups of sites. *Oikos* 119, 1674–1684. doi:10.1111/j.1600-0706.2010.18334.x.

Delaney, I., and Adhikari, S. (2020). Increased Subglacial Sediment Discharge in a Warming Climate: Consideration of Ice Dynamics, Glacial Erosion, and Fluvial Sediment Transport. *Geophys. Res. Lett.* 47, e2019GL085672. doi:10.1029/2019GL085672.

Dittmar, T., Koch, B., Hertkorn, N., and Kattner, G. (2008). A simple and efficient method for the solid-phase extraction of dissolved organic matter (SPE-DOM) from seawater. *Limnol. Oceanogr. Methods* 6, 230–235. doi:10.4319/lom.2008.6.230.

Dong, Z., Li, Z., Wang, F., and Zhang, M. (2009). Characteristics of atmospheric dust deposition in snow on the glaciers of the eastern Tien Shan, China. *J. Glaciol.* 55, 797–804. doi:10.3189/002214309790152393.

Dubnick, A. (2018). Hydrological Controls on the Biogeochemistry of Polar Glacier Ice and its Meltwater. Available at: https://doi.org/10.7939/R3VH5D103.

Dubnick, A., Barker, J., Sharp, M., Wadham, J., Lis, G., Telling, J., et al. (2010). Characterization of dissolved organic matter (DOM) from glacial environments using total fluorescence spectroscopy and parallel factor analysis. *Ann. Glaciol.* 51, 111–122. doi:10.3189/172756411795931912.

Dubnick, A., Kazemi, S., Sharp, M., Wadham, J., Hawkings, J., Beaton, A., et al. (2017). Hydrological controls on glacially exported microbial assemblages. *J. Geophys. Res. Biogeosciences* 122, 1049–1061. doi:10.1002/2016JG003685.

Dubnick, A., Sharp, M., Danielson, B., Saidi-Mehrabad, A., and Barker, J. (2020). Basal thermal regime affects the biogeochemistry of subglacial systems. *Biogeosciences* 17, 963–977. doi:https://doi.org/10.5194/bg-17-963-2020.

Dufrêne, M., and Legendre, P. (1997). Species Assemblages and Indicator Species:the Need for a Flexible Asymmetrical Approach. *Ecol. Monogr.* 67, 345–366. doi:https://doi.org/10.1890/0012-9615(1997)067[0345:SAAIST]2.0.CO;2.

Dunham, E. C., Dore, J. E., Skidmore, M. L., Roden, E. E., and Boyd, E. S. (2021). Lithogenic hydrogen supports microbial primary production in subglacial and proglacial environments. *Proc. Natl. Acad. Sci.* 118. doi:10.1073/pnas.2007051117.

Edwards, A., Mur, L. A. J., Girdwood, S. E., Anesio, A. M., Stibal, M., Rassner, S. M. E., et al. (2014). Coupled cryoconite ecosystem structure–function relationships are revealed by comparing bacterial communities in alpine and Arctic glaciers. *FEMS Microbiol. Ecol.* 89, 222–237. doi:10.1111/1574-6941.12283.

Elliott, S., Lead, J. R., and Baker, A. (2006). Characterisation of the fluorescence from freshwater, planktonic bacteria. *Water Res.* 40, 2075–2083. doi:10.1016/j.watres.2006.03.017.

Eng, A., and Borenstein, E. (2018). Taxa-function robustness in microbial communities. *Microbiome* 6, 45. doi:10.1186/s40168-018-0425-4.

Ewertowski, M. W., Evans, D. J. A., Roberts, D. H., and Tomczyk, A. M. (2016). Glacial geomorphology of the terrestrial margins of the tidewater glacier, Nordenskiöldbreen, Svalbard. *J. Maps* 12, 476–487. doi:10.1080/17445647.2016.1192329.

Fegel, T., Boot, C. M., Broeckling, C. D., Baron, J. S., and Hall, E. K. (2019). Assessing the Chemistry and Bioavailability of Dissolved Organic Matter From Glaciers and Rock Glaciers. *J. Geophys. Res. Biogeosciences* 124, 1988–2004. doi:10.1029/2018JG004874.

Feng, L., An, Y., Xu, J., and Kang, S. (2018). Characteristics and sources of dissolved organic matter in a glacier in the northern Tibetan Plateau: differences between different snow categories. *Ann. Glaciol.* 59, 31–40. doi:10.1017/aog.2018.20.

Feng, L., An, Y., Xu, J., Li, X., Jiang, B., and Liao, Y. (2020). Biochemical evolution of dissolved organic matter during snow metamorphism across the ablation season for a glacier on the central Tibetan Plateau. *Sci. Rep.* 10, 6123. doi:10.1038/s41598-020-62851-w.

Fischer, H., Siggaard-Andersen, M.-L., Ruth, U., Röthlisberger, R., and Wolff, E. (2007). Glacial/interglacial changes in mineral dust and sea-salt records in polar ice cores: Sources, transport, and deposition. *Rev. Geophys.* 45. doi:10.1029/2005RG000192.

Foght, J., Aislabie, J., Turner, S., Brown, C. E., Ryburn, J., Saul, D. J., et al. (2004). Culturable Bacteria in Subglacial Sediments and Ice from Two Southern Hemisphere Glaciers. *Microb. Ecol.* 47, 329–340. doi:10.1007/s00248-003-1036-5.

Franzetti, A., Tagliaferri, I., Gandolfi, I., Bestetti, G., Minora, U., Mayer, C., et al. (2016). Light-dependent microbial metabolisms drive carbon fluxes on glacier surfaces. *ISME J.* 10, 2984–2988. doi:10.1038/ismej.2016.72.

García-Descalzo, L., García-López, E., Alcázar, A., Baquero, F., and Cid, C. (2014). Proteomic analysis of the adaptation to warming in the Antarctic bacteria Shewanella frigidimarina. *Biochim. Biophys. Acta* 1844, 2229–2240. doi:10.1016/j.bbapap.2014.08.006.

Garcia-Lopez, E., and Cid, C. (2017). Glaciers and Ice Sheets As Analog Environments of Potentially Habitable Icy Worlds. *Front. Microbiol.* 8. doi:10.3389/fmicb.2017.01407.

Garcia-Lopez, E., Rodriguez-Lorente, I., Alcazar, P., and Cid, C. (2019). Microbial Communities in Coastal Glaciers and Tidewater Tongues of Svalbard Archipelago, Norway. *Front. Mar. Sci.* 5, 512. doi:10.3389/fmars.2018.00512.

Gardner, A. S., Moholdt, G., Wouters, B., Wolken, G. J., Burgess, D. O., Sharp, M. J., et al. (2011). Sharply increased mass loss from glaciers and ice caps in the Canadian Arctic Archipelago. *Nature* 473, 357–360. doi:10.1038/nature10089.

Gatza, E., Hammes, F., and Prest, E. (2013). Assessing Water Quality with the BD Accurri C6 Flow Cytometer. *White Pap. BD Accuri*.

Gill-Olivas, B., Telling, J., Tranter, M., Skidmore, M., Christner, B., O'Doherty, S., et al. (2021). Subglacial erosion has the potential to sustain microbial processes in Subglacial Lake Whillans, Antarctica. *Commun. Earth Environ.* 2, 1–12. doi:10.1038/s43247-021-00202-x.

Grannas, A. M., Hockaday, W. C., Hatcher, P. G., Thompson, L. G., and Mosley-Thompson, E. (2006). New revelations on the nature of organic matter in ice cores. *J. Geophys. Res. Atmospheres* 111. doi:10.1029/2005JD006251.

Grannas, A. M., Shepson, P. B., and Filley, T. R. (2004). Photochemistry and nature of organic matter in Arctic and Antarctic snow. *Glob. Biogeochem. Cycles* 18. doi:10.1029/2003GB002133.

Habtewold, T., Duchateau, L., and Christophides, G. K. (2016). Flow cytometry analysis of the microbiota associated with the midguts of vector mosquitoes. *Parasit. Vectors* 9, 167. doi:10.1186/s13071-016-1438-0.

Hansen, A. M., Kraus, T. E. C., Pellerin, B. A., Fleck, J. A., Downing, B. D., and Bergamaschi, B. A. (2016). Optical properties of dissolved organic matter (DOM): Effects of biological and photolytic degradation. *Limnol. Oceanogr.* 61, 1015–1032. doi:10.1002/lno.10270.

Harrison, J. C., Lynds, T., and Rainbird, R. H. (2016). Geology, Simplified tectonic assemblage map of the Canadian Arctic Islands, Northwest Territories–Nunavut; Geological Survey of Canada. *Can. Geosci. Map 80* scale 1: 2000000. doi:10.4095/297416.

Hawkings, J. R., Wadham, J. L., Tranter, M., Lawson, E., Sole, A., Cowton, T., et al. (2015). The effect of warming climate on nutrient and solute export from the Greenland Ice Sheet. *Geochem. Perspect. Lett.*, 94–104. doi:10.7185/geochemlet.1510.

Hawkings, J., Wadham, J., Tranter, M., Telling, J., Bagshaw, E., Beaton, A., et al. (2016). The Greenland Ice Sheet as a hot spot of phosphorus weathering and export in the Arctic. *Glob. Biogeochem. Cycles* 30, 191–210. doi:10.1002/2015GB005237.

Hetz, S. A., and Horn, M. A. (2021). Burkholderiaceae Are Key Acetate Assimilators During Complete Denitrification in Acidic Cryoturbated Peat Circles of the Arctic Tundra. *Front. Microbiol.* 12, 151. doi:10.3389/fmicb.2021.628269.

Hodson, A., Anesio, A. M., Tranter, M., Fountain, A., Osborn, M., Priscu, J., et al. (2008). Glacial Ecosystems. *Ecol. Monogr.* 78, 41–67.

Hodson, A. J., and Ferguson, R. I. (1999). Fluvial suspended sediment transport from cold and warm-based glaciers in Svalbard. *Earth Surf. Process. Landf.* 24, 957–974. doi:10.1002/(SICI)1096-9837(199910)24:11<957::AID-ESP19>3.0.CO;2-J.

Hodson, A. J., Mumford, P. N., Kohler, J., and Wynn, P. M. (2005). The High Arctic glacial ecosystem: new insights from nutrient budgets. *Biogeochemistry* 72, 233–256. doi:10.1007/s10533-004-0362-0.

Hodson, A., Mumford, P., and Lister, D. (2004). Suspended sediment and phosphorus in proglacial rivers: bioavailability and potential impacts upon the P status of ice-marginal receiving waters. *Hydrol. Process.* 18, 2409–2422. doi:https://doi.org/10.1002/hyp.1471.

Hood, E., Battin, T. J., Fellman, J., O'Neel, S., and Spencer, R. G. M. (2015). Storage and release of organic carbon from glaciers and ice sheets. *Nat. Geosci.* 8, 91–96. doi:10.1038/ngeo2331.

Hood, E., Fellman, J., Spencer, R. G. M., Hernes, P. J., Edwards, R., D'Amore, D., et al. (2009). Glaciers as a source of ancient and labile organic matter to the marine environment. *Nature* 462, 1044–1047. doi:10.1038/nature08580.

Hotaling, S., Hood, E., and Hamilton, T. L. (2017). Microbial ecology of mountain glacier ecosystems: biodiversity, ecological connections and implications of a warming climate. *Environ. Microbiol.* 19, 2935–2948. doi:10.1111/1462-2920.13766.

How, P., Messerli, A., Mätzler, E., Santoro, M., Wiesmann, A., Caduff, R., et al. (2021). Greenland-wide inventory of ice marginal lakes using a multi-method approach. *Sci. Rep.* 11, 4481. doi:10.1038/s41598-021-83509-1.

Hubbard, B., Cook, S., and Coulson, H. (2009). Basal ice facies: a review and unifying approach. *Quat. Sci. Rev.* 28, 1956–1969. doi:10.1016/j.quascirev.2009.03.005.

Hubbard, B., and Sharp, M. (1989). Basal ice formation and deformation: a review. *Prog. Phys. Geogr.* 13, 529–558.

Hubbard, and Sharp, M. (1993). Weertman regelation, multiple refreezing events and the isotopic evolution of the basal ice layer. *J. Glaciol.* 39, 275–291.

Iizuka, Y., Satake, H., Shiraiwa, T., and Naruse, R. (2001). Formation processes of basal ice at Hamna Glacier, Sôya Coast, East Antarctica, inferred by detailed co-isotopic analyses. *J. Glaciol.* 47, 223–231. doi:10.3189/172756501781832359.

Kayani, M. ur R., Doyle, S. M., Sangwan, N., Wang, G., Gilbert, J. A., Christner, B. C., et al. (2018). Metagenomic analysis of basal ice from an Alaskan glacier. *Microbiome* 6, 123. doi:10.1186/s40168-018-0505-5.

Kellerman, A. M., Hawkings, J. R., Wadham, J. L., Kohler, T. J., Stibal, M., Grater, E., et al. (2020). Glacier Outflow Dissolved Organic Matter as a Window Into Seasonally Changing Carbon Sources: Leverett Glacier, Greenland. *J. Geophys. Res. Biogeosciences* 125, e2019JG005161. doi:10.1029/2019JG005161.

Kellerman, A. M., Vonk, J., McColaugh, S., Podgorski, D. C., Winden, E. van, Hawkings, J. R., et al. (2021). Molecular Signatures of Glacial Dissolved Organic Matter From Svalbard and Greenland. *Glob. Biogeochem. Cycles* 35, e2020GB006709. doi:10.1029/2020GB006709.

Kida, M., Fujitake, N., Kojima, T., Tanabe, Y., Hayashi, K., Kudoh, S., et al. (2021). Dissolved Organic Matter Processing in Pristine Antarctic Streams. *Environ. Sci. Technol.* 55, 10175–10185. doi:10.1021/acs.est.1c03163.

Killawee, J. A., Fairchild, I. J., Tison, J.-L., Janssens, L., and Lorrain, R. (1998). Segregation of solutes and gases in experimental freezing of dilute solutions: implications for natural glacial systems. *Geochim. Cosmochim. Acta* 62, 3637–3655. doi:10.1016/S0016-7037(98)00268-3.

Kim, S., Kramer, R. W., and Hatcher, P. G. (2003). Graphical Method for Analysis of Ultrahigh-Resolution Broadband Mass Spectra of Natural Organic Matter, the Van Krevelen Diagram. *Anal. Chem.* 75, 5336–5344. doi:10.1021/ac034415p.

Kjeldsen, K. K., Khan, S. A., Bjørk, A. A., Nielsen, K., and Mouginot, J. (2017). Ice-dammed lake drainage in west Greenland: Drainage pattern and implications on ice flow and bedrock motion. *Geophys. Res. Lett.* 44, 7320–7327. doi:10.1002/2017GL074081.

Knight, P. G. (1997). The basal ice layer of glaciers and ice sheets. *Quat. Sci. Rev.* 16, 975–993. doi:10.1016/S0277-3791(97)00033-4.

Koch, B. P., Dittmar, T., Witt, M., and Kattner, G. (2007). Fundamentals of Molecular Formula Assignment to Ultrahigh Resolution Mass Data of Natural Organic Matter. *Anal. Chem.* 79, 1758–1763. doi:10.1021/ac061949s.

Koerner, R. M., Apollonio, S., Cowie, J. W., Voegtli, K., Cress, P., Wyness, R., et al. (1961). The Devon Island Expedition. *ARCTIC* 14, 252–265. doi:10.14430/arctic3683.

Koo, H., Mojib, N., Hakim, J. A., Hawes, I., Tanabe, Y., Andersen, D. T., et al. (2017). Microbial Communities and Their Predicted Metabolic Functions in Growth Laminae of a Unique Large Conical Mat from Lake Untersee, East Antarctica. *Front. Microbiol.* 8, 1347. doi:10.3389/fmicb.2017.01347.

Koppes, M., Hallet, B., Rignot, E., Mouginot, J., Wellner, J. S., and Boldt, K. (2015). Observed latitudinal variations in erosion as a function of glacier dynamics. *Nature* 526, 100–103. doi:10.1038/nature15385.

Kujawinski, E. B. (2002). Electrospray Ionization Fourier Transform Ion Cyclotron Resonance Mass Spectrometry (ESI FT-ICR MS): Characterization of Complex Environmental Mixtures. *Environ. Forensics* 3, 207–216. doi:10.1006/enfo.2002.0109.

Kujawinski, E. B., and Behn, M. D. (2006). Automated Analysis of Electrospray Ionization Fourier Transform Ion Cyclotron Resonance Mass Spectra of Natural Organic Matter. *Anal. Chem.* 78, 4363–4373. doi:10.1021/ac0600306.

Kujawinski, E. B., Longnecker, K., Blough, N. V., Vecchio, R. D., Finlay, L., Kitner, J. B., et al. (2009). Identification of possible source markers in marine dissolved organic matter using ultrahigh resolution mass spectrometry. *Geochim. Cosmochim. Acta* 73, 4384–4399. doi:10.1016/j.gca.2009.04.033.

Lamarche-Gagnon, G., Anesio, A. M., Wadham, J. L., Zarsky, J. D., Kohler, T. J., Bagshaw, E. A., et al. (2020). Meltwater runoff from the Greenland Ice Sheet reveals microbial consortia from contrasting subglacial drainage systems. *BioRxiv*, 2020.05.26.116566. doi:https://doi.org/10.1101/2020.05.26.116566.

Langille, M. G. I., Zaneveld, J., Caporaso, J. G., McDonald, D., Knights, D., Reyes, J. A., et al. (2013). Predictive functional profiling of microbial communities using 16S rRNA marker gene sequences. *Nat. Biotechnol.* 31, 814–821. doi:10.1038/nbt.2676.

Lanoil, B., Skidmore, M., Priscu, J. C., Han, S., Foo, W., Vogel, S. W., et al. (2009). Bacteria beneath the West Antarctic ice sheet. *Environ. Microbiol.* 11, 609–615. doi:10.1111/j.1462-2920.2008.01831.x.

Lawson, D. E., Strasser, J. C., Evenson, E. B., Alley, R. B., Larson, G. J., and Arcone, S. A. (1998). Glaciohydraulic supercooling: a freeze-on mechanism to create stratified, debris-rich basal ice: I. Field evidence. *J. Glaciol.* 44, 547–562. doi:10.3189/S0022143000002069.

Lawson, E. C., Bhatia, M. P., Wadham, J. L., and Kujawinski, E. B. (2014a). Continuous Summer Export of Nitrogen-Rich Organic Matter from the Greenland Ice Sheet Inferred by Ultrahigh Resolution Mass Spectrometry. *Environ. Sci. Technol.* 48, 14248–14257. doi:10.1021/es501732h.

Lawson, E. C., Wadham, J. L., Tranter, M., Stibal, M., Lis, G. P., Butler, C. E. H., et al. (2014b). Greenland Ice Sheet exports labile organic carbon to the Arctic oceans. *Biogeosciences* 11. doi:10.5194/bg-11-4015-2014.

Legendre, P., and Gallagher, E. (2001). Ecologically Meaningful Transformations for Ordination of Species Data. *Oecologia* 129, 271–280.

Legendre, P., and Legendre, L. (2012). *Numerical Ecology*. 3rd ed. Elsevier.

Lilbæk, G., and Pomeroy, J. W. (2008). Ion enrichment of snowmelt runoff water caused by basal ice formation. *Hydrol. Process.* 22, 2758–2766. doi:10.1002/hyp.7028.

Lister, H. (1981). Particle Size, Shape, and Load in a Cold and a Temperate Valley Glacier. *Ann. Glaciol.* 2, 39–44. doi:10.3189/172756481794352397.

Louca, S., Parfrey, L. W., and Doebeli, M. (2016). Decoupling function and taxonomy in the global ocean microbiome. *Science* 353, 1272–1277. doi:10.1126/science.aaf4507.

Louca, S., Polz, M. F., Mazel, F., Albright, M. B. N., Huber, J. A., O'Connor, M. I., et al. (2018). Function and functional redundancy in microbial systems. *Nat. Ecol. Evol.* 2, 936–943. doi:10.1038/s41559-018-0519-1.

Luckman, B. H. (1988). Dating the Moraines and Recession of Athabasca and Dome Glaciers, Alberta, Canada. *Arct. Alp. Res.* 20, 40–54. doi:10.2307/1551697.

Lutz, S., Anesio, A. M., Edwards, A., and Benning, L. G. (2017). Linking microbial diversity and functionality of arctic glacial surface habitats. *Environ. Microbiol.* 19, 551–565. doi:10.1111/1462-2920.13494.

Lutz, S., Anesio, A. M., Jorge Villar, S. E., and Benning, L. G. (2014). Variations of algal communities cause darkening of a Greenland glacier. *FEMS Microbiol. Ecol.* 89, 402–414. doi:10.1111/1574-6941.12351.

MacDonald, E. N., Tank, S. E., Kokelj, S. V., Froese, D. G., and Hutchins, R. H. S. (2021). Permafrost-derived dissolved organic matter composition varies across permafrost end-members in the western Canadian Arctic. *Environ. Res. Lett.* 16, 024036. doi:10.1088/1748-9326/abd971.

Malard, L. A., Anwar, M. Z., Jacobsen, C. S., and Pearce, D. A. (2019). Biogeographical patterns in soil bacterial communities across the Arctic region. *FEMS Microbiol. Ecol.* 95. doi:10.1093/femsec/fiz128.

Masella, A. P., Bartram, A. K., Truszkowski, J. M., Brown, D. G., and Neufeld, J. D. (2012). PANDAseq: paired-end assembler for illumina sequences. *BMC Bioinformatics* 13, 31. doi:10.1186/1471-2105-13-31.

McCutcheon, J., Lutz, S., Williamson, C., Cook, J. M., Tedstone, A. J., Vanderstraeten, A., et al. (2021). Mineral phosphorus drives glacier algal blooms on the Greenland Ice Sheet. *Nat. Commun.* 12, 570. doi:10.1038/s41467-020-20627-w.

McKnight, D. M., Boyer, E. W., Westerhoff, P. K., Doran, P. T., Kulbe, T., and Andersen, D. T. (2001). Spectrofluorometric characterization of dissolved organic matter for indication of precursor organic material and aromaticity. *Limnol. Oceanogr.* 46, 38–48. doi:https://doi.org/10.4319/lo.2001.46.1.0038.

Merder, J., Freund, J. A., Feudel, U., Hansen, C. T., Hawkes, J. A., Jacob, B., et al. (2020a). ICBM-OCEAN: Processing Ultrahigh-Resolution Mass Spectrometry Data of Complex Molecular Mixtures. *Anal. Chem.* 92, 6832–6838. doi:10.1021/acs.analchem.9b05659.

Merder, J., Freund, J. A., Feudel, U., Niggemann, J., Singer, G., and Dittmar, T. (2020b). Improved Mass Accuracy and Isotope Confirmation through Alignment of Ultrahigh-Resolution Mass Spectra of Complex Natural Mixtures. *Anal. Chem.* 92, 2558–2565. doi:10.1021/acs.analchem.9b04234.

Milner, A. M., Khamis, K., Battin, T. J., Brittain, J. E., Barrand, N. E., Füreder, L., et al. (2017). Glacier shrinkage driving global changes in downstream systems. *Proc. Natl. Acad. Sci.* 114, 9770–9778. doi:10.1073/pnas.1619807114.

Montross, S. N., and Skidmore, M. L. (2006). Geochemical Evidence of Microbially-Mediated Subglacial Mineral Weathering. *AGU Fall Meet. Abstr.* 31, C31A-1240.

Montross, S., Skidmore, M., Christner, B., Samyn, D., Tison, J.-L., Lorrain, R., et al. (2014). Debris-Rich Basal Ice as a Microbial Habitat, Taylor Glacier, Antarctica. *Geomicrobiol. J.* 31, 76–81. doi:10.1080/01490451.2013.811316.

Murphy, K. R., Stedmon, C. A., Graeber, D., and Bro, R. (2013). Fluorescence spectroscopy and multi-way techniques. PARAFAC. *Anal. Methods* 5, 6557–6566. doi:10.1039/C3AY41160E.

Murphy, K. R., Stedmon, C. A., Waite, T. D., and Ruiz, G. M. (2008). Distinguishing between terrestrial and autochthonous organic matter sources in marine environments using fluorescence spectroscopy. *Mar. Chem.* 108, 40–58. doi:10.1016/j.marchem.2007.10.003.

Murphy, K. R., Stedmon, C. A., Wenig, P., and Bro, R. (2014). OpenFluor– an online spectral library of auto-fluorescence by organic compounds in the environment. *Anal. Methods* 6, 658–661. doi:10.1039/C3AY41935E.

Musilova, M., Tranter, M., Bennett, S. A., Wadham, J., and Anesio, A. M. (2015). Stable microbial community composition on the Greenland Ice Sheet. *Front. Microbiol.* 6, 193. doi:10.3389/fmicb.2015.00193.

Nicholes, M. J., Williamson, C. J., Tranter, M., Holland, A., Poniecka, E., Yallop, M. L., et al. (2019). Bacterial Dynamics in Supraglacial Habitats of the Greenland Ice Sheet. *Front. Microbiol.* 10, 1366. doi:10.3389/fmicb.2019.01366.

Noël, B., Berg, W. J. van de, Lhermitte, S., Wouters, B., Schaffer, N., and Broeke, M. R. van den (2018). Six Decades of Glacial Mass Loss in the Canadian Arctic Archipelago. *J. Geophys. Res. Earth Surf.* 123, 1430–1449. doi:10.1029/2017JF004304.

Parada, A. E., Needham, D. M., and Fuhrman, J. A. (2016). Every base matters: assessing small subunit rRNA primers for marine microbiomes with mock communities, time series and global field samples. *Environ. Microbiol.* 18, 1403–1414. doi:10.1111/1462-2920.13023.

Price, P. B., Rohde, R. A., and Bay, R. C. (2009). Fluxes of microbes, organic aerosols, dust, sea-salt Na ions, non-sea-salt Ca ions, and methanesulfonate onto Greenland and Antarctic ice. *Biogeosciences* 6, 479–486. doi:10.5194/bg-6-479-2009.

Quince, C., Lanzen, A., Davenport, R. J., and Turnbaugh, P. J. (2011). Removing Noise From Pyrosequenced Amplicons. *BMC Bioinformatics* 12, 38. doi:10.1186/1471-2105-12-38.

Rada, C., and Schoof, C. (2018). Channelized, distributed, and disconnected: subglacial drainage under a valley glacier in the Yukon. doi:10.5194/TC-12-2609-2018.

Raes, E. J., Karsh, K., Sow, S. L. S., Ostrowski, M., Brown, M. V., van de Kamp, J., et al. (2021). Metabolic pathways inferred from a bacterial marker gene illuminate ecological changes across South Pacific frontal boundaries. *Nat. Commun.* 12, 2213. doi:10.1038/s41467-021-22409-4.

Rankin, A. M., Auld, V., and Wolff, E. W. (2000). Frost flowers as a source of fractionated sea salt aerosol in the polar regions. *Geophys. Res. Lett.* 27, 3469–3472. doi:10.1029/2000GL011771.

Retelletti Brogi, S., Ha, S.-Y., Kim, K., Derrien, M., Lee, Y. K., and Hur, J. (2018). Optical and molecular characterization of dissolved organic matter (DOM) in the Arctic ice core and the underlying seawater (Cambridge Bay, Canada): Implication for increased autochthonous DOM during ice melting. *Sci. Total Environ.* 627, 802–811. doi:10.1016/j.scitotenv.2018.01.251.

Riedel, T., Zark, M., Vähätalo, A. V., Niggemann, J., Spencer, R. G. M., Hernes, P. J., et al. (2016). Molecular Signatures of Biogeochemical Transformations in Dissolved Organic Matter from Ten World Rivers. *Front. Earth Sci.* 4. Available at: https://www.frontiersin.org/article/10.3389/feart.2016.00085 [Accessed February 6, 2022].

Sansupa, C., Wahdan, S. F. M., Hossen, S., Disayathanoowat, T., Wubet, T., and Purahong, W. (2021). Can We Use Functional Annotation of Prokaryotic Taxa (FAPROTAX) to Assign the Ecological Functions of Soil Bacteria? *Appl. Sci.* 11, 688. doi:10.3390/app11020688.

Santibáñez, P. A., Michaud, A. B., Vick-Majors, T. J., D'Andrilli, J., Chiuchiolo, A., Hand, K. P., et al. (2019). Differential Incorporation of Bacteria, Organic Matter, and Inorganic Ions Into Lake Ice During Ice Formation. *J. Geophys. Res. Biogeosciences* 124, 585–600. doi:10.1029/2018JG004825.

Santoro, A. E., Casciotti, K. L., and Francis, C. A. (2010). Activity, abundance and diversity of nitrifying archaea and bacteria in the central California Current. *Environ. Microbiol.* 12, 1989–2006. doi:https://doi.org/10.1111/j.1462-2920.2010.02205.x.

Sanyal, A., Antony, R., Samui, G., and Thamban, M. (2018). Microbial communities and their potential for degradation of dissolved organic carbon in cryoconite hole environments of Himalaya and Antarctica. *Microbiol. Res.* 208, 32–42. doi:10.1016/j.micres.2018.01.004.

Shade, A., Peter, H., Allison, S., Baho, D., Berga, M., Buergmann, H., et al. (2012). Fundamentals of Microbial Community Resistance and Resilience. *Front. Microbiol.* 3, 417. doi:10.3389/fmicb.2012.00417.

Shakil, S., Tank, S. E., Kokelj, S. V., Vonk, J. E., and Zolkos, S. (2020). Particulate dominance of organic carbon mobilization from thaw slumps on the Peel Plateau, NT: Quantification and implications for stream systems and permafrost carbon release. *Environ. Res. Lett.* 15, 114019. doi:10.1088/1748-9326/abac36.

Sharp, M., Parkes, J., Cragg, B., Fairchild, I. J., Lamb, H., and Tranter, M. (1999). Widespread bacterial populations at glacier beds and their relationship to rock weathering and carbon cycling. *Geology* 27, 107–110. doi:10.1130/0091-7613(1999)027<0107:WBPAGB>2.3.CO;2.

Shugar, D. H., Burr, A., Haritashya, U. K., Kargel, J. S., Watson, C. S., Kennedy, M. C., et al. (2020). Rapid worldwide growth of glacial lakes since 1990. *Nat. Clim. Change* 10, 939–945. doi:10.1038/s41558-020-0855-4.

Simon, C., Wiezer, A., Strittmatter, A. W., and Daniel, R. (2009). Phylogenetic diversity and metabolic potential revealed in a glacier ice metagenome. *Appl. Environ. Microbiol.* 75, 7519–7526. doi:10.1128/AEM.00946-09.

Singer, G. A., Fasching, C., Wilhelm, L., Niggemann, J., Steier, P., Dittmar, T., et al. (2012). Biogeochemically diverse organic matter in Alpine glaciers and its downstream fate. *Nat. Geosci.* 5, 710–714. doi:10.1038/ngeo1581.

Skidmore, M., Anderson, S. P., Sharp, M., Foght, J., and Lanoil, B. D. (2005). Comparison of Microbial Community Compositions of Two Subglacial Environments Reveals a Possible Role for Microbes in Chemical Weathering Processes. *Appl. Environ. Microbiol.* 71, 6986–6997. doi:10.1128/AEM.71.11.6986-6997.2005.

Skidmore, M. L., Foght, J. M., and Sharp, M. J. (2000). Microbial Life beneath a High Arctic Glacier. *Appl. Environ. Microbiol.* 66, 3214–3220. doi:10.1128/AEM.66.8.3214-3220.2000.

Smith, H., Dieser, M., McKnight, D., SanClements, M., and Foreman, C. (2018). Relationship between dissolved organic matter quality and microbial community composition across polar glacial environments. *FEMS Microbiol. Ecol.* 94. doi:10.1093/femsec/fiy090.

Smith, H. J., Foster, R. A., McKnight, D. M., Lisle, J. T., Littmann, S., Kuypers, M. M. M., et al. (2017). Microbial formation of labile organic carbon in Antarctic glacial environments. *Nat. Geosci.* 10, 356–359. doi:10.1038/ngeo2925.

Spencer, R. G. M., Guo, W., Raymond, P. A., Dittmar, T., Hood, E., Fellman, J., et al. (2014). Source and biolability of ancient dissolved organic matter in glacier and lake ecosystems on the Tibetan Plateau. *Geochim. Cosmochim. Acta* 142, 64–74. doi:10.1016/j.gca.2014.08.006.

Stedmon, C. A., and Bro, R. (2008). Characterizing dissolved organic matter fluorescence with parallel factor analysis: a tutorial. *Limnol. Oceanogr. Methods* 6, 572–579. doi:https://doi.org/10.4319/lom.2008.6.572.

Stedmon, C. A., and Markager, S. (2005). Resolving the variability in dissolved organic matter fluorescence in a temperate estuary and its catchment using PARAFAC analysis. *Limnol. Oceanogr.* 50, 686–697. doi:10.4319/lo.2005.50.2.0686.

Stedmon, C. A., Markager, S., and Bro, R. (2003). Tracing dissolved organic matter in aquatic environments using a new approach to fluorescence spectroscopy. *Mar. Chem.* 82, 239–254. doi:10.1016/S0304-4203(03)00072-0.

Stedmon, C. A., Markager, S., Tranvik, L., Kronberg, L., Slätis, T., and Martinsen, W. (2007). Photochemical production of ammonium and transformation of dissolved organic matter in the Baltic Sea. *Mar. Chem.* 104, 227–240. doi:10.1016/j.marchem.2006.11.005.

Stibal, M., Anesio, A. M., Blues, C. J. D., and Tranter, M. (2009). Phosphatase activity and organic phosphorus turnover on a high Arctic glacier. *Biogeosciences* 6, 913–922. doi:10.5194/bg-6-913-2009.

Stibal, M., Bradley, J. A., and Box, J. E. (2017). Ecological Modeling of the Supraglacial Ecosystem: A Process-based Perspective. *Front. Earth Sci.* 5, 52. doi:10.3389/feart.2017.00052.

Stibal, M., Gözdereliler, E., Cameron, K. A., Box, J. E., Stevens, I. T., Gokul, J. K., et al. (2015). Microbial abundance in surface ice on the Greenland Ice Sheet. *Front. Microbiol.* 6, 225. doi:10.3389/fmicb.2015.00225.

Stibal, M., Lawson, E. C., Lis, G. P., Mak, K. M., Wadham, J. L., and Anesio, A. M. (2010). Organic matter content and quality in supraglacial debris across the ablation zone of the Greenland ice sheet. *Ann. Glaciol.* 51, 1–8. doi:10.3189/172756411795931958.

Stibal, M., and Tranter, M. (2007). Laboratory investigation of inorganic carbon uptake by cryoconite debris from Werenskioldbreen, Svalbard. *J. Geophys. Res. Biogeosciences* 112. doi:10.1029/2007JG000429.

Stibal, M., Tranter, M., Benning, L. G., and Rehák, J. (2008a). Microbial primary production on an Arctic glacier is insignificant in comparison with allochthonous organic carbon input. *Environ. Microbiol.* 10, 2172–2178. doi:10.1111/j.1462-2920.2008.01620.x.

Stibal, M., Tranter, M., Telling, J., and Benning, L. G. (2008b). Speciation, phase association and potential bioavailability of phosphorus on a Svalbard glacier. *Biogeochemistry* 90, 1–13. doi:10.1007/s10533-008-9226-3.

Stibal, M., Wadham, J. L., Lis, G. P., Telling, J., Pancost, R. D., Dubnick, A., et al. (2012). Methanogenic potential of Arctic and Antarctic subglacial environments with contrasting organic carbon sources. *Glob. Change Biol.* 18, 3332–3345. doi:https://doi.org/10.1111/j.1365-2486.2012.02763.x.

St-Onge, M. R., Gool, J. A. M. V., Garde, A. A., and Scott, D. J. (2009). Correlation of Archaean and Palaeoproterozoic units between northeastern Canada and western Greenland: constraining the pre-collisional upper plate accretionary history of the Trans-Hudson orogen. *Geol. Soc. Lond. Spec. Publ.* 318, 193–235. doi:10.1144/SP318.7.

Stubbins, A., Hood, E., Raymond, P. A., Aiken, G. R., Sleighter, R. L., Hernes, P. J., et al. (2012). Anthropogenic aerosols as a source of ancient dissolved organic matter in glaciers. *Nat. Geosci.* 5, 198–201. doi:10.1038/ngeo1403.

Sułowicz, S., Bondarczuk, K., Ignatiuk, D., Jania, J. A., and Piotrowska-Seget, Z. (2020). Microbial communities from subglacial water of naled ice bodies in the forefield of Werenskioldbreen, Svalbard. *Sci. Total Environ.* 723, 138025. doi:10.1016/j.scitotenv.2020.138025.

Takeuchi, N. (2013). Seasonal and altitudinal variations in snow algal communities on an Alaskan glacier (Gulkana glacier in the Alaska range). *Environ. Res. Lett.* 8, 035002. doi:10.1088/1748-9326/8/3/035002.

Takeuchi, N., Tanaka, S., Konno, Y., Irvine-Fynn, T. D. L., Rassner, S. M. E., and Edwards, A. (2019). Variations in Phototroph Communities on the Ablating Bare-Ice Surface of Glaciers on Brøggerhalvøya, Svalbard. *Front. Earth Sci.* 7, 4. doi:10.3389/feart.2019.00004.

Telling, J., Anesio, A. M., Tranter, M., Stibal, M., Hawkings, J., Irvine-Fynn, T., et al. (2012). Controls on the autochthonous production and respiration of organic matter in cryoconite holes on high Arctic glaciers. *J. Geophys. Res. Biogeosciences* 117. doi:https://doi.org/10.1029/2011JG001828.

Thór Marteinsson, V., Rúnarsson, Á., Stefánsson, A., Thorsteinsson, T., Jóhannesson, T., Magnússon, S. H., et al. (2013). Microbial communities in the subglacial waters of the Vatnajökull ice cap, Iceland. *ISME J.* 7, 427–437. doi:10.1038/ismej.2012.97.

Tiago, I., Chung, A. P., and Veríssimo, A. (2004). Bacterial Diversity in a Nonsaline Alkaline Environment: Heterotrophic Aerobic Populations. *Appl. Environ. Microbiol.* doi:10.1128/AEM.70.12.7378-7387.2004.

Toubes-Rodrigo, M., Potgieter-Vermaak, S., Sen, R., Oddsdóttir, E. S., Elliott, D., and Cook, S. (2021). Active microbial ecosystem in glacier basal ice fuelled by iron and silicate comminution-derived hydrogen. *MicrobiologyOpen* 10, e1200. doi:10.1002/mbo3.1200.

Tranter, M., Sharp, M. J., Lamb, H. R., Brown, G. H., Hubbard, B. P., and Willis, I. C. (2002). Geochemical weathering at the bed of Haut Glacier d'Arolla, Switzerland—a new model. *Hydrol. Process.* 16, 959–993. doi:https://doi.org/10.1002/hyp.309.

Tranter, M., Skidmore, M., and Wadham, J. (2005). Hydrological controls on microbial communities in subglacial environments. *Hydrol. Process.* 19, 995–998. doi:10.1002/hyp.5854.

Vögtli, K. (1967). D.C. Resistivity Soundings on Devon Island, N.W.T., Canada. *J. Glaciol.* 6, 635–642. doi:10.3189/S0022143000019900.

Wadham, J. L., Bottrell, S., Tranter, M., and Raiswell, R. (2004a). Stable isotope evidence for microbial sulphate reduction at the bed of a polythermal high Arctic glacier. *Earth Planet. Sci. Lett.* 219, 341–355. doi:10.1016/S0012-821X(03)00683-6.

Wadham, J. L., Bottrell, S., Tranter, M., and Raiswell, R. (2004b). Stable isotope evidence for microbial sulphate reduction at the bed of a polythermal high Arctic glacier. *Earth Planet. Sci. Lett.* 219, 341–355. doi:10.1016/S0012-821X(03)00683-6.

Wagenbach, D., Ducroz, F., Mulvaney, R., Keck, L., Minikin, A., Legrand, M., et al. (1998). Sea-salt aerosol in coastal Antarctic regions. *J. Geophys. Res. Atmospheres* 103, 10961–10974. doi:10.1029/97JD01804.

Waller, R. I. (2001). The influence of basal processes on the dynamic behaviour of cold-based glaciers. *Quat. Int.* 86, 117–128. doi:10.1016/S1040-6182(01)00054-4.

Weisleitner, K., Perras, A., Moissl-Eichinger, C., Andersen, D. T., and Sattler, B. (2019). Source Environments of the Microbiome in Perennially Ice-Covered Lake Untersee, Antarctica. *Front. Microbiol.* 10, 1019. doi:10.3389/fmicb.2019.01019.

Whalen, J. B., Wodicka, N., Taylor, B. E., and Jackson, G. D. (2010). Cumberland batholith, Trans-Hudson Orogen, Canada: Petrogenesis and implications for Paleoproterozoic crustal and orogenic processes. *Lithos* 117, 99–118. doi:10.1016/j.lithos.2010.02.008.

Williams, P. L., Burgess, D. O., Waterman, S., Roberts, M., Bertrand, E. M., and Bhatia, M. P. (2021). Nutrient and Carbon Export From a Tidewater Glacier to the Coastal Ocean in the Canadian Arctic Archipelago. *J. Geophys. Res. Biogeosciences* 126, e2021JG006289. doi:10.1029/2021JG006289.

Williams, T. J., Lauro, F. M., Ertan, H., Burg, D. W., Poljak, A., Raftery, M. J., et al. (2011). Defining the response of a microorganism to temperatures that span its complete growth temperature range (-2°C to 28°C) using multiplex quantitative proteomics. *Environ. Microbiol.* 13, 2186–2203. doi:10.1111/j.1462-2920.2011.02467.x.

Wolff, E. W. (2013). Ice sheets and nitrogen. *Philos. Trans. R. Soc. B Biol. Sci.* 368, 20130127. doi:10.1098/rstb.2013.0127.

Woods, G. C., Simpson, M. J., Pautler, B. G., Lamoureux, S. F., Lafrenière, M. J., and Simpson, A. J. (2011). Evidence for the enhanced lability of dissolved organic matter following permafrost slope disturbance in the Canadian High Arctic. *Geochim. Cosmochim. Acta* 75, 7226–7241. doi:10.1016/j.gca.2011.08.013.

Wychen, W. V., Davis, J., Copland, L., Burgess, D. O., Gray, L., Sharp, M., et al. (2017). Variability in ice motion and dynamic discharge from Devon Ice Cap, Nunavut, Canada. *J. Glaciol.* 63, 436–449. doi:10.1017/jog.2017.2.

Wynn, P. M., Hodson, A. J., Heaton, T. H. E., and Chenery, S. R. (2007). Nitrate production beneath a High Arctic glacier, Svalbard. *Chem. Geol.* 244, 88–102. doi:10.1016/j.chemgeo.2007.06.008.

Xiang, S.-R., Shang, T.-C., Chen, Y., and Yao, T.-D. (2009). Deposition and postdeposition mechanisms as possible drivers of microbial population variability in glacier ice. *FEMS Microbiol. Ecol.* 70, 165–176. doi:10.1111/j.1574-6941.2009.00759.x.

Yamashita, Y., Fichot, C. G., Shen, Y., Jaffé, R., and Benner, R. (2015). Linkages among fluorescent dissolved organic matter, dissolved amino acids and lignin-derived phenols in a river-influenced ocean margin. *Front. Mar. Sci.* 2, 92. doi:10.3389/fmars.2015.00092.

Yang, G. L., Hou, S. G., Le Baoge, R., Li, Z. G., Xu, H., Liu, Y. P., et al. (2016). Differences in Bacterial Diversity and Communities Between Glacial Snow and Glacial Soil on the Chongce Ice Cap, West Kunlun Mountains. *Sci. Rep.* 6, 36548. doi:10.1038/srep36548.

Yang, Y., Hou, Y., Ma, M., and Zhan, A. (2020). Potential pathogen communities in highly polluted river ecosystems: Geographical distribution and environmental influence. *Ambio* 49, 197–207. doi:10.1007/s13280-019-01184-z.

Yde, J. C., Finster, K. W., Raiswell, R., Steffensen, J. P., Heinemeier, J., Olsen, J., et al. (2010). Basal ice microbiology at the margin of the Greenland ice sheet. *Ann. Glaciol.* 51, 71–79. doi:10.3189/172756411795931976.

Zaikova, E., Walsh, D. A., Stilwell, C. P., Mohn, W. W., Tortell, P. D., and Hallam, S. J. (2010). Microbial community dynamics in a seasonally anoxic fjord: Saanich Inlet, British Columbia. *Environ. Microbiol.* 12, 172–191. doi:10.1111/j.1462-2920.2009.02058.x.

Zhang, B., Wu, X., Zhang, G., Li, S., Zhang, W., Chen, X., et al. (2016). The diversity and biogeography of the communities of Actinobacteria in the forelands of glaciers at a continental scale. *Environ. Res. Lett.* 11, 054012. doi:10.1088/1748-9326/11/5/054012.

Zhang, S., Hou, S., Ma, X., Qin, D., and Chen, T. (2007). Culturable bacteria in Himalayan glacial ice in response to atmospheric circulation. *Biogeosciences* 4, 1–9. doi:10.5194/bg-4-1-2007.

SUPPLEMENTARY INFORMATION

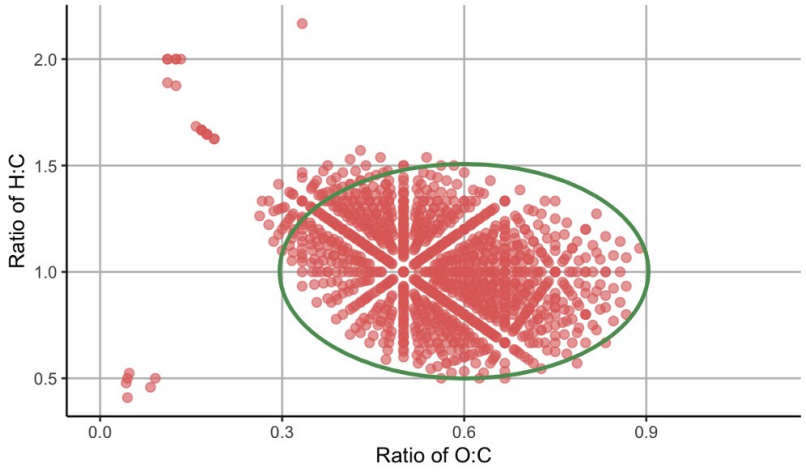

Figure S1. Van Krevalan plot of H:C and O:C ratios derived from molecular formulae associated with the resolved *m/z* peaks (red dots) detected in the Suwanee River Fulvic Acid (SRFA) standard, which has been used as a reference for terrestrially derived DOM in this and past studies. The green circle indicates the approximate range of H:C and O:C ratios used to characterize channel waters and basal ice *m/z* peaks as terrestrial-like.

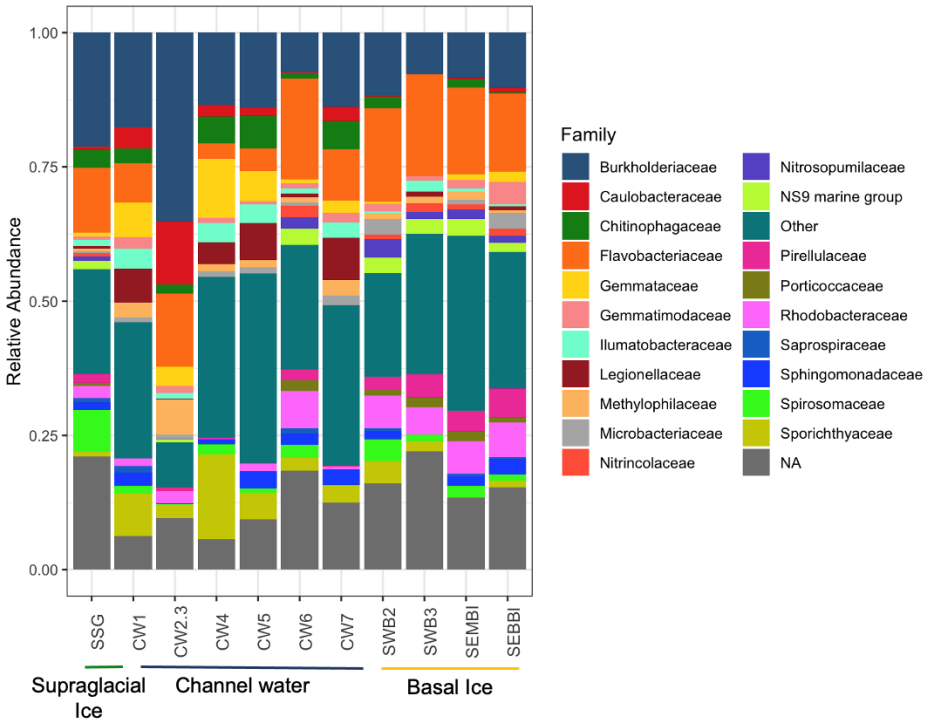

Figure S2. Relative distribution of the most abundant (top 20) families found in the supraglacial ice (green), channel waters (blue), and basal ice (yellow) samples; 'NA' refers to taxa that were unresolved/unidentified

at the family rank and higher, whereas 'Other' indicates taxa that were identified but less abundant than the top 20 displayed here.

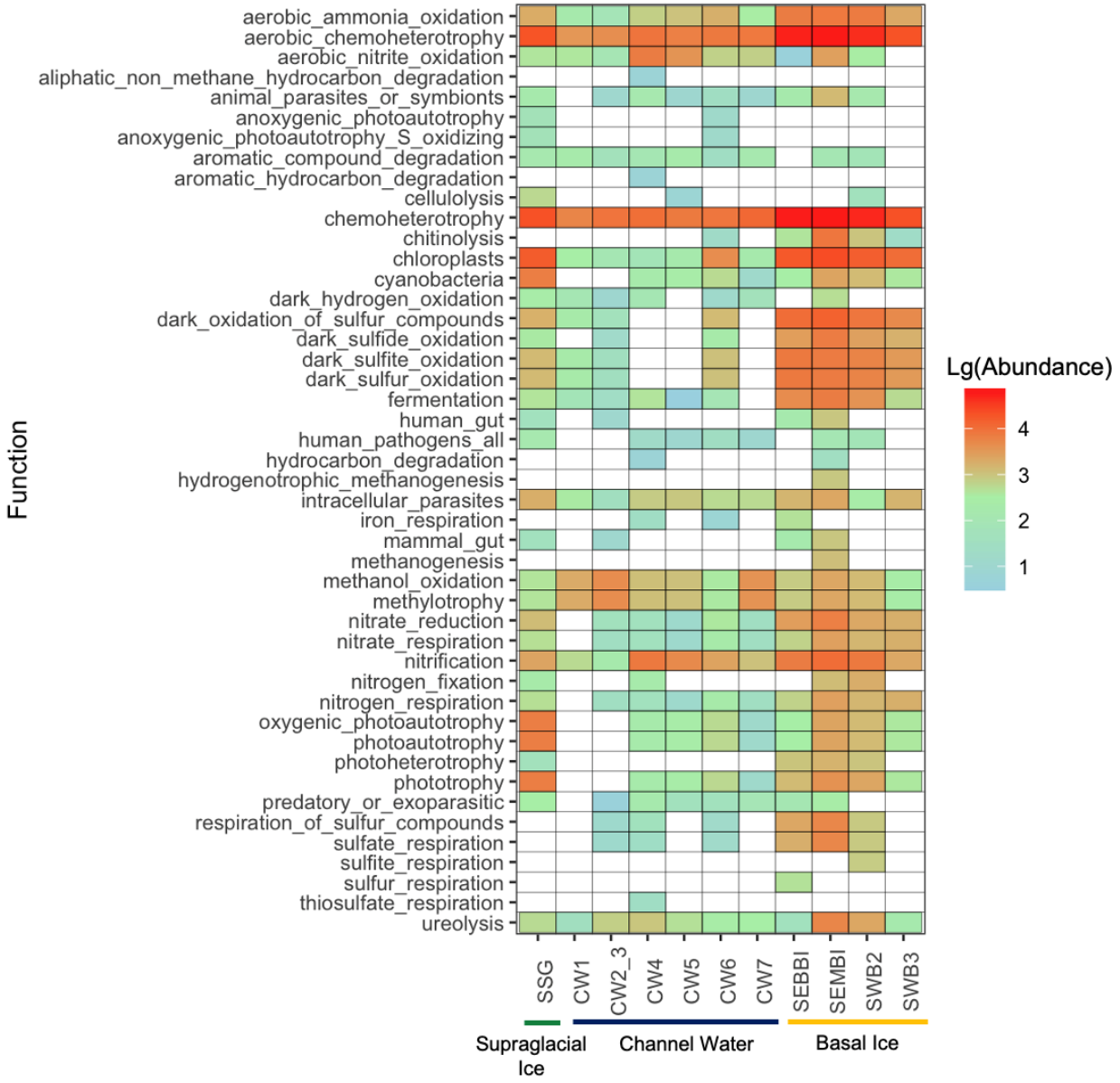

Figure S3. Log abundances of metabolic functions were observed in the supraglacial ice (green), channel waters (blue), and basal ice (yellow) environments. Based on 30% of our resolved ASVs, a total of 47 metabolic functions were identified using the FAPROTAX pipeline (Louca et al., 2016), which are all displayed here.